DTIC FILE COPY

(1)

AD-A206 024

DTIC
ELECTE
MAR 3 0 1989
S D
H

DEPARTMENT OF THE AIR FORCE

AIR UNIVERSITY

AIR FORCE INSTITUTE OF TECHNOLOGY

Wright-Patterson Air Force Base, Ohio

DISTRIBUTION STATEMENT A
Approved for public release;
Distribution Unlimited

89 3 28 056

(1)

AFIT/GE/ENG/89M-5

CONTROL DESIGN OF AN UNSTABLE NON-MINIMUM PHASE AIRCRAFT SUBJECT TO CONTROL SURFACE SATURATION

THESIS

Oliver J. Merwin
Captain, USAF

AFIT/GE/ENG/89M-5

DTIC
ELECTE
MAR 3 0 1989
S D
H

Revised pages A, 1 thru A-7 added
5 Jun 89

Approved for public release; distribution unlimited

AFIT/GE/ENG/89M-5

CONTROL DESIGN OF AN UNSTABLE NON-MINIMUM PHASE AIRCRAFT SUBJECT TO CONTROL SURFACE SATURATION

THESIS

Presented to the Faculty of the School of Engineering

of the Air Force Institute of Technology

Air University

In Partial Fulfillment of the

Requirements for the Degree of

Master of Science in Electrical Engineering

Oliver J. Merwin, B.S.A.E.

Captain, USAF

March 1989

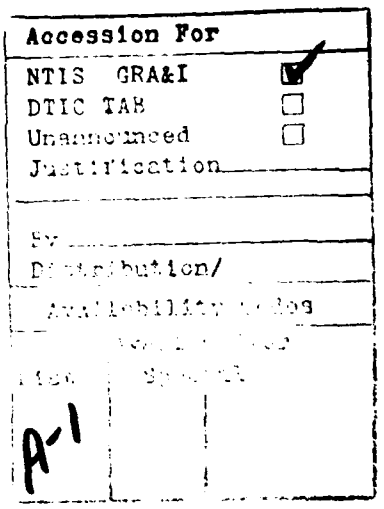

Approved for public release; distribution unlimited

Acknowledgements

I would like to express my sincere appreciation to my committee members, Dr. Constantine Houpis, Dr. Isaac Horowitz, and Dr. John D'Azzo for their instruction, guidance and support. I would also like to thank my classmates Lt. Tom Kobylarz, Capt. Kurt Neumann, and Capt. Darryl Hammond for letting me bounce my ideas off of them. Finally I want to express gratitude to my wife Carmen. Her love, understanding and support through the rigors of AFIT kept me sane and made this thesis possible.

Oliver J. Merwin

Table of Contents

List of Figures

List of Tables

Abstract

The purpose of this study is to validate a design technique for the control of unstable aircraft which are subject to limited control authority. This thesis applies the technique to a realistic aircraft model, instead of the simplified models used in the theoretical development, to produce a pitch rate controller for widely spaced regions of the flight envelope.

First the aircraft is stabilized by feeding back pitch rate. Then an adjustable command limiter is placed in the input path for the stable effective plant. The saturation level of the limiter is adjusted by a second feedback loop feeding back the stabilator deflection angle. An outer feedback loop provides the proper command tracking response when the command limiter is not saturated. The final element is a minor feedback loop around the command limiter to provide a second degree of freedom to ensure the limiter comes out of saturation as quickly as possible.

Simulations for step commands ranging from 1 to 50 degrees/second pitch rate show the design is quite successful. The stabilator does not saturate in a manner which causes instability even when responding to extreme commands. Simulations of a pulse command show that the command limiter unstaurates rapidly and the aircraft responds appropriately to a reduced pitch command even when the stabilator is near the limit.

The technique applies relatively simple linear design tools to the non linear problem of control surface saturation.

CONTROL DESIGN FOR AN UNSTABLE NON-MINIMUM PHASE AIRCRAFT SUBJECT TO CONTROL SURFACE SATURATION

I. Introduction

1.1 Background

In the aggressive search for improved performance of modern fighter aircraft, it is becoming increasingly popular to intentionally design aircraft to be open loop unstable. While this removes the weight and drag burden of basic aircraft stability, it requires a full time, active flight control system to regain the stability the pilot needs to perform the mission (11). It becomes obvious, then, that control surface limits of rate or amplitude cannot be allowed to interfere with the application of the additional control power needed to restabilize the airplane. When an unstable aircraft departs equilibrium, either from pilot command or some external force, it tends to diverge from the original condition. The forces necessary to return the aircraft to equilibrium may require rapid, large control surface deflections. If, at any time, the flight controller demands a deflection that is beyond the physical capabilities of the surface, the effect is the same as if there is no flight controller present at all. Horowitz says that "if feedback is not reasserted soon enough, the instability becomes uncorrectable" (6:1137). Therefore, it becomes essential to design the controller so that the control surface does not saturate.

In 1972, Horowitz and Sidi proposed a control synthesis technique which promised to provide an organized approach to obtain satisfactory system performance despite the uncertainties guaranteed to exist in any physical system (8:677-699). The technique is called Quantitative Feedback Theory (QFT) because of the systematic

and quantitative manner in which feedback compensators are designed. QFT is a methodical technique for designing control systems in the presence of uncertainty of the plant characteristics. QFT admits the impossibility of exactly modeling the real world and assumes only that the limits of the modeling inaccuracy are known. Controllers are synthesized to produce satisfactory performance for any arbitrary plant within the defined limits. The reader is assumed to have a basic knowledge of linear control theory and QFT and these are not extensively explained here. For further information on linear control theory and QFT, the reader should refer to references 2 and 9.

All past AFIT thesis work using Quantitative Feedback Theory has concentrated on applying the technique to as wide a range of plant parameters as possible to explore the limits of the technique. This effort excluded the consideration of either rate of amplitude surface saturation. Plant variation due to control surface failures or battle damage is typical.

A critical assumption in linear control theory is that the device behaves in a linear manner. This implies that the control surfaces will be able to supply any forces deemed necessary by the controller. In other words, the control surface deflection is not limited by either rate or amplitude. This removes a highly nonlinear device from the plant and greatly simplifies the design. Obviously, this is an unreasonable assumption. Although it works quite well for small perturbations about the nominal condition, large commands may require control surface movement beyond its capabilities producing highly non-linear behavior. This is often handled by synthesizing a linear design and then performing simulations. If the simulation shows control surface movement beyond capabilities, the engineer must go back and "tweak" the design to give satisfactory response (10).

In 1983, Horowitz extended QFT to include plants that contain elements which saturate. Horowitz was able to guarantee acceptable system performance even during "hard" saturation and for conditionally stable plants. The control system was first designed as if the non-linear element was not present, using the procedures outlined in 1972. Then an additional feedback loop and feedback compensator were added around the saturating element to provide a rapid return to the linear range of operation. (5:169-187).

In 1984, Horowitz dealt specifically with the problem of rate and amplitude saturation in elements which represent translational power amplifiers such as the hydraulic actuators used on aircraft flight control surfaces. In this particular class of problem, it is often impossible to directly sense the actual quantity which saturates. For instance, it may not be practical to place a deflection rate sensor directly on the control surface. This makes placing the extra feedback loop required by the procedures of 1983 difficult. The procedure is basically unchanged although Horowitz stresses that the feedback must be taken from as near the saturating element as possible. The farther from the element the feedback is taken, the less freedom the designer has to tailor the loop response under saturation. He points out that if the saturating quantity can be sensed directly, the extra degree of freedom afforded by the additional feedback loop gives great flexibility to design the loop performance even under "hard" saturation. This paper also discusses the complexity of having more than one element susceptible to limiting. Horowitz assumes that only one element dominates and is the constraining case. All other saturating components can be ignored (7:1215-1229). Horowitz and Liao considered the added difficulty of an open-loop unstable plant in 1986 (6).

1.2 General Approach

A representative block diagram of a system containing saturating elements is shown in Figure 1.1. The linear dynamics of the basic aircraft is represented by block P. The linear dynamics of the control surface actuator is shown by block A. The actuator also contains one or more saturating elements shown by block N1. The plant is first stabilized with a minor feedback loop utilizing the compensators G_1 and H_1. This results in a stable effective plant P_e.

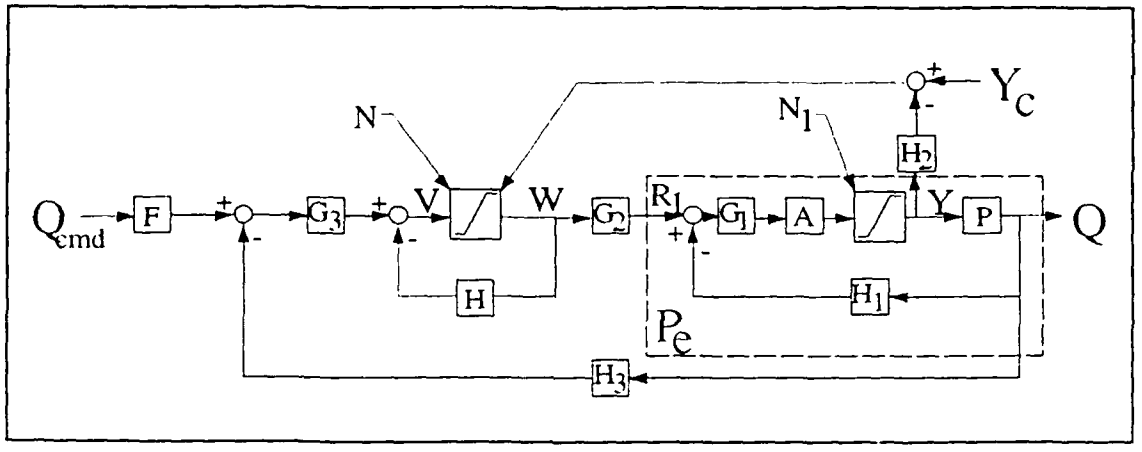

Figure 1.1. Basic Block Diagram.

Assuming that the subsequent design is satisfactory and the control surface never saturates, this guarantees that the commands to the effective plant will always "see" a stable system. Then another saturation element, N, is deliberately added in the input path. This new element reduces the magnitude of the input to the effective plant P_e as N_1 approaches saturation. This reduction ensures that the input does not aggravate the unstable tendencies of the plant beyond the stabilizing capability of the limited control surface. The compensators G_2 and H_2 and the input Y_c govern the saturation level of N based on Y where Y is the control surface deflection and Y_c is the maximum allowable value of Y.

A minor feedback loop is placed around the new saturation element to achieve the desired loop response during saturation of the input limiter. The compensator H, together with G_3 and H_3, adjust the open loop characteristics of the final system and guarantee that N remains saturated for as short a time as possible. A prefilter F is added to adjust the closed loop characteristics. This is now essentially the same process as was developed in 1983. The only factor not specifically accounted for is unwanted disturbance in the plant stabilization loop. An example might be wind gust effects. Such a disturbance would look like an input to the loop which cannot be limited by the newly introduced element. Horowitz and Liao say that if the disturbance is large enough, the system will unavoidably be driven into saturation and instability. However, it may be possible to design the loop gain such that a certain tolerance to disturbance is achieved (6:1137-1146).

The deflection angle and rate of the control surface must be continually monitored (or discretely sampled if the sample rate is high enough) to determine when it is approaching its limit. This is done by placing sensors on the control surface or on the mechanical linkages actuating the surface to measure the quantities of interest. The nearer the sensor is to the actual saturating quantity, the better the control system is able to handle the problem. If any uncertain plant elements are between the surface and the sensor, the more stringent the control loop will have to be. This is because the loop design must be based upon the worst case of the uncertain elements. But by measuring the output of the saturating element, an additional feedback loop "can be used to control to some extent the system behavior under saturation" (6:1137).

1.3 Objective

The purpose of this research is to verify that the apriori knowledge of the nonlinearities of an aircraft system can be used in a QFT design of a practical flight con-

trol system. This thesis applies QFT techniques to an actual aircraft flight control problem instead of the simplified models used in the theoretical development. The aircraft to be used is the STOL/Maneuver Technology Demonstrator (SMTD). The SMTD is a modified McDonnell Aircraft Company F-15.

1.4 Scope

The actual aircraft model including the actual actuator model is used. Stabilator amplitude and rate limits are incorporated into the design. Although the actual aircraft has canards, flaps, and thrust vectoring in addition to the stabilator for longitudinal control, the design is treated, in theis thesis, as a single-input single-output problem in order to limit the scope of the research. The stabilator is used to control pitch rate. While this simplifies the details of the design, it forces the stabilator to do double duty as the only stabilization device and also to provide the required tracking response.

1.5 Assumptions

1. The aircraft model is linearized about the equilibrium (trim) flight condition and the perturbations about the trim condition do not invalidate the model.

2. The only sources of non-linearities are in the stabilator actuator and the command limiter in the control system.

3. The mass of the aircraft remains constant.

4. The aircraft is a rigid body.

5. The lateral and longitudinal modes are independent of each other for these trim conditions.

6. The earth's surface is flat and inertially fixed.

7. The atmosphere is fixed to the earth and homogeneous in the vicinity of each trim point.

8. Aircraft pitch rate is measurable and can be fed back for stabilization and tracking control.

9. Stabilator deflection angle is measurable and can be fed back for command limiting.

10. The stabilator deflection angle sensor operates very quickly relative to the rest of the system and its dynamics can be neglected.

11. Sensor noise is negligible.

1.6 Units and Transfer Functions

Unless otherwise noted, the units used in this thesis are feet, pounds, seconds, and radians.

Transfer functions are displayed in the following format:

$$TF = \frac{k(a)}{s(\omega_n, \zeta)} \tag{1.1}$$

where

$$(a) \quad \text{and} \quad (\omega_n, \zeta) \tag{1.2}$$

indicate factors of the form

$$(s - a) \quad \text{and} \quad [s^2 + 2(\zeta\omega_n)s + (\omega_n)^2] \tag{1.3}$$

respectively. Left half plane roots are indicated by negative values of a and positive values of ζ.

1.7 Presentation

Chapter II presents the aircraft model and the desired performance specifications. Chapter III discusses the stabilization control loop. Chapter IV presents the design of the tracking control loop and the design of the compensator around the command limiter. Design of the saturation control loop is discussed in Chapter V. Simulation results are shown in Chapter VI, and Chapter VII presents conclusions and recommendations.

II. Aircraft Model and Specifications

2.1 Introduction

This chapter defines the linear dynamics model used in the design. Transfer functions representing pitch rate output due to stabilator command input are derived from the state space representation of the aircraft at each of six flight conditions.

Figure 2.1 shows the relative position of each condition in the flight envelope.

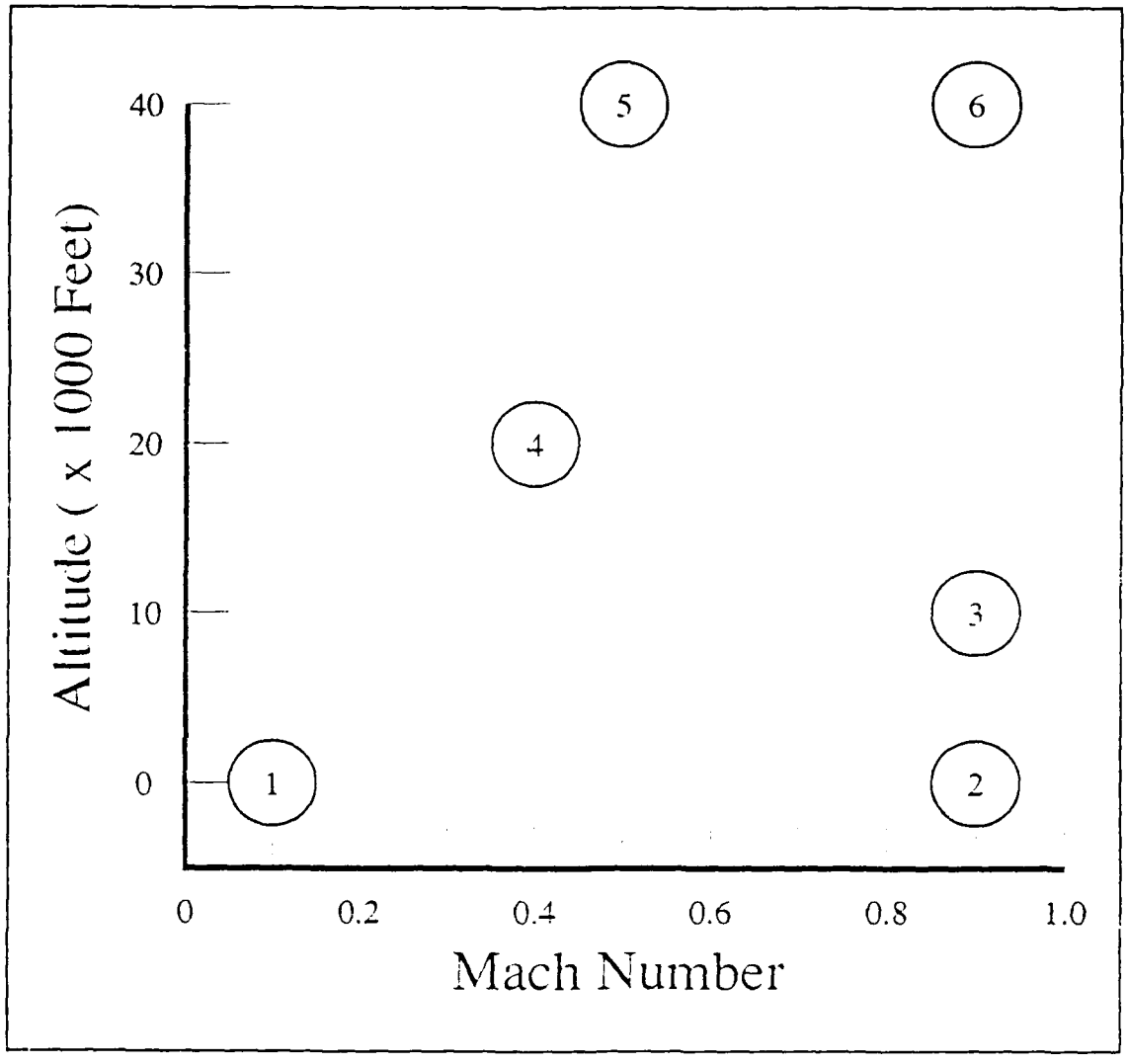

Figure 2.1. Flight Envelope

2.2 Basic Aircraft State Equations

Using the pertinent aerodynamic data, listed in Table 2.1 for the six flight conditions, the general state equations for longitudinal motion of the SMTD in stability axes are (1)

$$\begin{bmatrix} \dot{u} \\ \dot{q} \\ \dot{\theta} \\ \dot{\alpha} \end{bmatrix} = \begin{bmatrix} X_u & X_q & -g\cos\theta_1 & X_\alpha \\ M_u & M_q & 0 & M_\alpha \\ 0 & 1 & 0 & 0 \\ \dfrac{Z_u}{U_1} & \dfrac{Z_q + U_1}{U_1} & \dfrac{-g\sin\theta_1}{U_1} & \dfrac{Z_\alpha}{U_1} \end{bmatrix} \begin{bmatrix} u \\ q \\ \theta \\ \alpha \end{bmatrix} + \begin{bmatrix} X_\delta \\ M_\delta \\ 0 \\ \dfrac{Z_\delta}{U_1} \end{bmatrix} \delta_{STAB} \qquad (2.1)$$

where

u = Forward Velocity Perturbation (Feet/Second)

q = Pitch Rate Perturbation (Radians/Second)

θ = Pitch Angle Perturbation (Radians)

α = Angle of Attack Perturbation (Radians)

$\dot{x}$ = Indicates First Time Derivative of x

X_y = Longitudinal Force Stability Derivative with respect to State y

M_y = Pitching Moment Stability Derivative

Z_y = Vertical Force Stability Derivative

θ_1 = Initial Pitch Angle (Radians)

g = Gravitational Constant

Table 2.1. Aerodynamic Data

	Flight Condition					
	1	2	3	4	5	6
Altitude	0	0	10000	20000	40000	40000
Mach No.	0.2	0.9	0.9	0.4	0.5	0.9
U_1	222.73	1002.34	831.22	302.00	239.56	431.22
X_u	-0.0867	-0.0563	-0.0422	-0.0205	-0.0272	-0.0118
M_u	0.00168	0.00336	0.00243	0.000588	0.000795	-0.00249
Z_u	-0.3988	-0.1508	-0.1464	-0.2341	-0.1873	-0.1489
X_q	0	0	0	0	0	0
M_q	-0.5409	-2.319	-1.687	-0.5240	-0.2988	-0.5192
Z_q	0	0	0	0	0	0
X_α	-19.739	-27.217	-15.255	-14.5088	-20.8079	1.85032
M_α	1.4021	30.4289	20.448	1.81577	1.3548	4.82617
Z_α	-105.788	-2886.1	-2005.5	-244.43	-139.08	-555.08
X_δ	1.932	-9.876	-8.583	0.879	3.065	0.818
M_δ	1.002	20.064	14.202	1.828	1.079	4.683
Z_δ	-9.487	-67.397	-51.836	-9.069	-11.721	-18.209
θ_1	0.245	0.00853	0.0136	0.1312	0.1985	0.0573

Table 2.2 lists the gains, poles, and zeros of each of the transfer functions for the listed flight conditions. The tabulated data refers to a transfer function of the form:

$$P = \frac{Ks(s-z_1)(s-z_2)}{(s-p_1)(s-p_2)(s-p_3)(s-p_4)} \tag{2.2}$$

Table 2.2. Basic Aircraft Transfer Functions.

	Numerator			Denominator			
Trim Point	K	Z_1	Z_2	P_1	P_2	P_3	P_4
1	1.00	-0.51	0.0024	-1.74	0.67	-0.013+0.21i	-0.013-0.21i
2	20.06	-2.77	-0.054	-8.12	2.92	-0.11	0.063
3	14.20	-2.26	-0.041	-6.55	2.51	-0.085	0.051
4	1.83	-0.78	-0.0056	-2.03	0.69	-0.034+0.14i	-0.034-0.14i
5	1.08	-0.54	0.0055	-1.63	0.72	0.011+0.12i	0.011-0.12i
6	4.68	-1.15	-0.012	-3.08	1.38	-0.007+0.12i	-0.007-0.12i

2.3 Actuator Model

Figure 2.2 shows a block diagram of the actuator model A used in this design. The stabilator is subject to limits of +15 to -29 degrees deflection, shown by element N_1, and ± 46 degrees/second deflection rate, shown by N_2.

The stabilator actuator has the following dynamic model:

$$A = \frac{Y}{Y_{cmd}} = \frac{(31.27)(231.3)^2}{(s+31.27)[s^2+2(0.618)(231.3)s+(231.3)^2]} \tag{2.3}$$

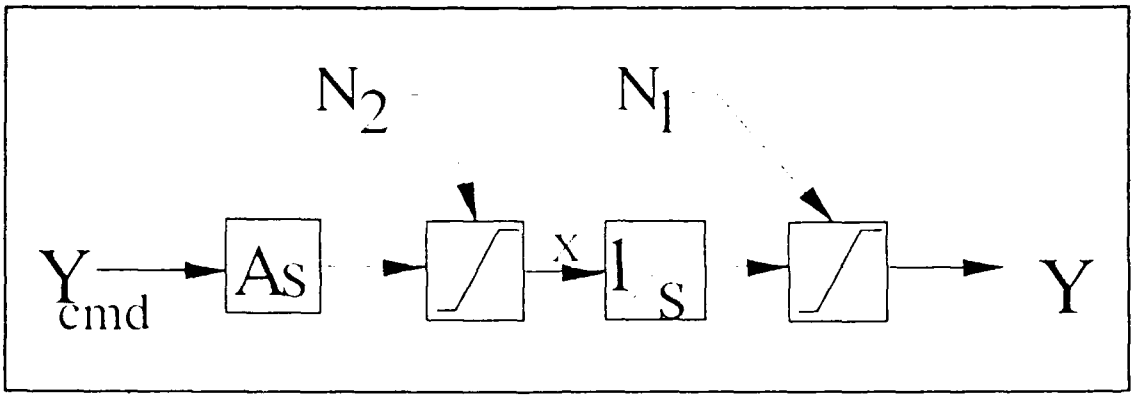

Figure 2.2. Actuator Block Diagram

2.4 Specifications

A second order pitch rate response is desired for the overall system shown in Figure 1.1. The preferred equivalent transfer function is:

$$\frac{Q}{Q_{cmd}} = \frac{2^2}{s^2 + 2(0.8)(2)s + 2^2} \tag{2.4}$$

The aircraft should follow this model from 0.1 radians/second (r/s) to 20 r/s as a minimum. A Type 1 open loop transfer function is also desired to produce zero steady state error.

2.5 Observations

Figure 2.3 shows a portion of the arithmetic complex plane showing the locations of the dominant poles and zeros of the basic plant transfer function for each of the six cases. In examining the transfer functions for the basic airplane, it should be noted that cases 1 and 5 each have one right half plane (RHP) zero. This is a highly unusual characteristic for the pitch rate transfer function of a realistic airplane and casts some suspicion on the validity of the model. Another unusual feature is that none of the six cases have an oscillatory short period mode.

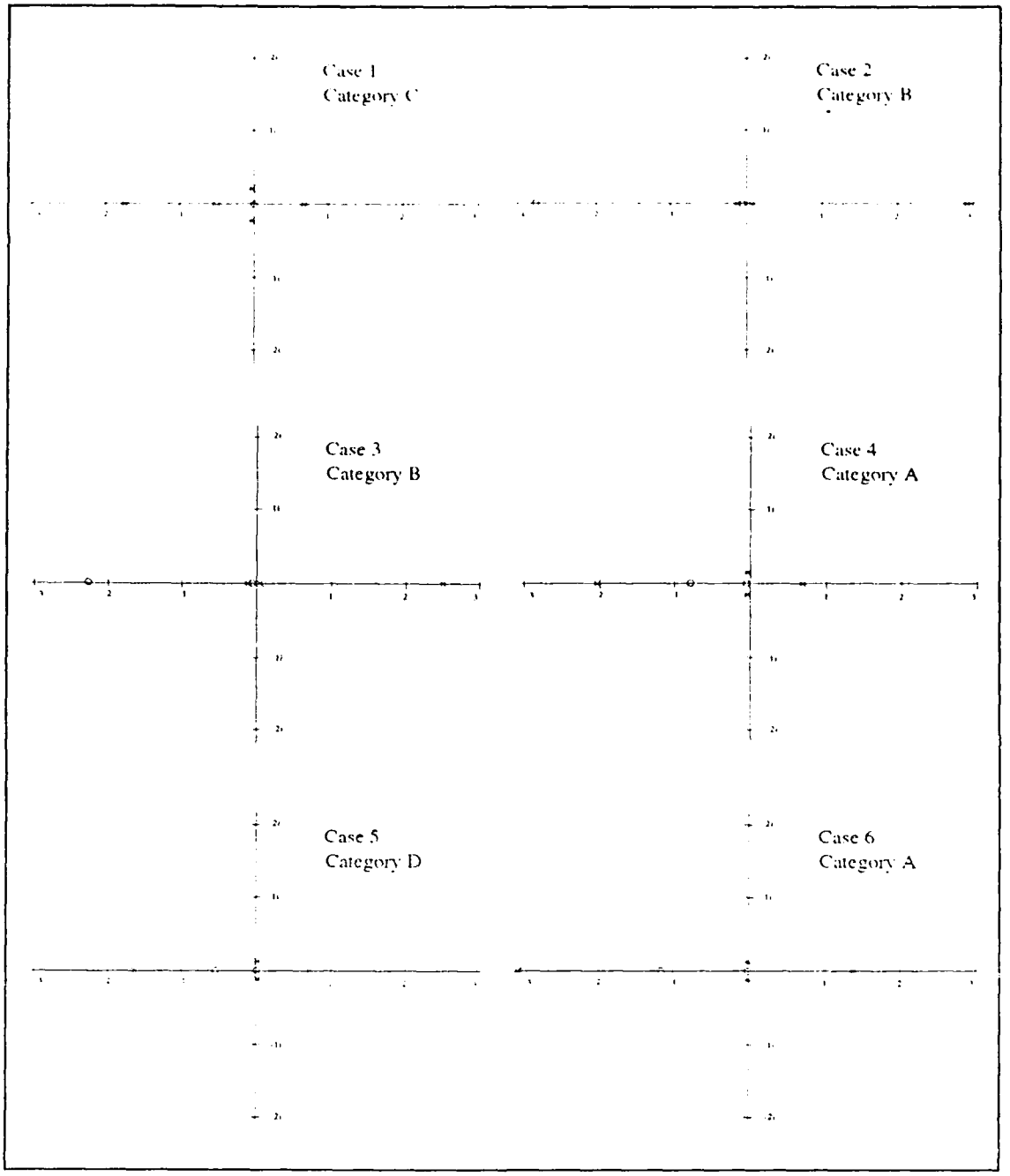

Figure 2.3. Dominant Root Locations for the Basic Plants

Notice also that the transfer functions fall into four basic categories which roughly correspond to changes in dynamic pressure. The first category is characterized by transfer functions with one RHP pole and no RHP zeros. Cases 4 and 6 are

in this category. Case 4 is at medium speed and altitude while case 6 is at high speed and high altitude, giving medium dynamic pressure in each case. Cases 2 and 3 are in a second category with two RHP poles and no RHP zeros. These cases occur at low altitude and high speed, producing a high dynamic pressure. Cases 1 and 5 are at a fairly low speed and have low dynamic pressures and represent the third and fourth categories respectively. The third category has one RHP pole and one RHP zero. The fourth category has 3 RHP poles and one RHP zero. Table 2.3 summarizes the four categories represented in this problem.

Table 2.3. Basic Transfer Function Categories

Category	# RHP Zeros	# RHP Poles	Flight Condition
A	0	1	4,6
B	0	2	2,3
C	1	1	1
D	1	3	5

The various categories correspond to the various possible combinations of RHP poles and zeros. Each of the transfer functions has two zeros and four poles (excluding the zero at the origin). This yields 15 possible combinations and only four of these combinations are represented by the given transfer functions.

Cases 2 and 3 each have two RHP poles. One is quite near the origin and the other is in the range of 2.5 - 3.0. Cases 4 and 6 have a single RHP pole approximately at 1.0. Cases 1 and 5 have a RHP pole at about 0.7 and also a RHP zero

quite near the origin. Additionally, the phugoid mode of case 5 is unstable. The large differences between the six models pose a severe challenge to the design process.

2.6 Frequency Response Templates

In order to apply QFT to the problem, the plant variations must be characterized as a region of uncertainty, called a template, on the Nichols chart. Each template should be sub-divided into regions corresponding to the categories defined in Table 2.3. Assuming the aircraft dynamics can be represented by a set of linear time invariant (LTI) transfer functions, region A contains the frequency response mapping of all Category A transfer functions (Cases 4 and 6) and Region B encloses the frequency responses of all Category B transfer functions (Cases 2 and 3) and so on, as illustrated in Figure 2.4.

Awareness of these distinct regions is vital because the dynamics do not necessarily vary smoothly between the regions. For instance, if the phugoid roots of Case 1, which are in the LHP, are moved slightly to the right in the complex plane, they move into the RHP (like in Case 5). This causes an abrupt -360° phase jump at very low frequency. The regions are not mutually exclusive and may overlap. The dynamics of the aircraft are assumed to change fairly smoothly within each region. Unfortunately, six cases are hardly sufficient to fully characterize even one region. Many more flight conditions would need to be studied to be able to accurately characterize the frequency response of all four regions.

Figure 2.5 shows the relative positions on the Nichols chart of the frequency response of each of the six cases for four representative frequencies. For the purposes of this study, the templates are assumed to be bounded by straight lines on the Nichols chart as shown. Appendix A lists templates for frequencies from 0.0001 to

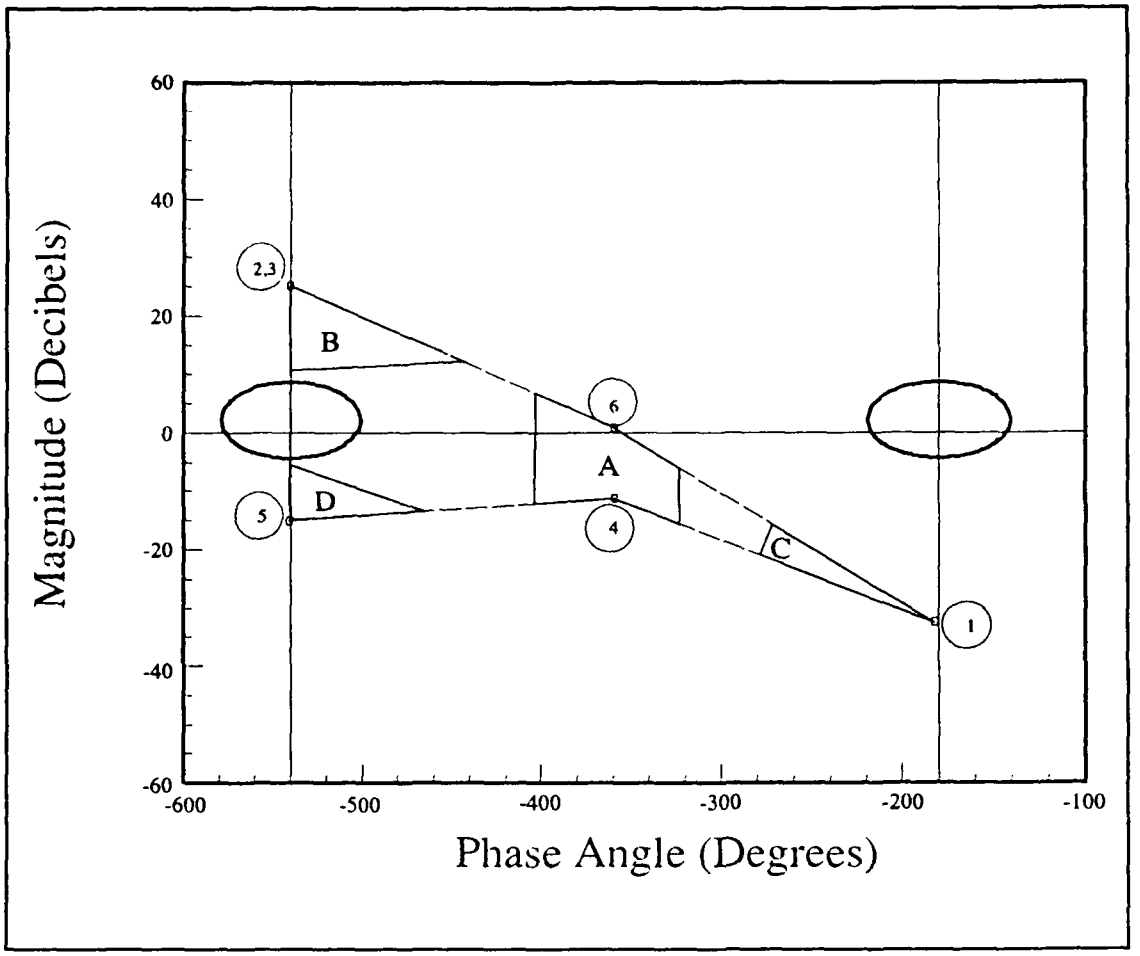

Figure 2.4. Example Template Regions

562 radians/second. Notice that the templates are 360 degrees wide at very low frequency. This is due to the fact that Category C plants, which have one RHP pole and one RHP zero, produce no phase shift at very low frequency, while Category B and D plants, which each have two more RHP poles than RHP zeros, produce -360 degrees of phase shift at very low frequency. As the frequency increases, the templates narrow until, in the limit as frequency approaches ∞, the templates become a vertical line 26 dB tall.

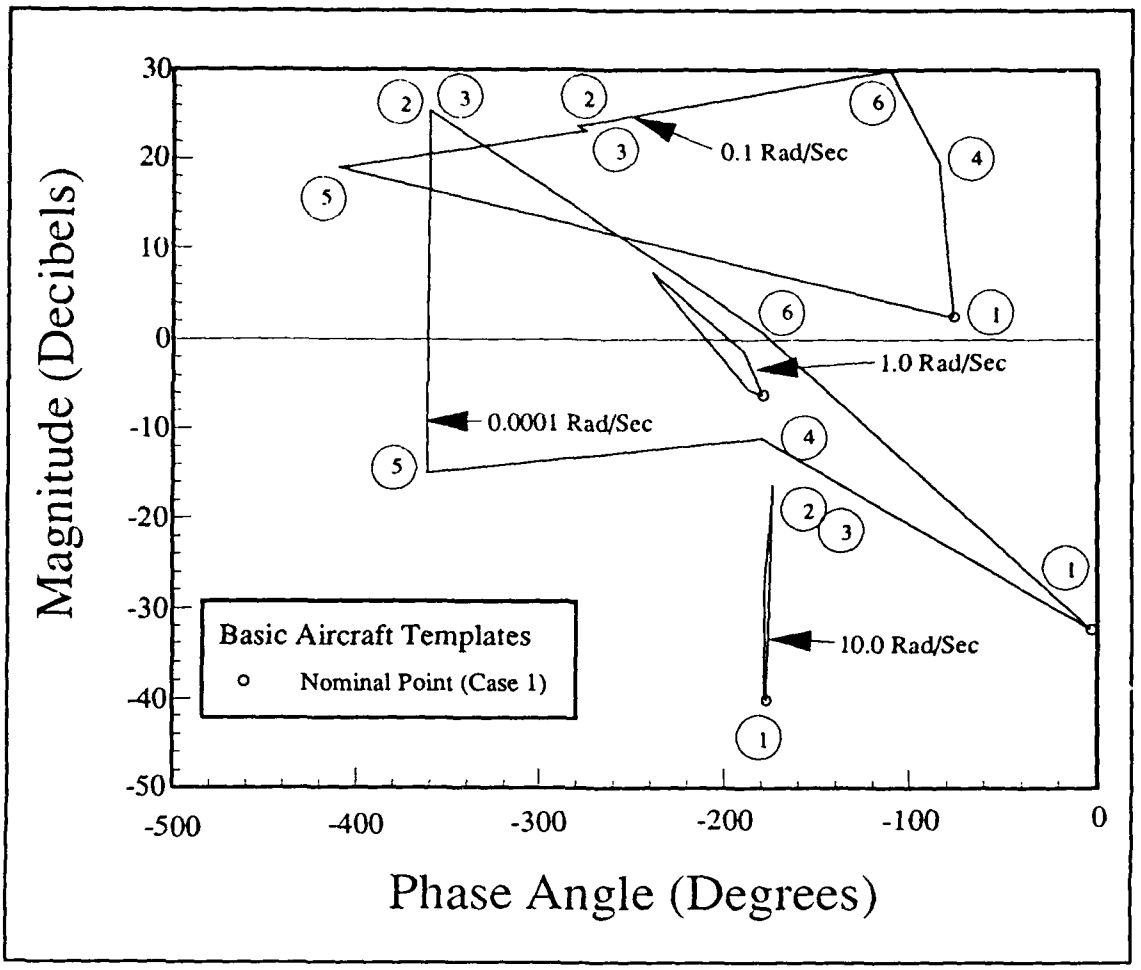

Figure 2.5. Basic Plant Templates

III. Stabilization

3.1 QFT Compensator Requirements

3.1.1 Design Philosophy. Figure 3.1 shows a block diagram representing the possible locations of compensators to be placed in the stabilization minor feedback loop shown in Figure 1.1. While the cascade compensator G_1 and the feedback compensator H_1 of Figure 3.1 each have effects on the closed loop response, the characteristic equation of Q/R_1 is $1+G_1H_1AP$ regardless of the position of the compensator or how it is broken up around the loop. Therefore, only the product G_1H_1 need be considered for stability purposes.

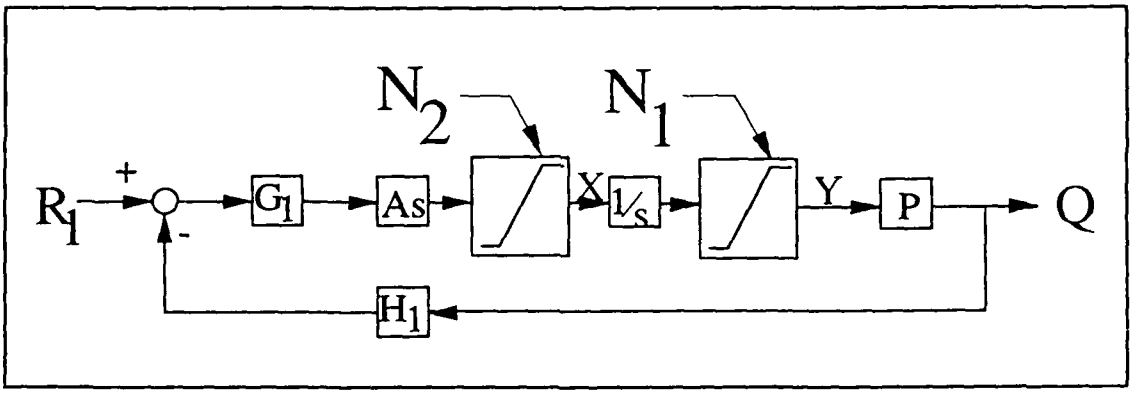

Figure 3.1. Stabilization Control Loop Block Diagram

3.1.2 Nyquist Stability Analysis. In order to determine the form of a single compensator to stabilize all four categories, it is first necessary to examine the various combinations of RHP poles and zeroes in the separate plants. Categories C and D (Cases 1 and 5 respectively) each have one RHP pole on the real axis and one RHP zero. If negative feedback and a compensator with all left half plane (LHP) poles and zeros and positive gain is used, a root of the characteristic equation must lie on the real axis between the pole and the zero in the right half plane. This will, for all

values of positive gain, produce a pole of the closed loop transfer function in the right half plane. Therefore, a compensator with negative gain is required if the compensator has only LHP poles and zeros.

The Nyquist plot is useful for determining stability for a proposed compensator form. For example, consider the simple unity feedback uncompensated system shown in Figure 3.2(a). The Nyquist stability criterion requires that, for no RHP roots of the characteristic equation, there must be exactly one counter-clockwise encirclement of the -1 point for each open loop RHP pole as frequency ranges from $-\infty$ to $+\infty$ (2:287).

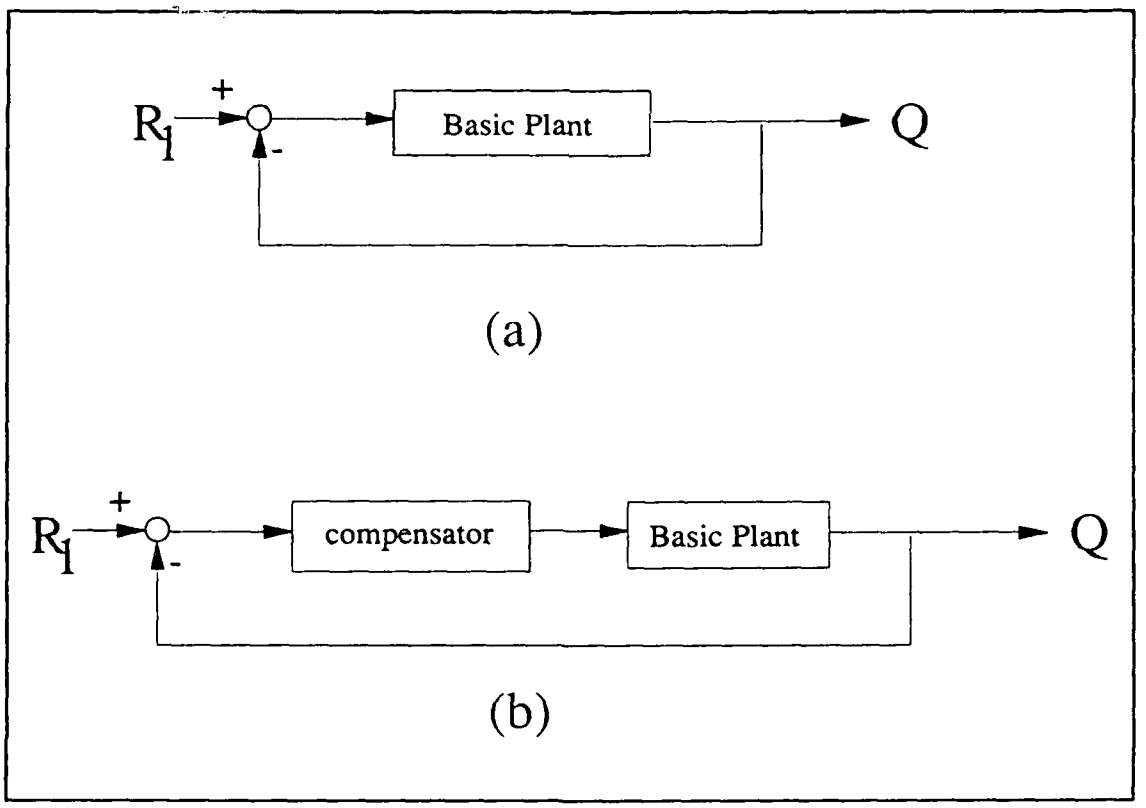

Figure 3.2. Basic Feedback System (a) Uncompensated
(b) with Cascade Compensator

The unity feedback system of Figure 3.2(a) might not produce a stable closed loop or may have undesirable open loop characteristics. To correct this, a compensator may be added to the loop as in Figure 3.2(b).

This compensator might have one or more poles or zeros in the RHP and its gain may be positive or negative. Figure 3.3 shows that Categories B (Cases 2 and 3) and C (Case 1) can each be stabilized by a compensator with negative gain and all poles in the LHP. Category C shows one half encirclement (one full encirclement as frequency goes from $-\infty$ to ∞) and must have a gain greater than 1.0 at zero frequency. Category B shows one encirclement and must have a gain less than 1.0 at zero frequency. Unfortunately, at zero frequency, Case 2 (Category B) actually has a larger gain than Case 1 (Category C) as shown in the low frequency templates. So a compensator with all LHP poles cannot stabilize Categories B and C simultaneously.

An additional RHP pole (provided by the compensator) changes this situation. Figures 3.4 and 3.5 show that with positive gain, Category C produces the one required encirclement, Category B gives one and one half encirclements, Category A shows one encirclement, Category D shows two, and the relative gains now agree with the actual plants. Figure 3.6 shows the equivalent Nichols plots. The loop transmission, G_1H_1AP, must be designed so that, at zero frequency, ALL Category B plants have gains greater than 1.0 and ALL Category C and D plants must have gains less than 1.0. Category A plants, since they begin at -360 degrees at zero frequency, may begin at any gain as long as the gain is greater than 1.0 at -180 degrees.

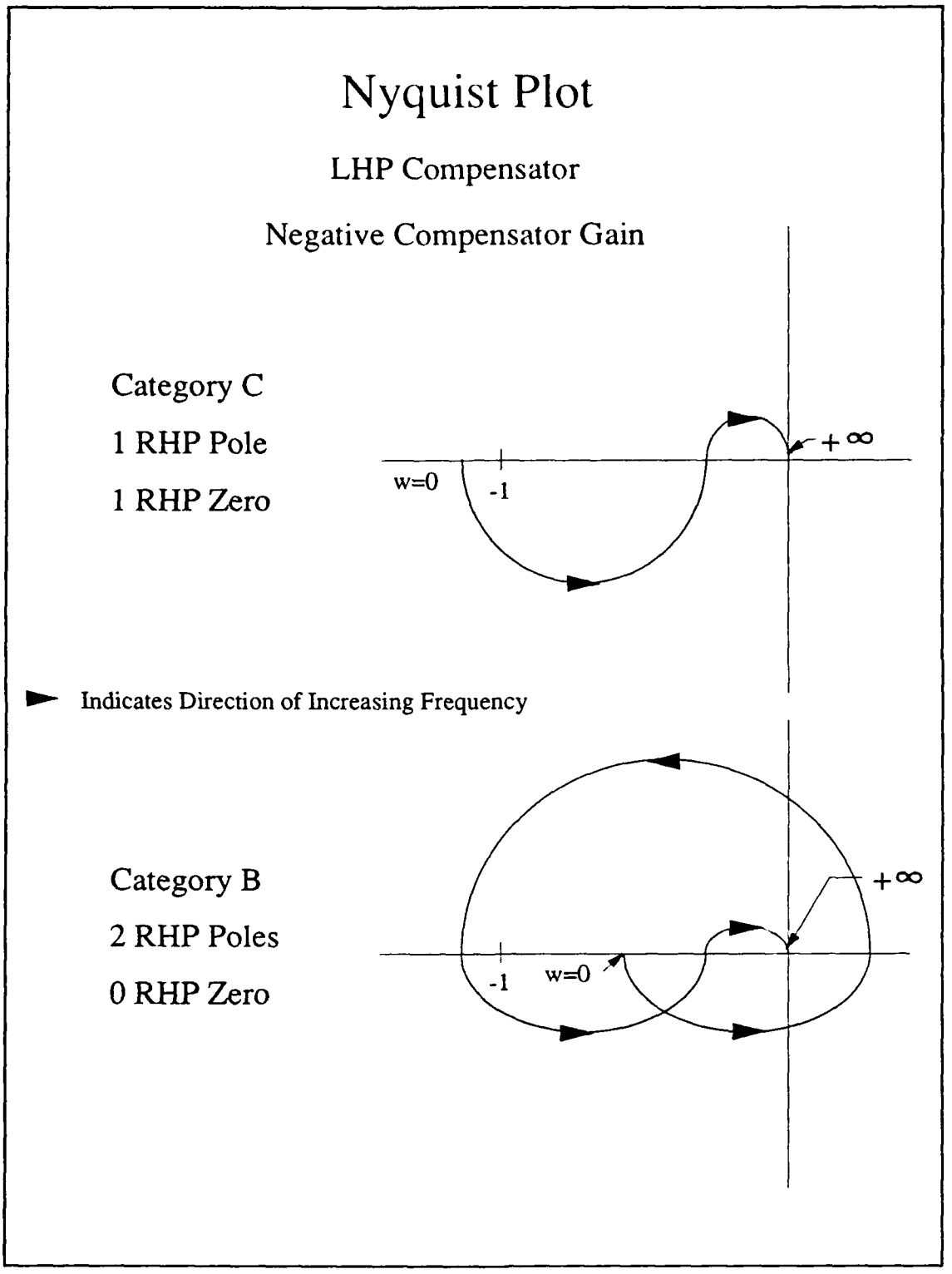

Figure 3.3. Nyquist Plot for Category B and C Plants with a Stable Compensator (Positive Frequency Portion)

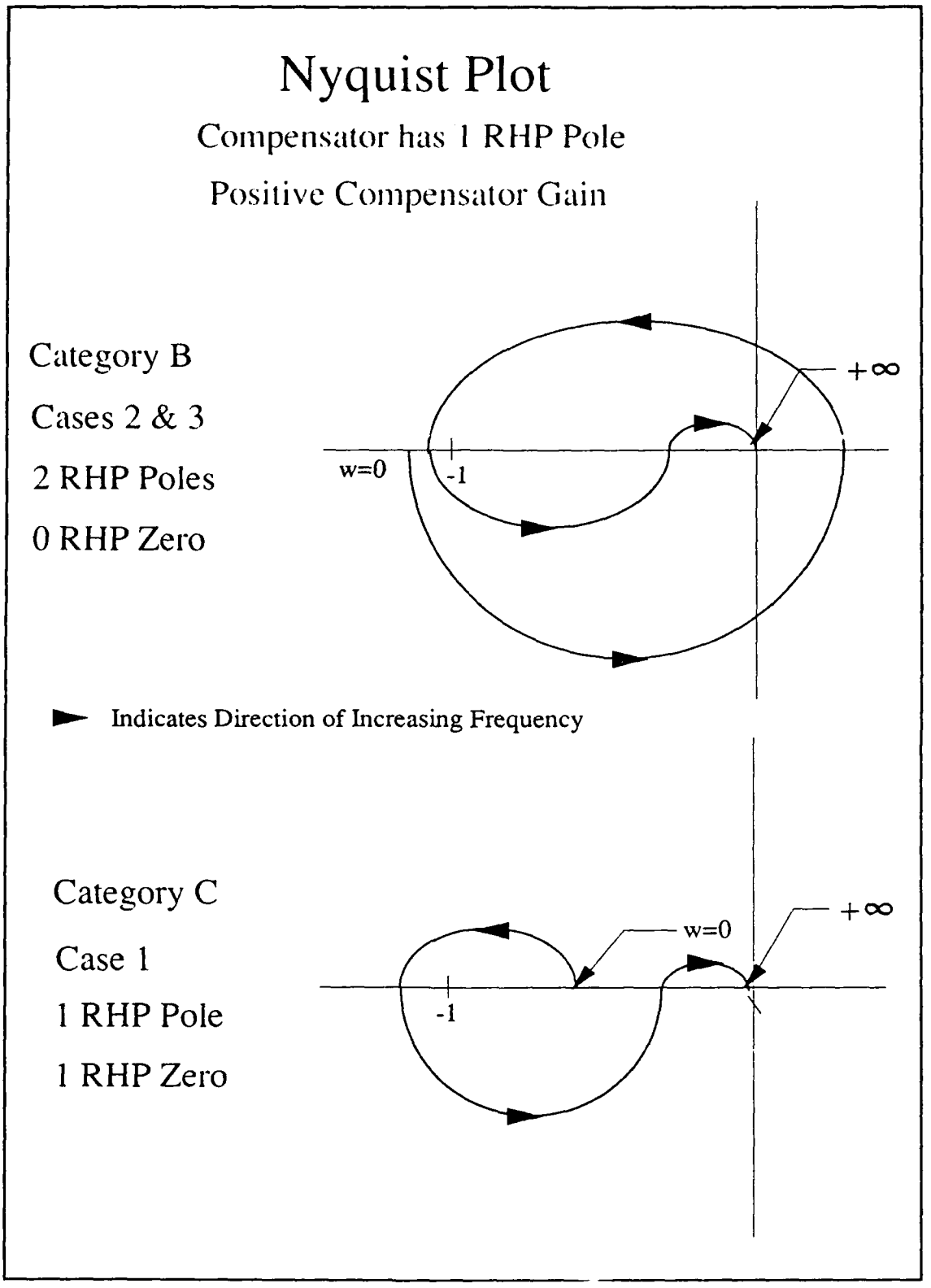

Figure 3.4. Nyquist Plot for Cat. B and C Plants with 1 Extra RHP Pole
(Positive Frequency Portion)

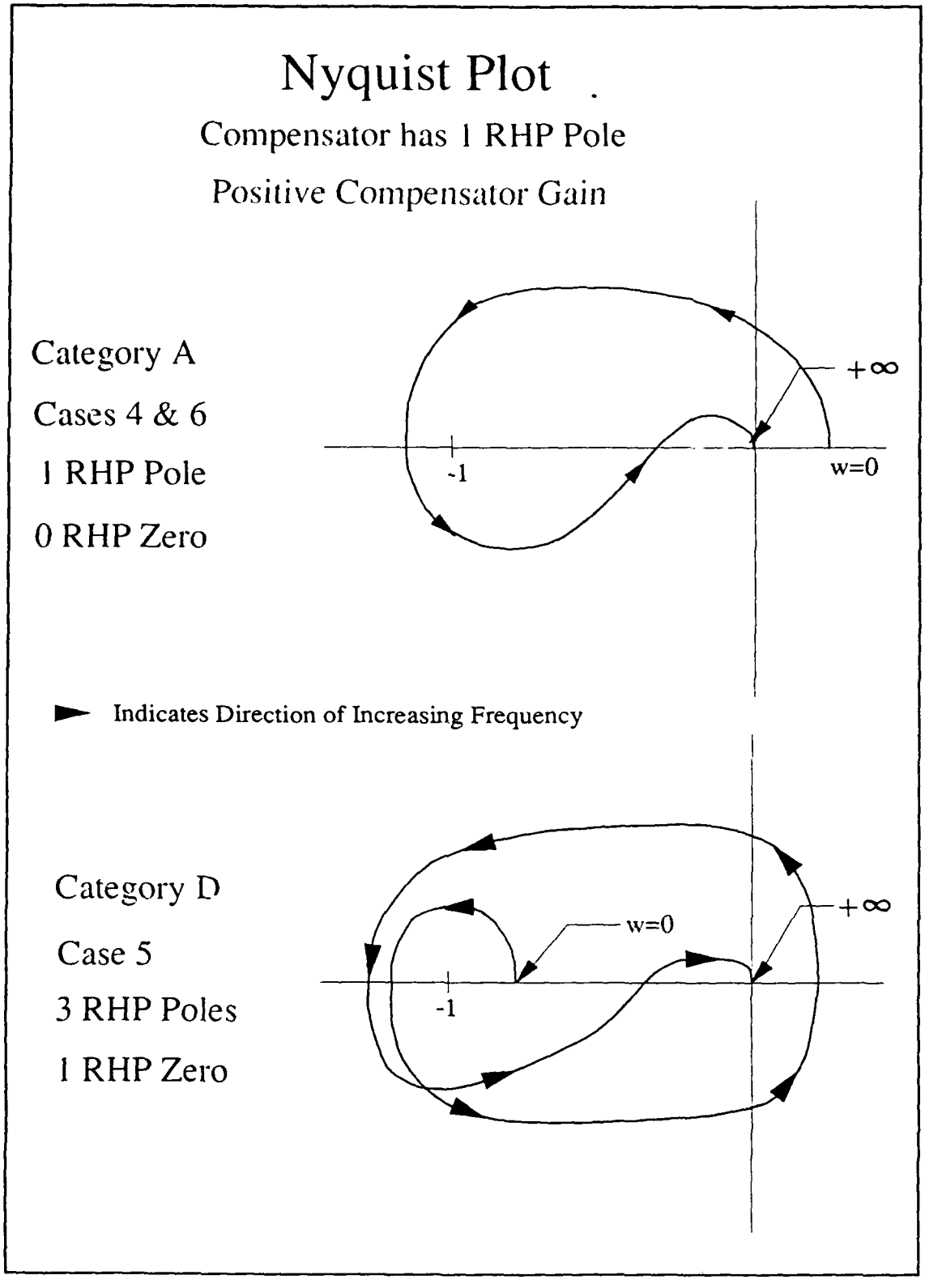

Figure 3.5. Nyquist Plot for Cat. A and D Plants with 1 Extra RHP Pole
(Positive Frequency Portion)

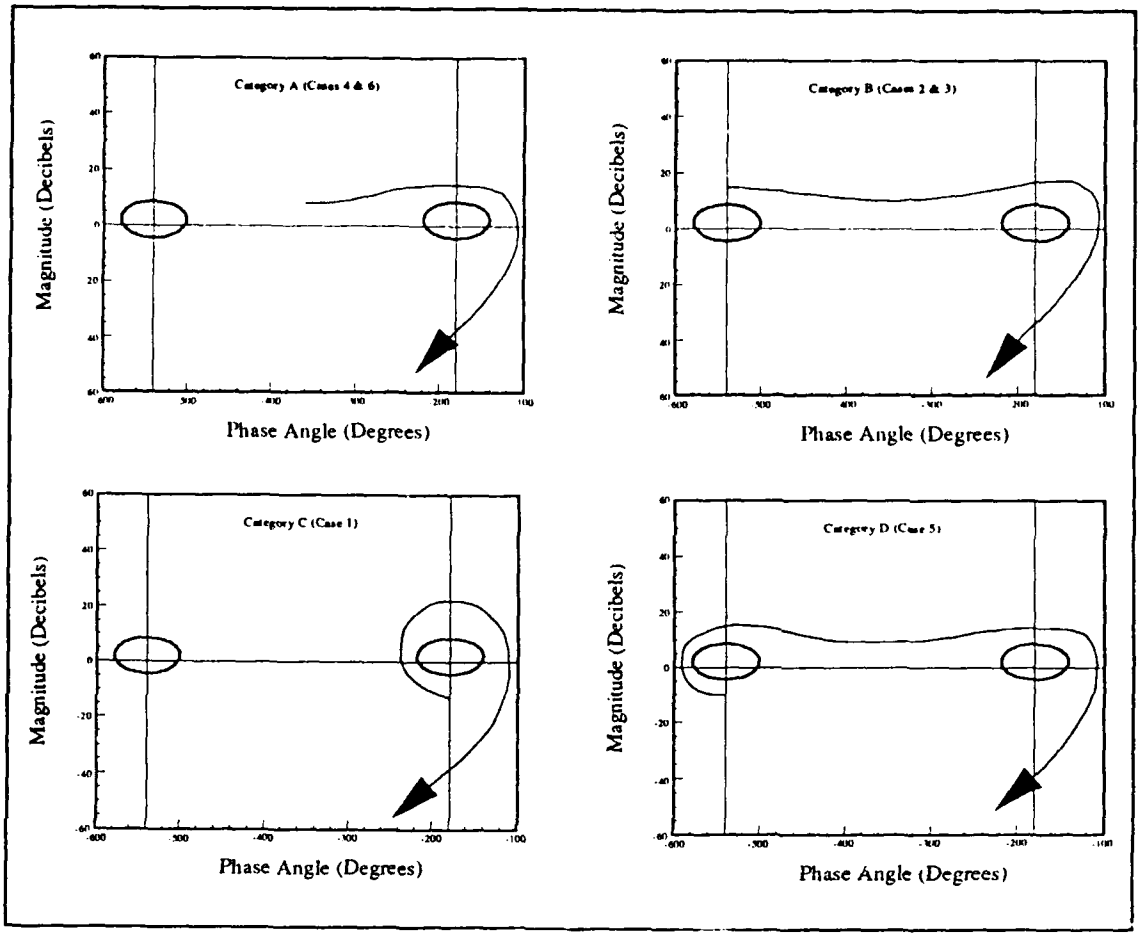

Figure 3.6. Representative Nichols Plots for each Category

3.1.3 Nichols Chart Stability Bounds Now, the stability bounds for the system of Figure 3.2(b) must be plotted on the Nichols chart. Case 1 is chosen as nominal because its phase will vary the least with frequency and because it is at the bottom of each template. The purpose of this feedback loop is purely stability and the only criteria for bound generation is that none of the separate regions of a template may penetrate the chosen closed loop magnitude (M_m) contour. It must also be remembered that the pattern of M_m contours repeats every 360°.

Consider the template for very low frequency in Figure 2.4 (which is repeated here) with the Regions A, B, C, and D as shown. Attempting to place the template in

such a manner that the magnitude of Region B is greater than 0 dB, the magnitude of Region D is less than 0 dB, and Region C has a phase of -180° (or any odd multiple of 180°), results in enclosing about half of the M_m contour at -540° with the template.

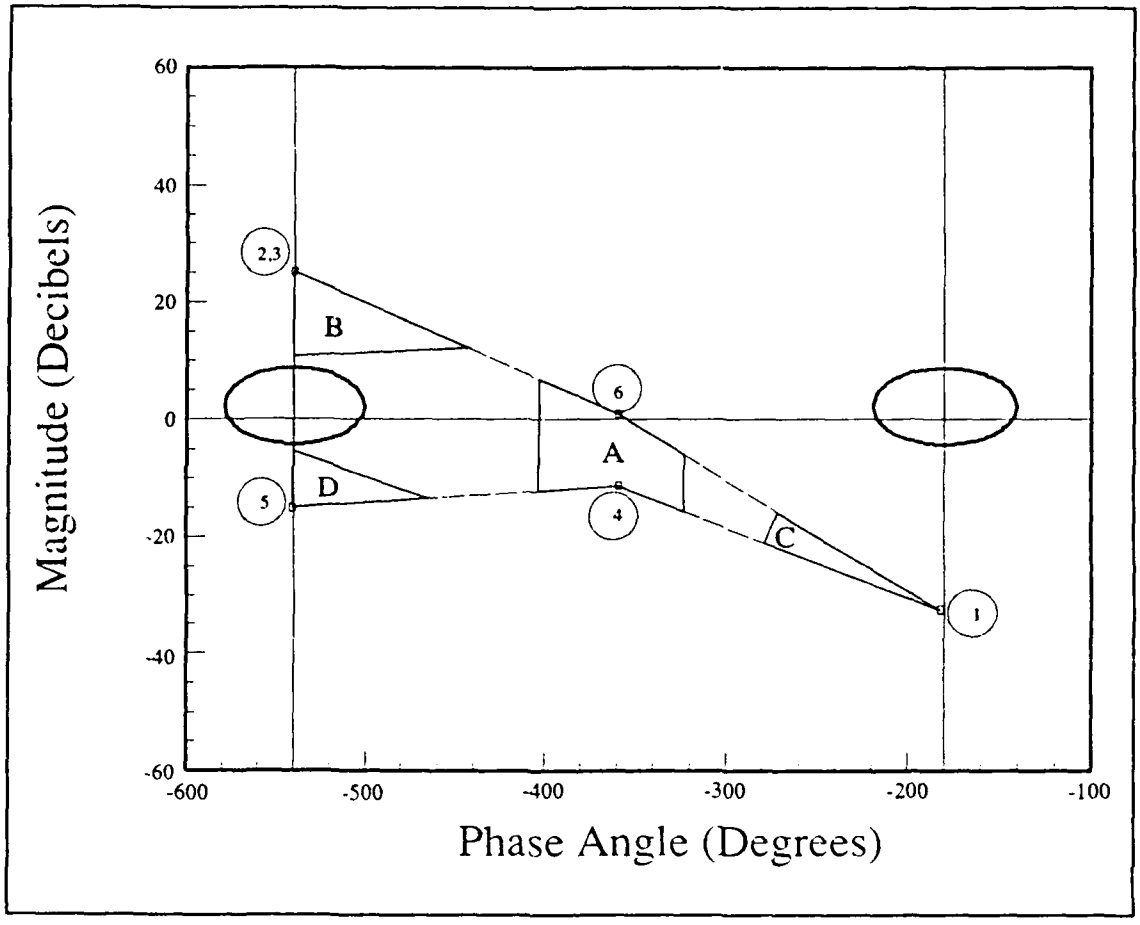

Figure 2.4. Example Template Regions

Also consider the movement of the poles and zeros as the aircraft moves from Case 4 (Region A), which has 1 real RHP pole, to Case 2 (Region B), which has 2 real RHP poles. To make this transition, one of the LHP poles from Case 4 must move into the RHP. Therefore, it is reasonable to expect at least one plant in the total range of uncertainty to have a pole at the origin. At zero frequency, this plant

will have infinite gain. This implies that, at very low frequency, Regions A and B actually extend upwards farther than Figure 2.4 shows. The transition produces a -180° phase "jump" at infinite gain. So far, this does not cause a problem because Section 3.1.2 does not place an upper limit on the steady state gain of Category A or B plants.

Consider the movement from Region A (Case 4) to Region C (Case 1), which has one real RHP pole and one real RHP zero. In this case one of the LHP zeros of the Region A plant must move into the RHP. This gives a probable plant with a zero at the origin which has zero steady state gain. Thus, at very low frequency, Regions A and C in Figure 2.4 probably actually extend much farther down than shown. The transition produces a +180° phase "jump" at zero gain. Again this is not a problem since Section 3.1.2 does not place a lower limit on Category A or C plants.

Now consider the movement from Region C (Case 1) to Region D (Case 5). For this transition, the pair of lightly damped LHP complex poles of the Region C plant must move into the RHP. Presumably, during the transition, a case will exist which has a pair of purely imaginary poles. This does not necessarily affect the steady state gain (since the poles are not at the origin). However, at some non zero frequency, an infinite gain can be expected. The effect of the transition, at zero frequency, is to produce a -360° "jump" in the phase with little change in gain. The frequency response of the hypothesized "transition" plant places it in Region C at very low frequency. As frequency increases past the imaginary pole value the gain increases to infinity (decreasing again past the pole) and the phase "jumps" 180° to the left on the Nichols chart.

At zero frequency, the template is probably infinitely tall. Region A probably extends from $-\infty$ dBs to $+\infty$ dBs. Region B probably extends from some non zero gain to $+\infty$ dBs and Regions C and D probably extend from $-\infty$ dBs to some finite gain. At some finite frequency greater than zero, Region C probably becomes 180°

wide and infinitely tall with a lower bound at some non-zero gain. Thus, it is possible for the plant to transition smoothly from any region to any other region (although, not necessarily directly) without moving outside the template or violating the low frequency gain requirements of Section 3.1.2.

Because, as flight conditions change, the particular plant which represents the current condition of the airplane "jumps" from region to region (caused by poles or zeros moving across the imaginary axis), it is only necessary that none of the separate regions penetrate the M_m contours. The portions of the templates between the regions need not be considered because none of the plants actually have frequency responses in this area.

Note that if Region B overlaps Region D at very low frequency, stabilization of all cases will not be possible with a single compensator because the conditions specified in Section 3.1.2 cannot be met. Indeed, there must be a gap between these regions at least as tall as the chosen M_m contour. This is only critical at very low frequency when the templates are nearly 360° wide. The transition between Regions C and D (Cases 1 and 5) is also troublesome. The size of the template may make loop shaping difficult. Note that the aircraft does not necessarily transition form region to region in the manner described. The actual aircraft may go through far more complicated transitions (possibly including other plant categories) which may invalidate the design. Many more flight condition need to be studied to accurately characterize the transition process. Assuming that the given six conditions adequately describe the behavior of the aircraft and that none of the transitions adversely affect stability, the design can proceed.

Each bound is a closed contour surrounding the 0 dB/-180° point on the Nichols Chart and represents a forbidden region for a given frequency. At the bound's frequency, the nominal loop transmission must lie outside the contour. This guarantees that, regardless of where in the range of uncertainty the frequency

response of the actual plant lies, the closed loop frequency response will not violate the chosen M_m contour. In other words, $|L/(1+L)| \leq M_m$. A maximum closed loop magnitude of 4 dB is used for this problem.

A bound must be plotted for several discrete frequencies ranging from 0 to 10 radians/second. Above 10 radians/second (for this problem), the templates become essentially vertical lines 26 dB tall. Figure 3.7 shows the placement of the low frequency template on the Nichols plot to generate the bound. All other bounds are generated in the same manner. Figure 3.8 shows the plotted bounds for five representative frequencies assuming that, at very low frequency, Region D is concentrated at the single point represented by Case 5.

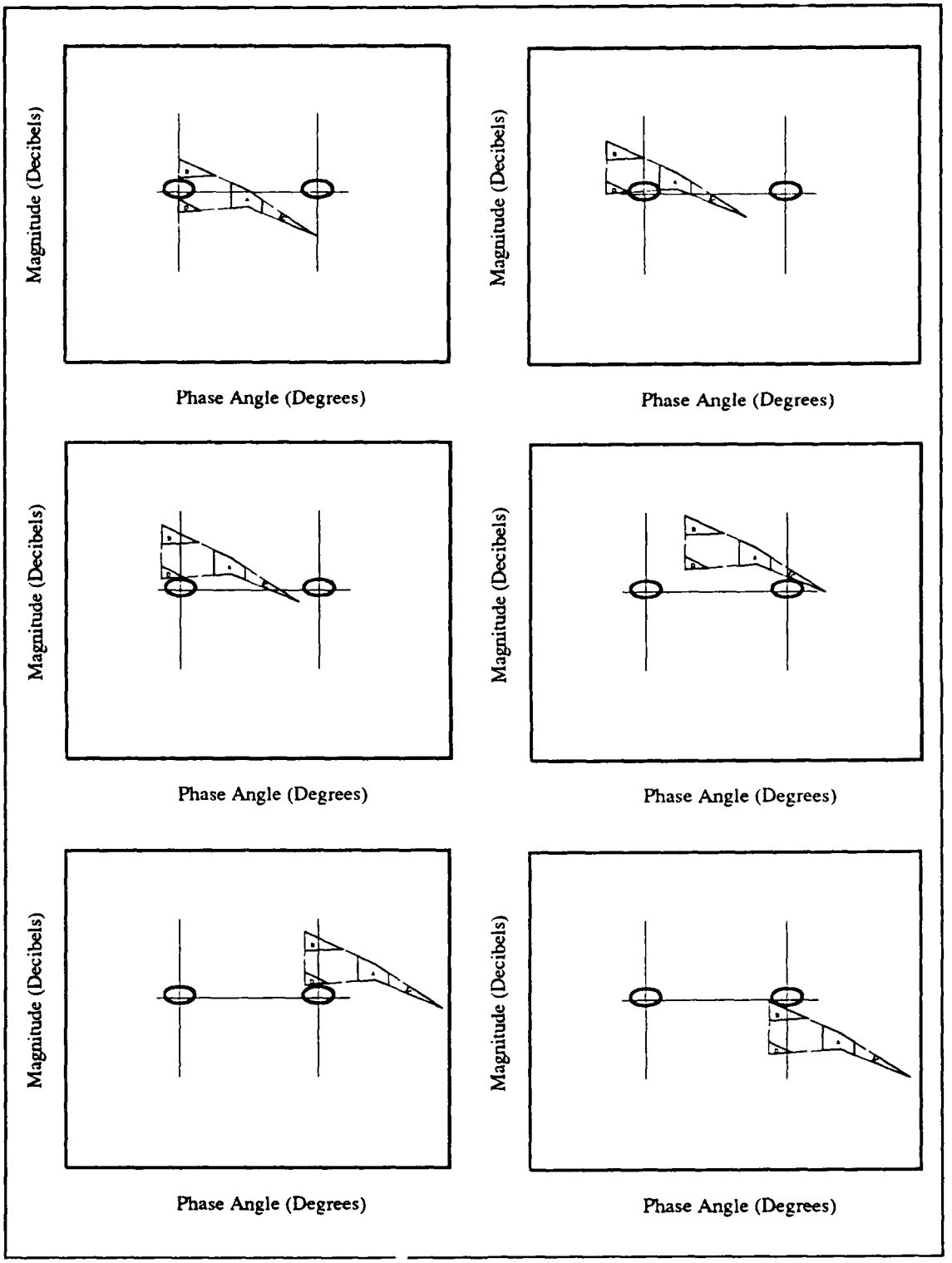

Figure 3.7. Nichols Chart Template Placement

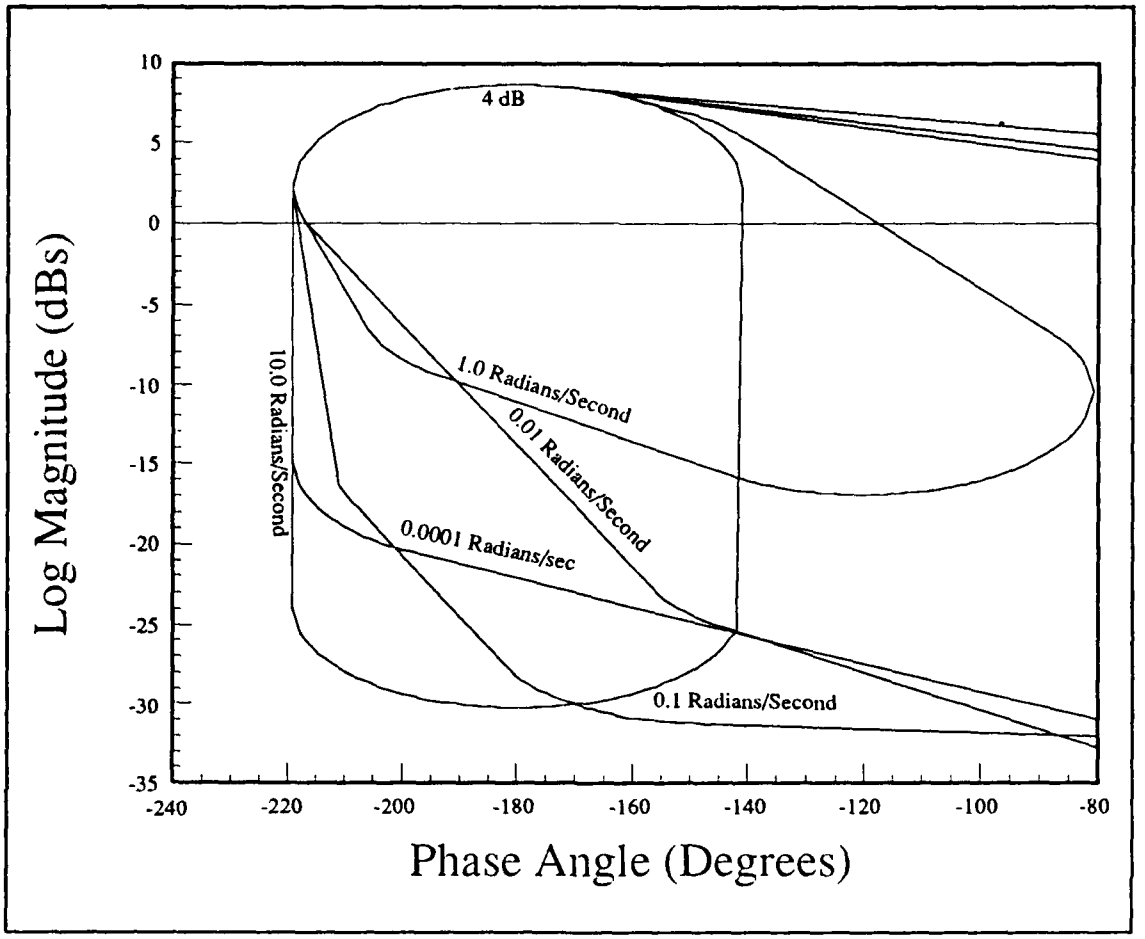

Figure 3.8. Nichols Chart Stabilization Bounds

Referring back to Figure 3.6 for Category C, it can be seen that, at zero frequency, the phase angle must be -180 degrees with the gain less than 1.0. Additionally, since Category D plants must also start at a gain less than 1.0, and Category B plants must start greater than 1.0, the steady state gain of the nominal loop transmission must be between -22 and -48 dB. This constraint also keeps Cases 2, 3, and 5 out of the 4 dB M_m contour at -540°. As frequency increases the phase must decrease (become more negative) while gain increases until the gain is greater than 1.0. Then the phase may be allowed to increase (become less negative) beyond -180 degrees. Figure 3.9 shows the general Nichols plot phase and magnitude trends that

can be expected from poles or zeros in the right or left half plane. From this figure, it can be seen that, in order to achieve the necessary initial phase lag and gain increase, a RHP zero is required to dominate the frequency response at very low frequency.

As frequency continues to increase, phase lead and gain reduction must occur. Figure 3.9 shows this requires a RHP pole. A single RHP pole will return the phase to -180 degrees and the gain becomes constant (at some value above the zero frequency value) because of an equal number of poles and zeros. The phase angle must be made to continue to increase toward zero while the gain begins to decrease. This requires another RHP pole. Once the gain is reduced below 1.0, LHP poles are added to further increase the phase lag and to ensure physically realizable compensators. Additional poles and zeros are added to conform, as closely as possible, to the plotted bounds. Since any attempt to cancel a RHP pole or zero in the plant results in a RHP pole in the closed loop transfer function (because perfect cancellation is impossible), the RHP poles or zeros present in the plant must also be in the loop transmission.

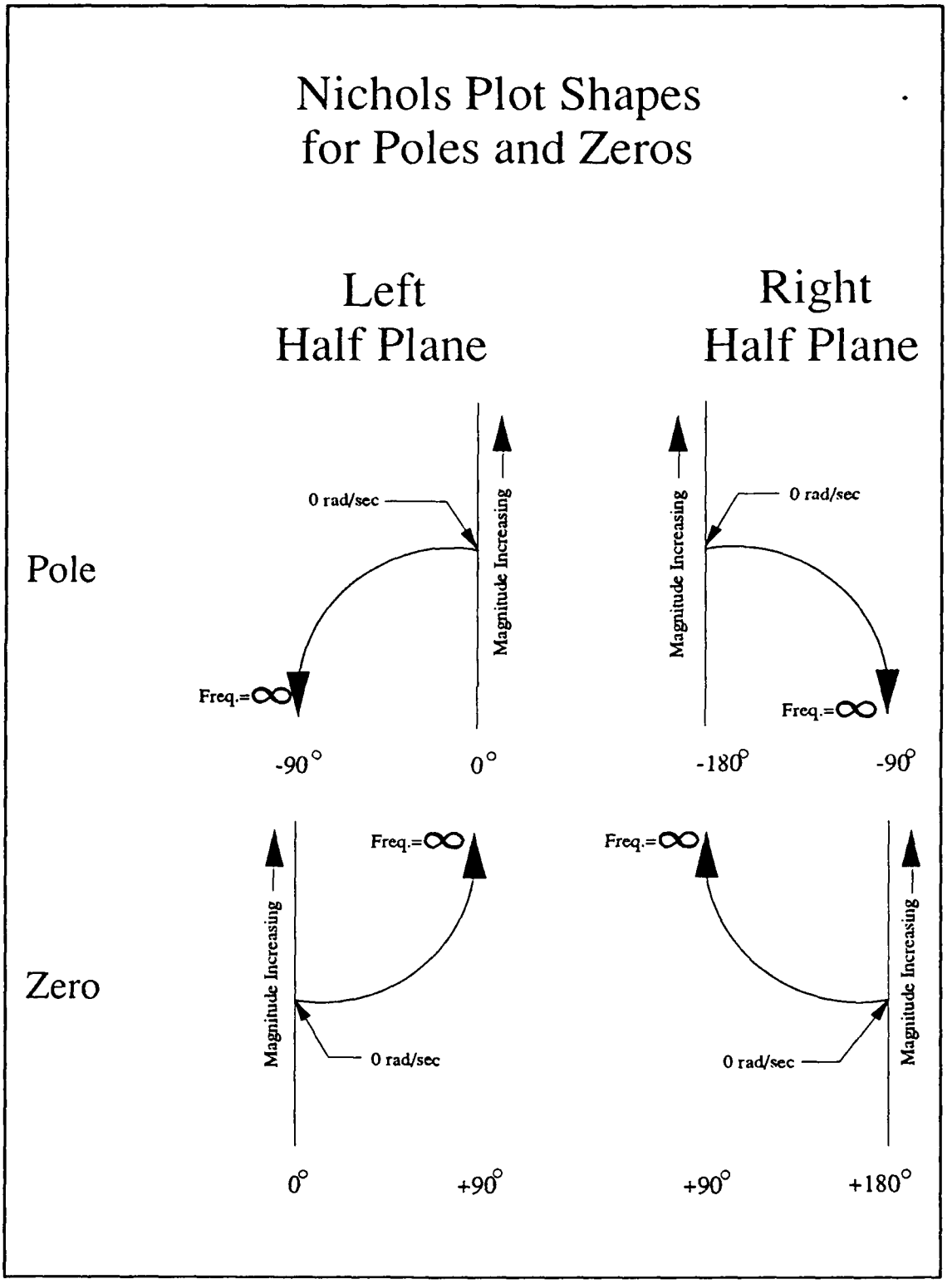

Figure 3.9. Nichols Plot Magnitude and Phase Trends for Poles and Zeros

3.1.4 Nominal Loop Shaping. The previous discussion shows that, to stabilize all six cases, the nominal loop transmission (Case 1 and the compensator G_1) must have two RHP poles and one RHP zero and the two RHP poles of the loop transmission must be farther from the origin than the RHP zero to exert their influence at higher frequencies. Fortunately, the nominal plant has a RHP zero at 0.0024 and a RHP pole at 0.668 to produce this characteristic. The second RHP pole is placed at 0.2. A nominal loop transmission which satisfies the plotted bounds is:

$$L_{1nom} = G_1 H_1 P_0 = \frac{2.95 \times 10^9 (-0.025)(-4.5)(-0.51)(0.0024)}{(-31.27)(231.3, 0.618)(-1000)(-0.7)(-0.05)(-1.74)(0.2)(0.67)} \quad (3.1)$$

and its frequency response is plotted in Figure 3.10. Figure 3.11 shows the frequency response plots for all 6 cases and demonstrates that all six cases are stable and avoid the M_m contours. The loop compensator is found by dividing the loop transmission by the nominal plant:

$$P_0 = A P_{Case1} = \frac{1.6766 \times 10^6 s(-0.51)(0.0024)}{(-31.27)(231.3, 0.618)(-1.74)(0.21, 0.062)(0.67)} \quad (3.2)$$

Notice that the nominal plant is Type (-1) (one free "s" in the numerator). This forces the product $G_1 H_1$ to be the following Type 1 transfer function:

$$G_1 H_1 = \frac{L_{1nom}}{P_0} = \frac{1762(-0.025)(-4.5)(0.21, 0.062)}{s(-0.05)(-0.7)(-1000)(0.2)} \quad (3.3)$$

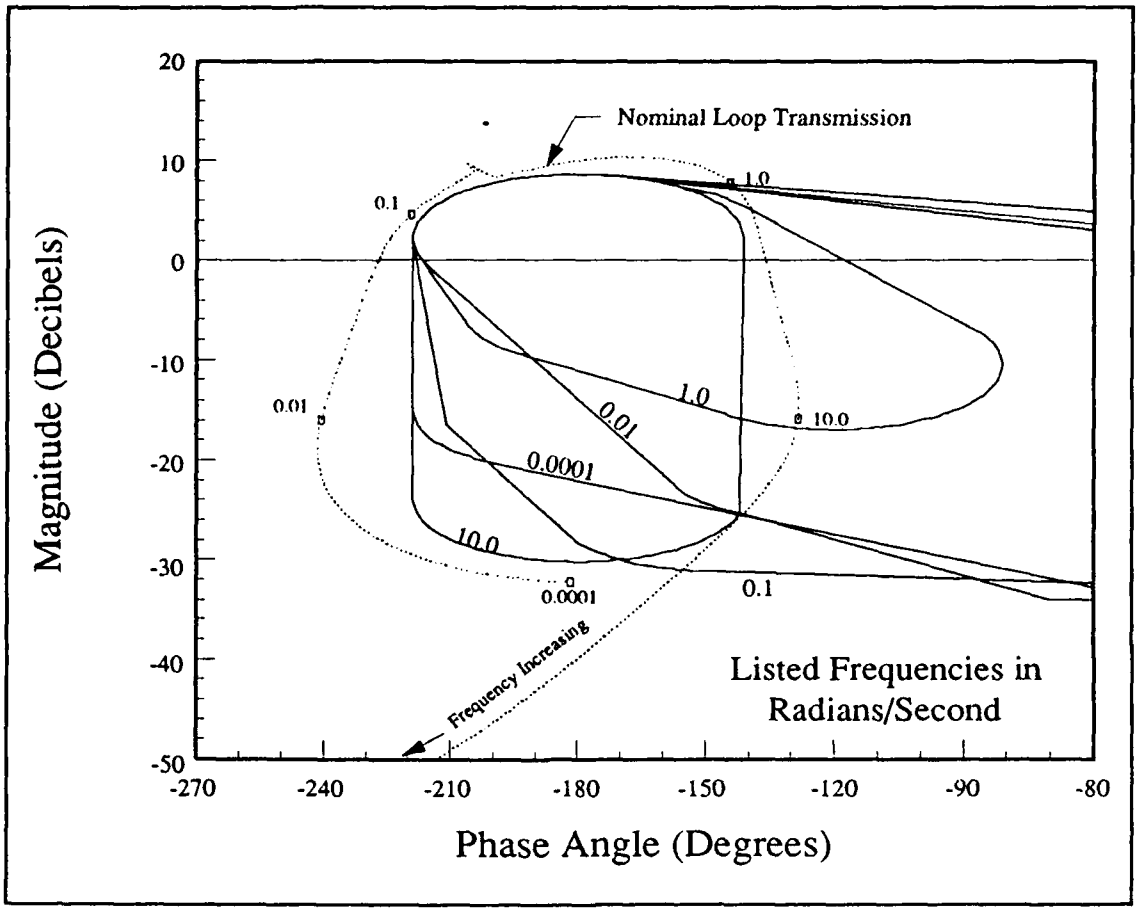

Figure 3.10. Nominal Loop Transmission Nichols Plot

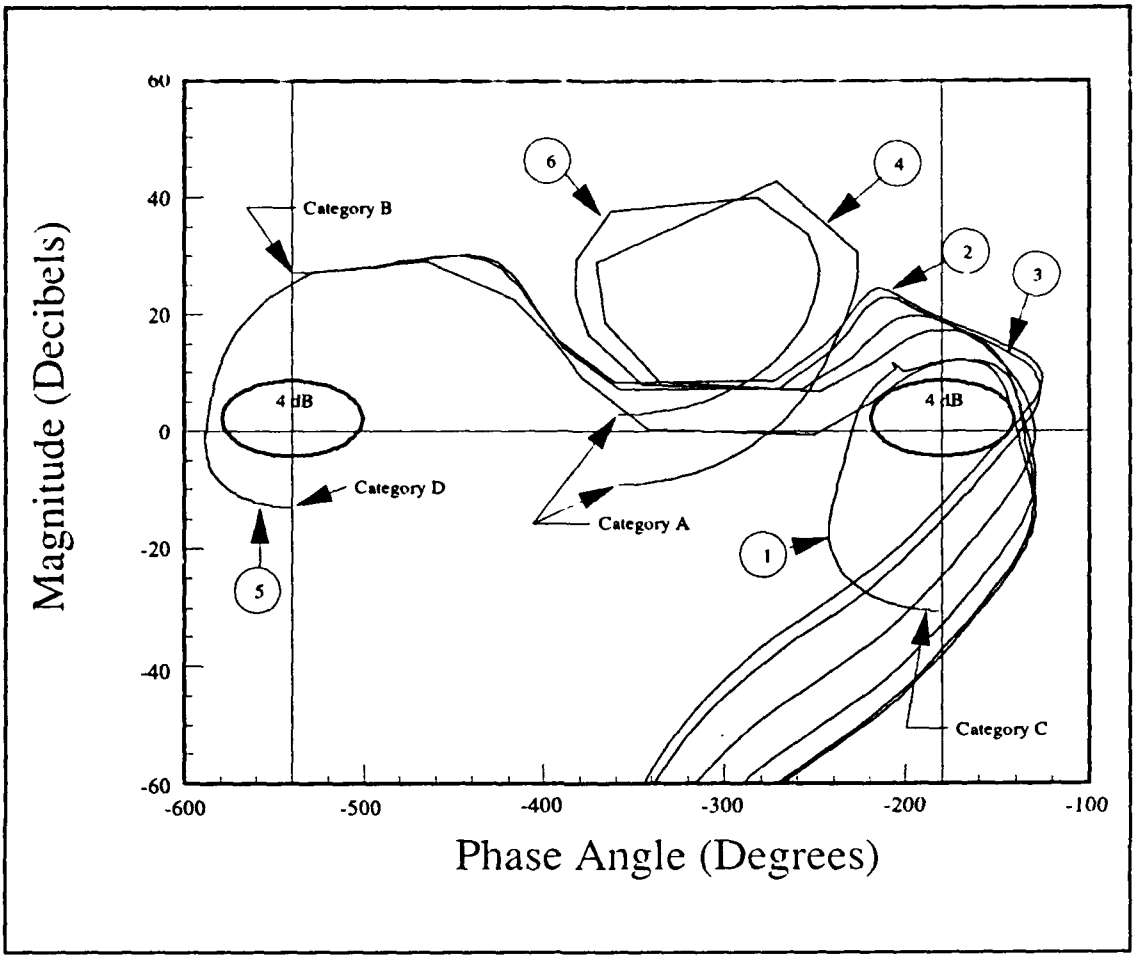

Figure 3.12. Transmission Nichols Plot for All Six Cases

3.1.5 Compensator Placement. In deciding whether to place the compensator in the forward path (G_1) or in the feedback path (H_1), an examination of the form of the transfer functions involved is necessary. Two closed loop transfer functions are of interest in this problem. Both pitch rate and stabilator deflection are to be controlled by outer feedback loops and their transfer functions due to a command to the effective plant must both be considered. Figure 3.1 is repeated here to illustrate the locations of the possible compensators G_1 and H_1.

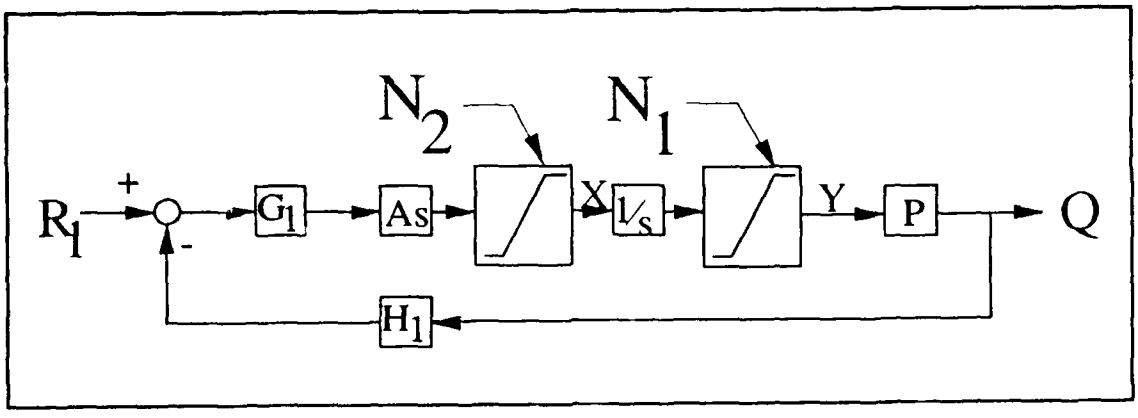

Figure 3.1. Stabilization Control Loop Block Diagram

If the entire stabilization compensator calculated in Section 3.1.3 is placed in the feedback path ($G_1 = 1$), the two transfer functions are

$$P_e = \frac{Q}{R_1} = \frac{AP}{1 + APH_1} \tag{3.4}$$

and

$$P_y = \frac{Y}{R_1} = \frac{A}{1 + APH_1} \tag{3.5}$$

This configuration has two undesirable features. Because the basic plant is Type (-1) and the stabilization compensator (H_1) is Type 1, P_e is Type (-1). This forces the use of a second order integrator in the outer control loop to produce the desired Type 1 open loop transfer function. The other problem is that the RHP pole in H_1 shows up as a RHP zero in both P_e and P_y.

Another possibility is to place the entire compensator in the forward path and letting $H_1 = 1$. The closed loop transfer functions then become

$$P_\epsilon = \frac{G_1 A P}{1 + G_1 A P} \tag{3.6}$$

and

$$P_y = \frac{G_1 A}{1 + G_1 A P} \tag{3.7}$$

In this configuration, the compensator no longer contributes RHP zeroes or differentiators to either transfer function. An additional effect of this placement is that P_y becomes Type 1 and P_ϵ is Type 0.

A third possibility is to split the compensator into two parts, placing one part in the feedback path and the other in the forward path. This might be useful if the compensator contained any RHP zeroes. Placing the RHP zeroes in the feedback path removes them from either of the closed loop transfer functions. This is not necessary in this case and unity feedback with a compensator in the forward path is used ($H_1 = 1$).

Letting H_1=1 and substituting Eqs (2.3), (3.3) and each of the basic plants listed in Table 2.2 into Eqs (3.6) and (3.7) yields a family of transfer functions P_e and P_y. Table 3.1 lists P_e for all six cases and Table 3.2 lists P_y. P_e and P_y are of the form

$$P_e = \frac{K(-0.025)(-4.5)(0.21,0.062)(s-z_1)(s-z_2)}{(s-p_1)(s-p_2)(s-p_3)(s-p_4)(s-p_5)(s-p_6)(s-p_7)(s-p_8)(s-p_9)(s-p_{10})(s-p_{11})} \quad (3.8)$$

and

$$P_y = \frac{2.95\times 10^9(-0.025)(-4.5)(0.21,0.062)(s-z_1)(s-z_2)(s-z_3)(s-z_4)}{s(s-p_1)(s-p_2)(s-p_3)(s-p_4)(s-p_5)(s-p_6)(s-p_7)(s-p_8)(s-p_9)(s-p_{10})(s-p_{11})} \quad (3.9)$$

Notice that P_e is Type 0 and P_y is Type 1.

Table 3.1. Effective Plant Transfer Function

	Flight Condition					
	1	2	3	4	5	6
K	2.95×10^{9}	5.33×10^{10}	3.77×10^{10}	4.68×10^{9}	2.87×10^{9}	1.24×10^{10}
z_1	-0.51	-2.77	-2.26	-0.78	-0.54	-1.15
z_2	0.0024	-0.054	-0.041	-0.0056	0.0055	-0.012
p_1	-1000	-1001i	-1001i	-1000	-1000i	-1000i
p_2	-143+182	-146+181i	-146+182i	-143+182i	-143+182i	-144+182i
p_3	-143-182i	-146-181i	-146-182i	-143-182i	-143-182i	-144-182i
p_4	-29.3	-11.4+29.9i	-12.1+23.6i	-27.5	-29.1	-18.5
p_5	-1.37+2.30i	-11.4-29.9i	-12.1-23.6i	-2.06+3.18i	-1.30+2.45i	-5.98+4.95i
p_6	-1.37-2.30i	-3.34+1.28i	-3.17+0.83i	-2.06 3.18i	-1.30-2.45i	-5.98-4.95i
p_7	-0.436	-3.34-1.28i	-3.17-0.83i	-0.803	-0.492	-1.26
p_8	-0.013+0.21i	-0.019+0.21i	-i0.019+0.22	-0.018+0.22i	-0.028+0.23i	-0.019+0.22i
p_9	-0.013-0.21i	-0.019-0.21i	-0.019-0.22i	-0.018-0.22i	-0.028-0.23i	-0.019-0.22i
p_{10}	-0.032+0.039i	-0.054	-0.041	-0.019+0.015i	-0.014+0.018i	-0.021+0.010i
p_{11}	-0.032-0.039i	-0.024	-0.023	-0.019-0.015i	-0.014-0.018i	-0.021-0.010i

Table 3.2. Stabilator Deflection Transfer Function

	Flight Condition					
	1	2	3	4	5	6
z_1	-1.74	-8.12	-6.55	-2.03	-1.63	-3.08
z_2	0.67	2.92	2.51	0.69	0.72	1.38
z_3	-0.013+0.21i	-0.11	-0.085	-0.034+0.14i	0.011+0.21i	-0.007+0.12i
z_4	-0.013-0.21i	0.063	0.051	-0.034-0.14i	0.011-0.21i	-0.007-0.12i
p_1	-1000	-1001i	-1001i	-1000	-1000i	-1000i
p_2	-143+182	-146+181i	-146+182i	-143+182i	-143+182i	-144+182i
p_3	-143-182i	-146-181i	-146-182i	-143-182i	-143-182i	-144-182i
p_4	-29.3	-11.4+29.9i	-12.1+23.6i	-27.5	-29.1	-18.5
p_5	-1.37+2.30i	-11.4-29.9i	-12.1-23.6i	-2.06+3.18i	-1.30+2.45i	-5.98+4.95i
p_6	-1.37-2.30i	-3.34+1.28i	-3.17+0.83i	-2.06-3.18i	-1.30-2.45i	-5.98-4.95i
p_7	-0.436	-3.34-1.28i	-3.17-0.83i	-0.803	-0.492	-1.26
p_8	-0.013+0.21i	-0.019+0.21i	-i0.019+0.22	-0.018+0.22i	-0.028+0.23i	-0.019+0.22i
p_9	-0.013-0.21i	-0.019-0.21i	-0.019-0.22i	-0.018-0.22i	-0.028-0.23i	-0.019-0.22i
p_{10}	-0.032+0.039i	-0.054	-0.041	-0.019+0.015i	-0.014+0.018i	-0.021+0.010i
p_{11}	-0.032-0.039i	-0.024	-0.023	-0.019-0.015i	-0.014-0.018i	-0.021-0.010i

3.2 Individual Compensators

Regardless of whether cascade compensation, feedback compensation or a combination is used, the RHP poles of the plant show up as RHP zeroes of P_y. This means that the saturation control loop compensator(s) (G_2 and/or H_2 from Figure 1.1) must contend with RHP zeroes ranging from 0.051 to 2.92. Since it is difficult to

achieve a loop gain greater than 1.0 within one octave of a RHP zero location, there can be little feedback benefit from about 0.025 to 6.0 rad/sec if a single compensator is used (4).

Additionally, not all the cases have the same number of RHP zeroes. The transfer functions P_y for Cases 1, 4, and 6 each have one RHP zero while cases 2 and 3 have two RHP zeros and case 5 has three. Any stable Type 1 open loop transfer function with an even number of RHP zeros requires negative feedback to produce a stable closed loop transfer function. Any stable Type 1 function with an odd number of RHP zeros needs positive feedback or else a root of the characteristic equation will exist in the right half plane between the origin and the first RHP zero. Therefore, a single compensator set (G_2 and/or H_2) cannot produce a stable saturation control loop for all six cases.

Although the stabilization issue can possibly be circumvented by adding a differentiator to the compensator (G_2 and/or H_2) to produce a Type 0 open loop transfer function, the large frequency range of very little loop gain is enough reason to consider separate designs for each case. These might be implemented by gain scheduling or by switching the compensator set as the aircraft enters a particular region of the flight envelope (4). For the remainder of this thesis, case 6 is used to illustrate the design process. The design details for each case are presented in the appendices.

From Table 2.2, for case 6, the basic plant is

$$P = \frac{4.68s(-1.15)(-0.012)}{(-3.08)(1.38)(0.12, 0.062)} \tag{3.10}$$

Stabilizing case 6 does not require a RHP pole. A compensator can be designed by any conventional technique to obtain a stable effective plant. Nichols plot loop shaping is used here. A simple (although probably sub-optimal) approach is to design

a loop transmission which resembles the loop transmission obtained with the single compensator. Because this compensator need only handle Case 6, a somewhat more conservative value of M_m can be used. $M_m = 3\text{dB}$ is used here giving the following loop transmission:

$$L_1 = \frac{1.54 \times 10^8}{(-31.27)(231.3, 0.618)(-15)(1.38)} \tag{3.11}$$

where

$$L_1 = G_1 AP \tag{3.12}$$

Figure 3.12 shows the Nichols plot for the stabilization loop transmission. Substituting Eq (3.10) and Eq (2.3) into Eq (3.12) yields

$$G_1 = \frac{L_1}{AP} = \frac{19.677(-3.08)(0.12, 0.062)}{s(-15)(-1.15)(-0.012)} \tag{3.13}$$

Substituting Eqs (2.3), (3.10), and (3.13), into Eqs (3.6) and (3.7) yields

$$P_e = \frac{1.54 \times 10^8}{(231, 0.62)(-35.8)(7.91, 0.58)} \tag{3.14}$$

and

$$P_y = \frac{3.29 \times 10^7(-3.08)(1.38)(0.12, 0.062)}{s(231, 0.62)(-35.8)(7.91, 0.58)(-1.15)(0.012)} \tag{3.15}$$

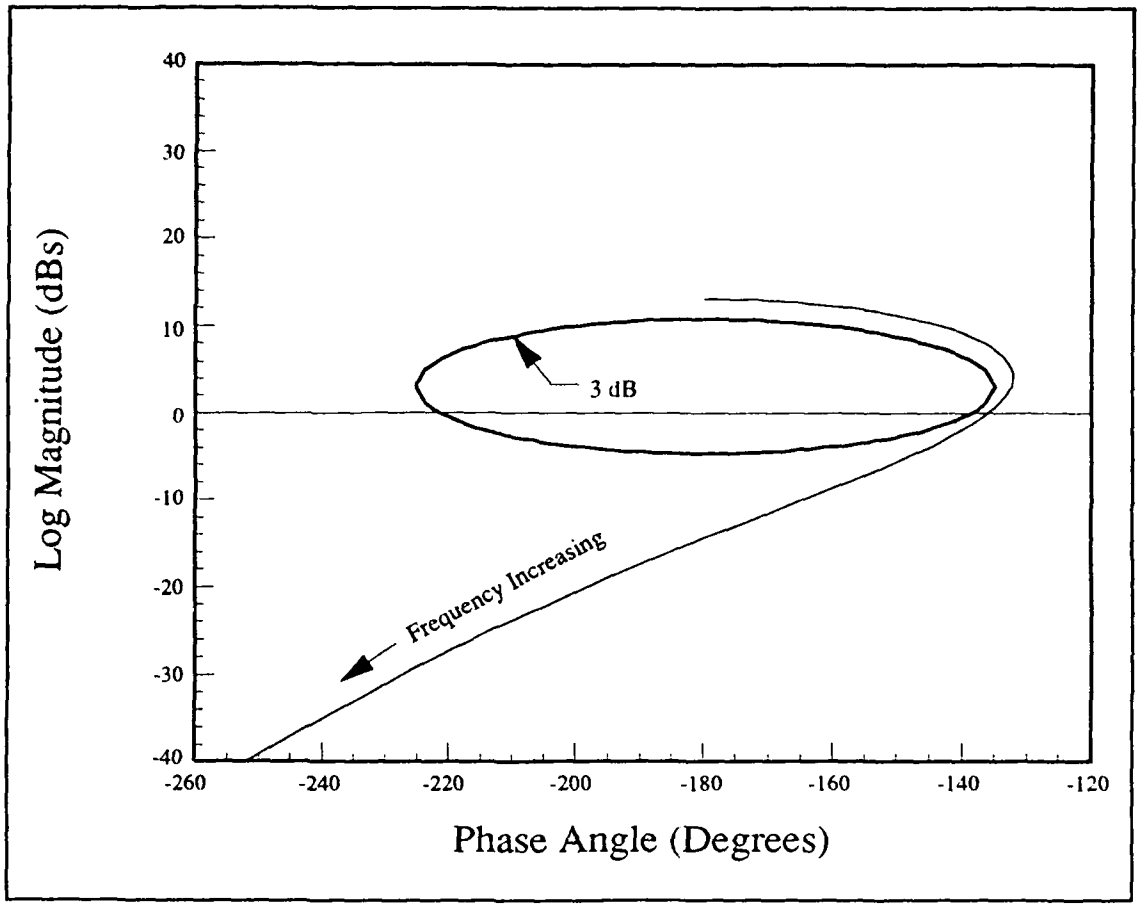

Figure 3.12. Stabilization Loop Nichols Plot for Case 6

IV. Saturation Control Loop

4.1 Design Philosophy

The control system developed in this thesis can be thought of as a dual mode control system. The first mode is the standard pilot command tracking mode. Chapters III and V present the design of the necessary components for this mode. The second mode is a maximum pitch performance mode. In this mode, the control system recognizes that the commanded input exceeds the capabilities of the aircraft and the control system delivers what it can.

Whenever the tracking control loop gains control of the airplane, it commands the stabilator to go to a steady state value somewhere near maximum deflection. This gives the maximum pitch rate the aircraft can produce without sacrificing stability. Figure 4.1 shows the saturation control loop block diagram.

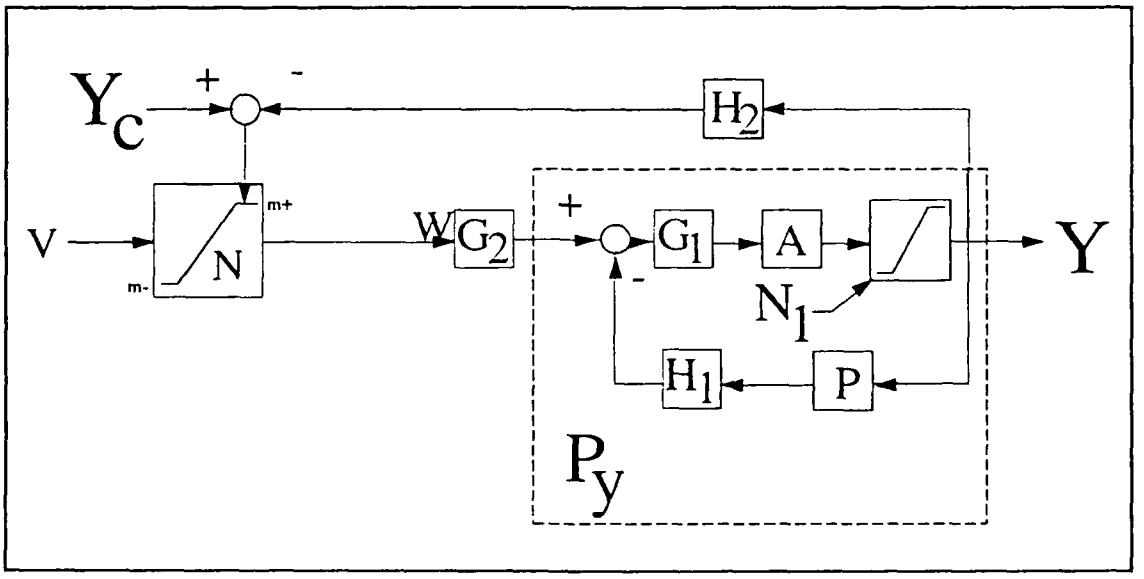

Figure 4.1. Saturation Control Loop Block Diagram

The stabilator deflection angle is continually compared to the maximum allowable deflection angle Y_c. The input/output relationship of the command limiter (N) is shown graphically in Figure 4.2. The saturation level of the command limiter is adjusted according to

$$m^+ = Y_c^+ - H_2 Y \tag{4.1}$$

$$m^- = Y_c^- - H_2 Y \tag{4.2}$$

where

y_c^+ = Maximum Allowable Positive Deflection Angle

y_c^- = Maximum Allowable Negative Deflection Angle

m^+ = Positive Command Limit

m^- = Negative Command Limit

Whenever the input V is larger than the saturation level m^+ (or m^- for negative commands), the saturation control loop gains control. The input to G_2 now comes directly from the saturation control loop instead of the tracking control loop. Although pitch rate is continually being monitored by the tracking control loop, it is no longer being directly controlled. At some time in the future, when the actual pitch rate rises above the commanded value, the input V falls below the saturation value and the tracking control loop regains control.

The output of interest is the step response of the stabilator deflection angle (Y of Figure 4.1). The deflection angle should have very little overshoot above the final value. This minimizes the necessary "safety factor" between Y_c and the actual stabilator limits. And since maximum performance is desired, settling time should be as short as possible.

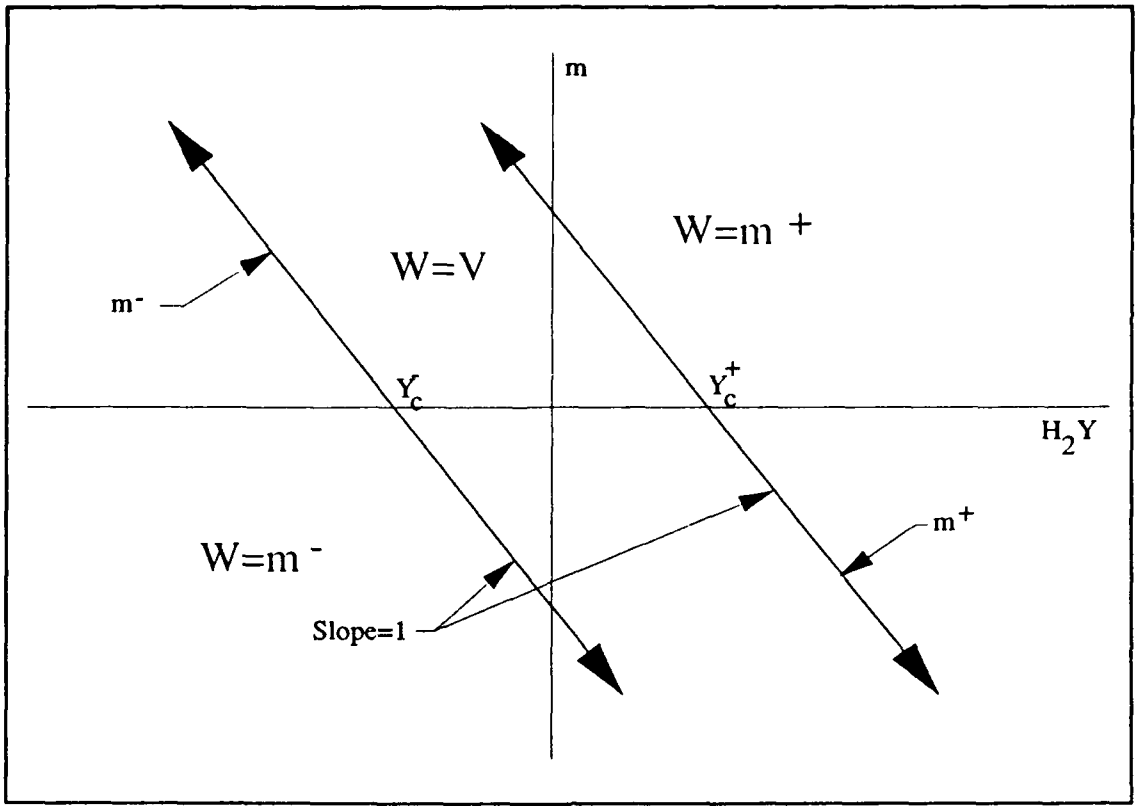

Figure 4.2. Command Limiter Input/Output Relationship

4.2 Stabilator Response

4.2.1 Cases 1, 4, 5, and 6. It is useful to qualitatively consider the movement of the stabilator as it responds to pitch commands (from the pilot) and stabilization commands (from the stabilization control loop) in the simplest of the six cases. The transfer functions P_y for cases 1, 4, 5, and 6 are all Type 1 with one real RHP zero. Figure 4.3 shows a representative stabilator deflection angle plot in response to a positive step pitch rate command.

Initially, the stabilator moves in a positive direction. This drives the airplane away from the equilibrium condition in the desired direction. Since the aircraft is unstable, the pitch rate continues to build and a stabilator reversal is required to arrest the pitch rate. If the aircraft is stable, a step input to the stabilator will produce zero steady state pitch rate because the transfer function is Type (-1). Although oscillation

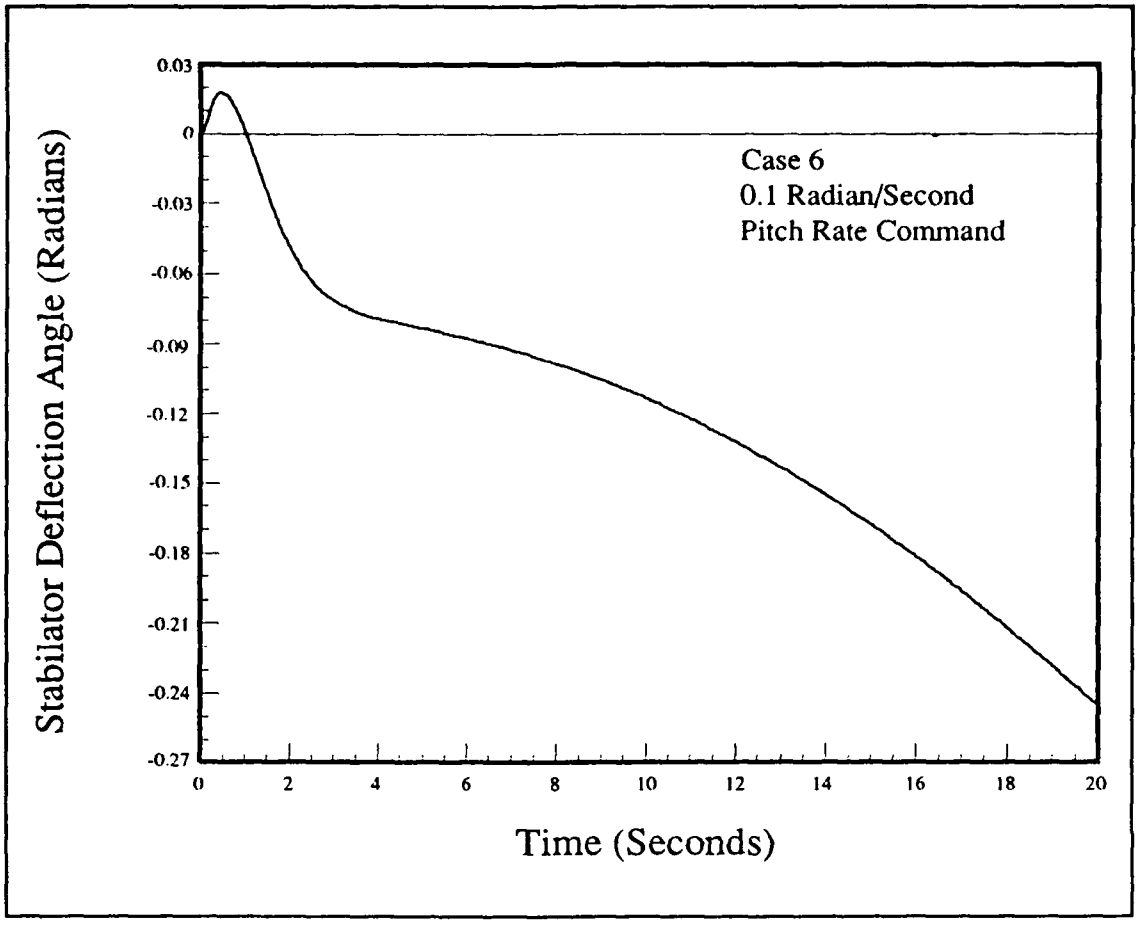

Figure 4.3. Example Stabilator Deflection Angle Plot for Case 6

might occur, a reversal of the stabilator would not be necessary. The stabilization control loop performs this function. A negative steady state stabilator deflection is necessary to maintain a constant positive pitch rate. As the aircraft continues to pitch up, the airplane's airspeed begins to decrease due to gravity and due to the increased drag caused by the increased lift during the pitch up. As airspeed drops, the effectiveness of the stabilator also drops since the force developed by an airfoil is proportional to the velocity squared. To maintain the necessary stabilizing pitching forces, the stabilator deflection angle magnitude must increase (14). Notice that the deflection angle does not approach a constant steady state value (caused by the Type

1 transfer function P_y).

Figure 4.3 shows that there are two distinct regions where saturation might occur. The positive limit might be reached in the initial positive going region if a particularly large command is applied suddenly. Secondly, the negative limit might be reached if a large command is applied for an extended period. Even a relatively small command will eventually produce a negative saturation if maintained long enough. Since the need for stability causes the negative steady state deflection, it is the negative limit which is of primary concern for a positive pitch rate command. As the commands increase, the peak in the initial region gets larger and the magnitude of the reversal gets larger. Eventually, the positive limit is reached. If the command is increased further, the control surface will remain saturated in the initial region for some period of time. It will come out of saturation when the pitch rate begins to approach the commanded value. If the control surface has sufficient control authority to arrest the pitch rate, instability does not result. If a large enough command is applied the stabilator, saturation in the initial region will continue too long and even full opposite control will not be able to arrest the pitch rate. The purpose of the command limiter is to limit the input to the effective plant so that this does not occur. Assuming a successful saturation control loop design, if the stabilator saturates in the initial region, the result is a sluggish departure from equilibrium. If the stabilator saturates in the final region, the result is loss of control because further negative deflection is required to slow the pitch rate.

4.2.2 Cases 2 and 3. Cases 2 and 3 are somewhat more complicated. They each contain a second RHP zero in their transfer functions (P_y). This causes a second reversal in the stabilator deflection. Figure 4.4 shows the stabilator deflection angle plot for case 2.

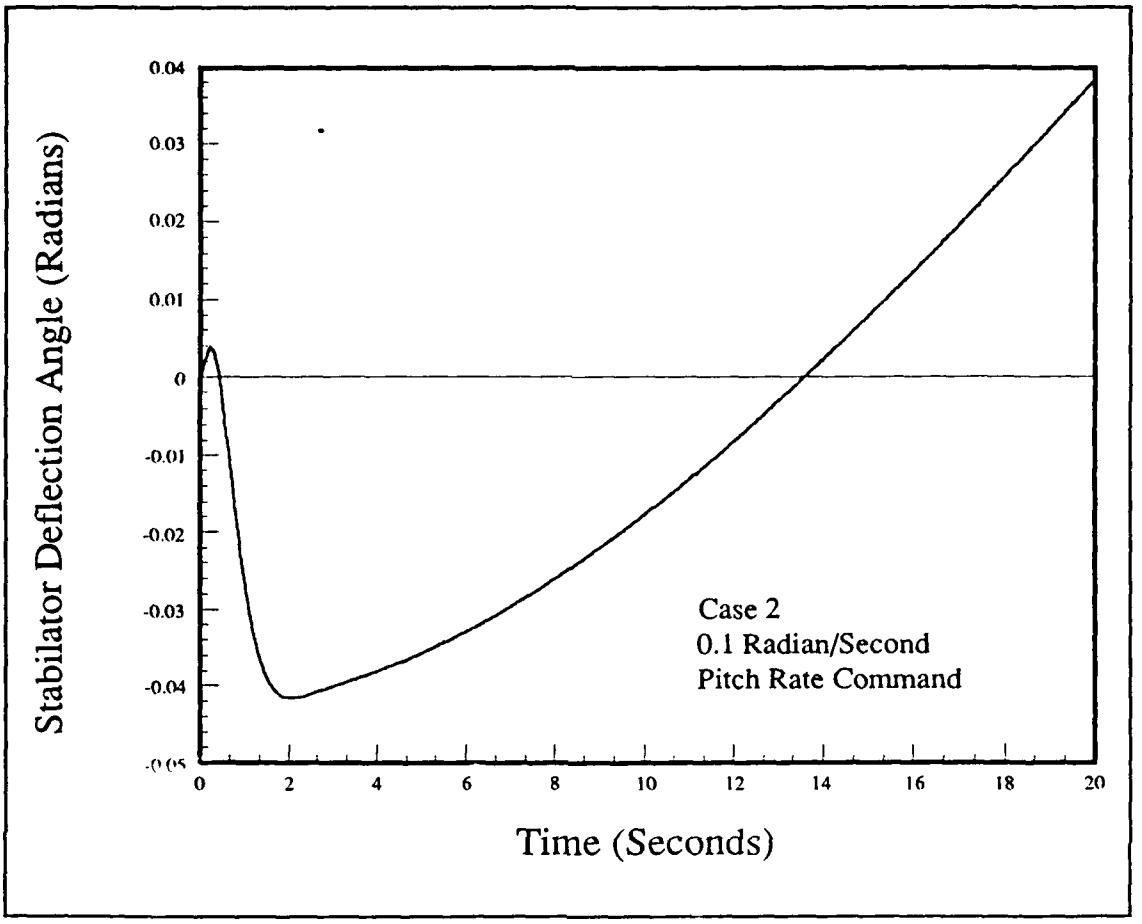

Figure 4.4. Example Stabilator Deflection Angle Plot for Case 2

There are now three distinct regions to consider. The first region, as before, drives the airplane in the desired direction away from the equilibrium condition. Saturation in this region causes only sluggishness. The two reversals are stability motivated and saturation in the later two regions causes loss of control.

4.2.3 Time Response Design. The ultimate goal of the saturation control loop is to detect an excessive pitch rate command and move the stabilator to maximum allowable deflection as quickly as possible. However, each of the transfer functions contain one or more RHP zeros which hinder this goal. To determine the placement of the dominant poles of the closed loop transfer function to best achieve

the goal, consider the second order transfer function

$$\frac{C(s)}{R(s)} = \frac{\omega_n^2}{a} \frac{(s-a)}{(s^2 + 2\zeta\omega_n s + \omega_n^2)} \tag{4.3}$$

To study the effects of the relative placement of the RHP zero and the dominant poles of the transfer function, let $a = K\omega_n$. Thus

$$\frac{C(s)}{R(s)} = \frac{\omega_n}{K} \frac{(s-K\omega_n)}{(s^2 + 2\zeta\omega_n s + \omega_n^2)} \tag{4.4}$$

Since small overshoot is desired let $\zeta = 0.8$ and, for simplicity, let $\omega_n = 1$.

$$\frac{C(s)}{R(s)} = \frac{1}{K} \frac{(s-K)}{(s^2 + 1.6s + 1)} \tag{4.5}$$

By varying K, the effects of placement of the RHP zero relative to the dominant poles can be seen. Figure 4.5 shows the time response plots for several values of K.

As the value of K decreases, the peak value of the initial positive region increases. In other words, the nearer the RHP zero is to the origin, for a given set of dominant poles, the larger the initial peak. Similarly, as the system is made faster (dominant poles move farther from the origin), for a given RHP zero location, the likelihood of saturation in the initial region increases. For the cases discussed in section 4.2.1, which have only one reversal, this is not terribly important because initial saturation does not cause loss of control. However, for the other cases with

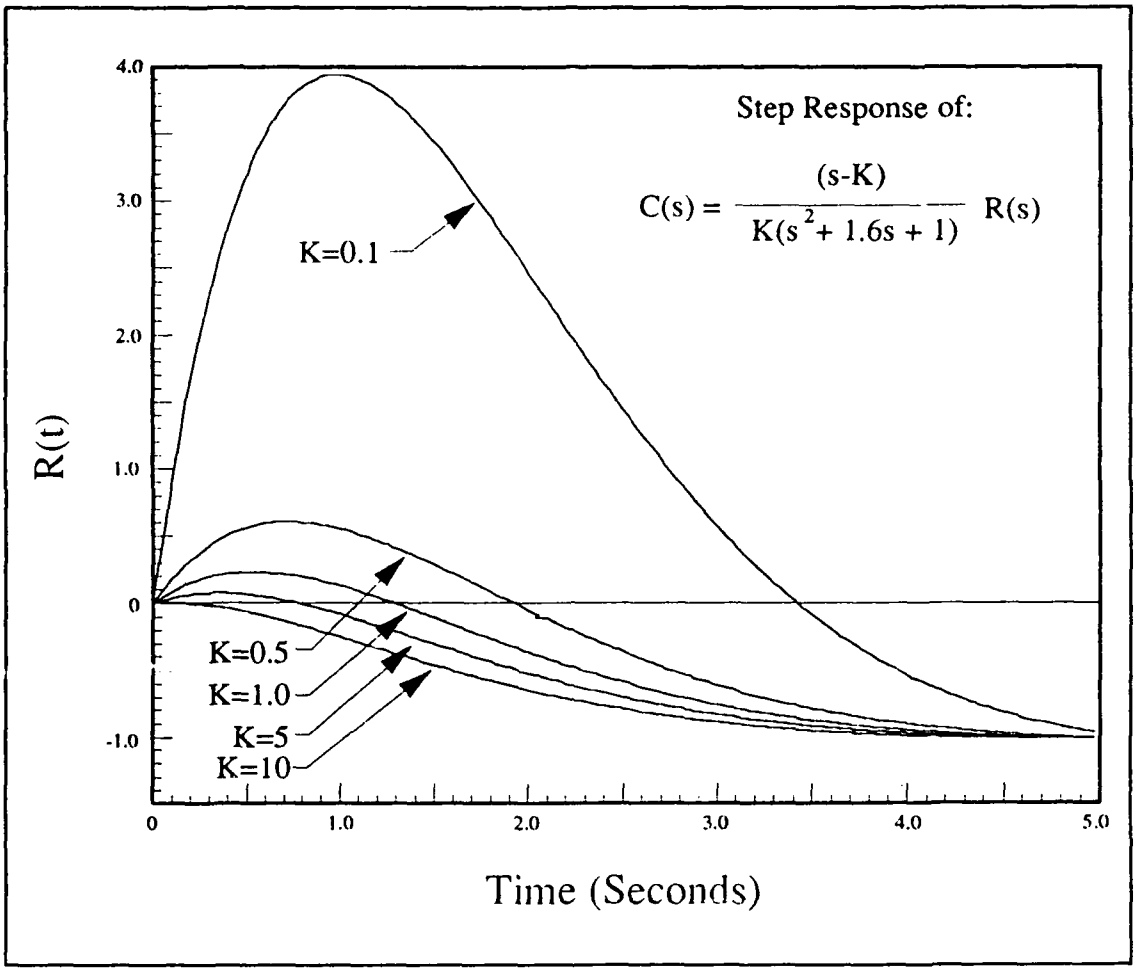

Figure 4.5. Sensitivity of Time Response to RHP Zero Placement

additional regions with saturation potential, any saturation in another region is potentially disastrous. Therefore, it becomes imperative to not make the saturation control loop "too fast". This directly conflicts with the desire for a very quick system.

On the other hand, RHP zeros have a natural limiting effect on the open loop bandwidth, as mentioned in Section 3.2, which automatically slows down the system (11). The engineer must keep in mind that this natural slowing may or may not be sufficient after a maximum open loop bandwidth system is designed. It may be necessary to further slow the system to avoid excessive peak values during the reversals.

4.3 Saturation Control Loop Shaping.

4.3.1 System Type. Consider letting the product $L_{2c} = G_2H_2$ be Type 0. Section 5.3 discusses the reasons why the forward path compensator G_2 should be Type 1. And since Eq (3.15) (P_y) is Type 1, the feedback compensator H_2 becomes Type (-1). From the block diagram of Figure 4.1

$$\frac{Y}{Y_c} = \frac{G_2P_y}{1 + G_2H_2P_y} \tag{4.6}$$

Letting G_2 be Type 1 and H_2 be Type (-1) gives

$$\frac{Y}{Y_c} = \frac{1}{s^2}\frac{G_2^0P_y^0}{[1 + (G_2^0H_2^0P_y^0)/s]} \tag{4.7}$$

where

G_2^0 = Type 0 Part of G_2

H_2^0 = Type 0 Part of H_2

P_y^0 = Type 0 Part of P_y

Rearranging Eq (4.7) gives

$$\frac{Y}{Y_c} = \frac{G_2^0P_y^0}{s(s + G_2^0H_2^0P_y^0)} \tag{4.8}$$

which is Type 1.

For a constant input Y_c, Y will not approach a constant value in steady state. This is obviously unacceptable for controlling amplitude saturation. However, since deflection rate is simply the derivative of the deflection angle

$$X = sY \tag{4.9}$$

substitution of Eq (4.9) into Eq (4.8) gives

$$P_2 = \frac{Y}{Y_c} = s\frac{X}{Y_c} = \frac{G_2^0 P_y^0}{s(s + G_2^0 H_2^0 P_y^0)} \tag{4.10}$$

Rearranging Eq (4.10) gives

$$\frac{X}{Y_c} = \frac{G_2^0 P_y^0}{s + G_2^0 H_2^0 P_y^0} \tag{4.11}$$

which is Type 0 and approaches a constant steady state value for a constant input Y_c. Therefore, although unsuitable for amplitude saturation, this configuration is useful for controlling control surface rate saturation. None of the six cases studied here requires protection from rate saturation.

Try letting H_2 be Type 0. Eq (4.7) becomes

$$P_2 = \frac{1}{s^2}\frac{G_2^0 P_y^0}{[1 + (G_2^0 H_2^0 P_y^0)/s^2]} \tag{4.12}$$

Rearranging Eq (4.12) gives

$$P_2 = \frac{G_2^0 P_y^0}{s^2 + G_2^0 H_2^0 P_y^0} \tag{4.13}$$

which is Type 0 and has constant steady state output. Therefore, to control amplitude, H_1 should be Type 0. Since G_2 and P_y are Type 1, $L_2 = G_2 H_2 P_y$ is Type 2. Notice that a single control loop cannot ensure safety from both rate and amplitude saturation.

4.3.2 Stability. Figure 4.6(a) shows the Nyquist plot for a representative Type 1 transfer function with one RHP zero (like P_y for Case 6). For a stable closed loop transfer function, a Type 2 open loop transfer function with no RHP poles must have a Nyquist plot which resembles Figure 4.6(b).

Examination of Figure 4.6(b) shows there are no net encirclements of the -1 point. Obviously, a pole at the origin is necessary in the compensator to produce the desired Type 2 transfer function. Adding an integrator to Figure 4.6(a) "rotates" the positive frequency portion of the plot 90° clockwise to the vicinity of 0°. But since the phase at 0 radians/second must be -180°, as shown in Figure 4.6(b), the compensator must be multiplied by -1. Therefore, to create the proper Nyquist plot, $G_2 h_2$ must be Type 1 with negative steady state gain.

It is more convenient to use the Nichols chart to shape the frequency response of the saturation loop transmission. Since small overshoot is desired, a somewhat more conservative value of M_m is used. For this loop $M_m = 2.3\text{dB}$ is used. The required loop transmission is:

$$L_2 = L_{2c}P_y = P_y = \frac{-1.53 \times 10^7(-3.08)(1.38)(-0.03)}{s^2(231, 0.62)(-35.8)(7.91, 0.58)(-1.15)} \tag{4.14}$$

Substituting Eq (3.15) into Eq (4.14) gives the required compensator:

$$L_{2c} = \frac{-0.464(-0.012)(-0.03)}{s(0.12, 0.062)} \tag{4.15}$$

where

$$L_{2c} = G_2H_2 \tag{4.16}$$

This gives the open loop frequency response of L_2 shown in Figure 4.7.

Example Nyquist Plots

Uncompensated
Type 1 System
with 1 RHP Zero

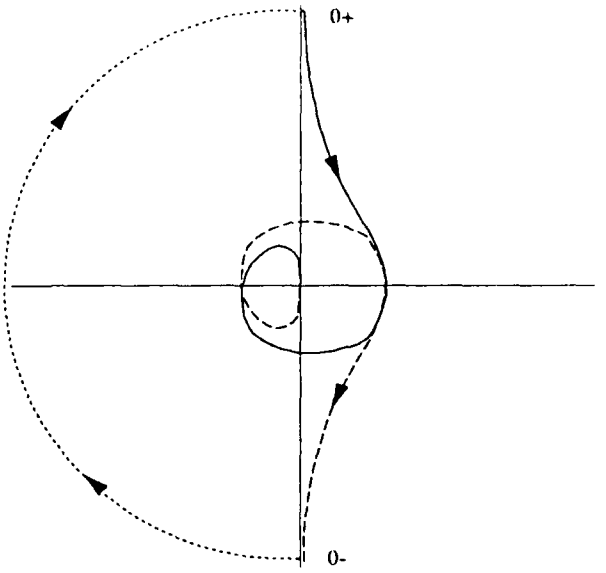

(a)

Type 2 System

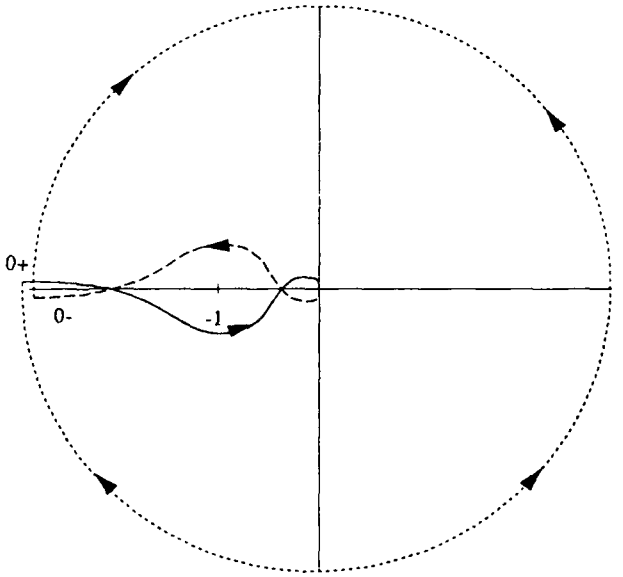

(b)

Figure 4.6. Stabilator Response Nyquist Plot (a) Uncompensated (b) Compensated

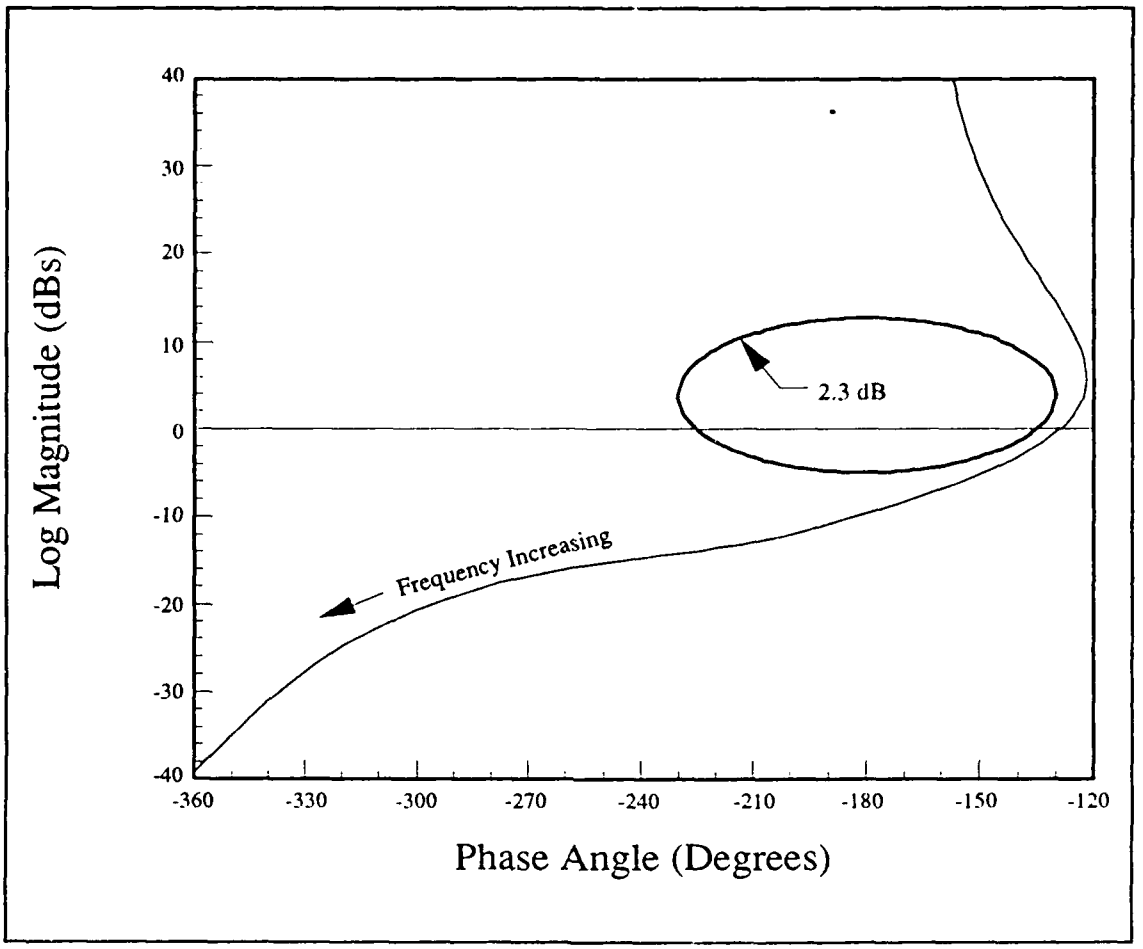

Figure 4.7. Saturation Control Open Loop Frequency Response for Case 6

4.3.3 Compensator Placement. As before, loop shaping only determines the product of the two compensators in the loop (G_2H_2 in this case). It is again necessary to decide whether cascade compensation, feedback compensation, or a combination of the two is appropriate. Consider the transfer function:

$$\frac{Y}{Y_c} = \frac{G_2 P_y}{1 + G_2 H_2 P_y} \tag{4.17}$$

Which can be rewritten using Eq (4.14) and Eq (4.16) as

$$\frac{Y}{Y_c} = \frac{G_2 H_2 P_y}{H_2(1 + G_2 H_2 P_y)} = \frac{1}{H_2}\frac{L_2}{1 + L_2} = F_2 P_2 \tag{4.18}$$

where

$$P_2 = \frac{L_2}{1 + L_2} \qquad \text{and} \qquad F_2 = \frac{1}{H_2} \tag{4.19}$$

If the time response of P_2 is inadequate, improvement may be possible through the use of the "prefilter" F_2. Placing a real prefilter on the input would be ineffective because Y_c is constant. Eventually, the output from this filter will reach steady state and the only effect would be to scale Y_c by some constant. To solve for G_2 and H_2, use Eq (4.16) and Eq (4.19) and rearrange, giving

$$H_2 = \frac{1}{F_2} \tag{4.20}$$

and

$$G_2 = \frac{L_{2c}}{H_2} = L_{2c} F_2 \tag{4.21}$$

Notice that both F_2 and its inverse must be implemented. Incidentally, H_2 can also be used to "hide" any RHP zeros in L_{2c}.

Substituting Eq (4.14) into Eq (4.19) gives

$$P_2 = \frac{1.53 \times 10^7 (-0.03)(-3.08)(1.38)}{(231, 0.62)(-35.3)(7.52, 0.67)(0.78, 0.54)(-0.032)} \tag{4.22}$$

Figure 4.8 shows the linear time response of the saturation control loop for Case 6 to a unit step input. Although smaller overshoot is desirable, the time response is adequate and a prefilter is not needed. Thus, $H_2 = (1/F_2) = 1$ and from Eq (4.15) and Eq (4.16)

$$G_2 = L_{2c} F_2 = \frac{-0.464(-0.012)(-0.03)}{s(0.12, 0.062)} \tag{4.23}$$

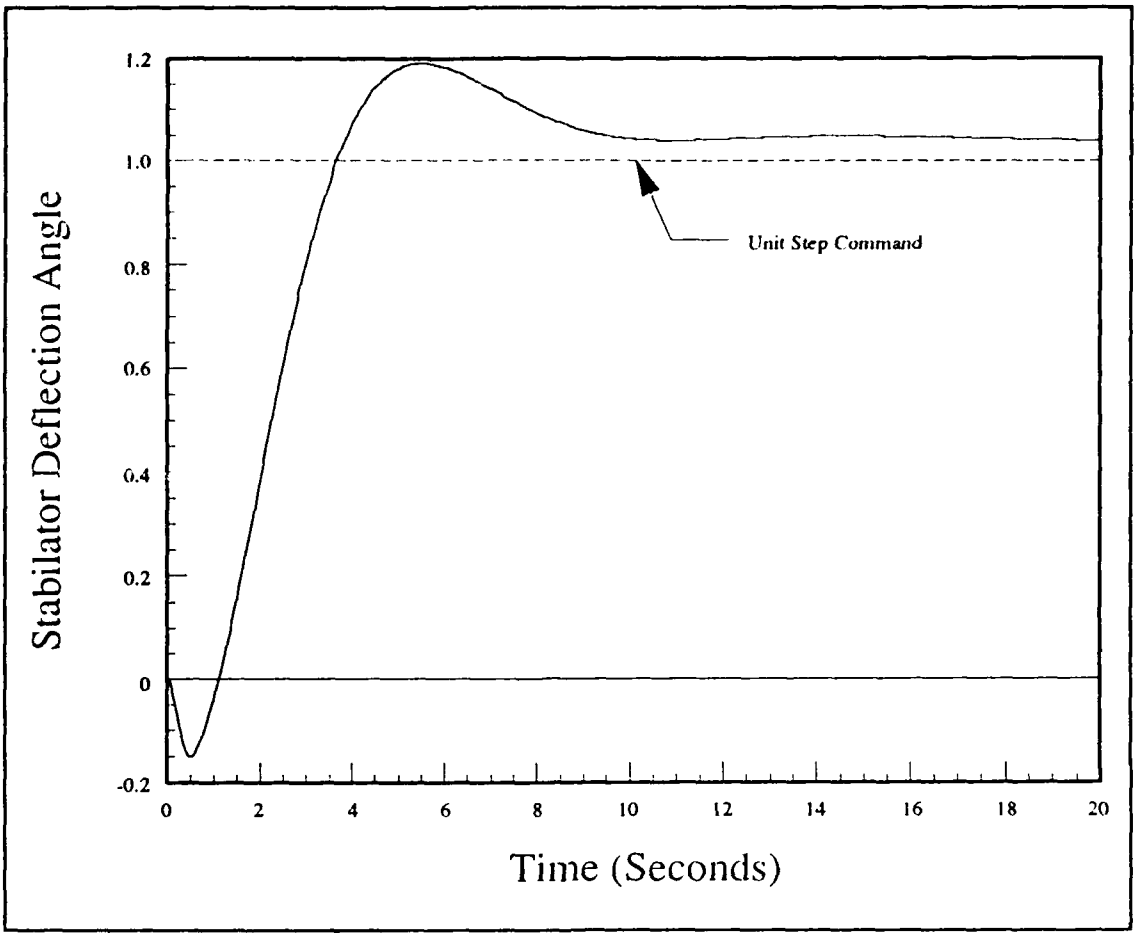

Figure 4.8. Step Response of the Saturation Control Loop for Case 6

V. Tracking Control Loop

5.1 Loop Compensation

Most of the time the system is in operation, neither the command limiter nor the control surface is in saturation. During this condition, the system can be represented by the block diagram shown in Figure 5.1.

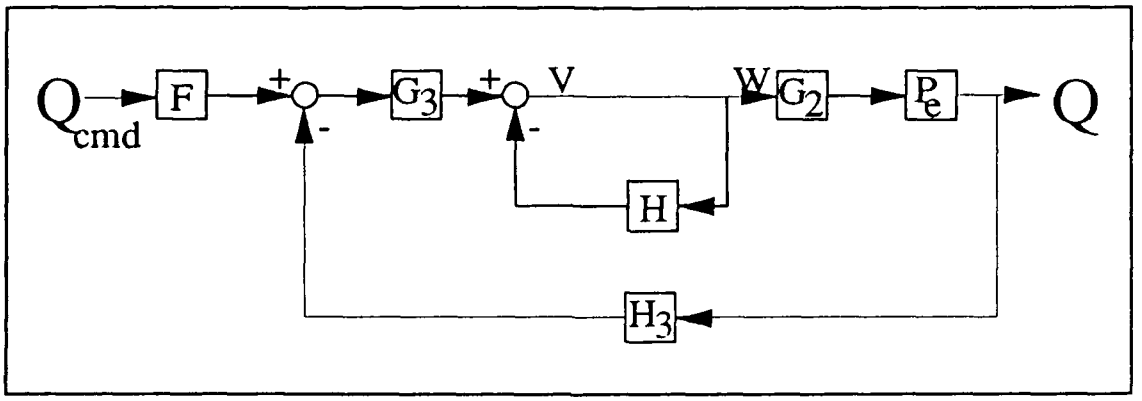

Figure 5.1. Tracking Control for No Command Limiting

The system has the open loop transfer function

$$L_3 = \frac{G_3 H_3 G_2 P_e}{1 + H} \tag{5.1}$$

For simplicity define

$$L_{3c} = \frac{G_3 H_3 G_2}{1 + H} \tag{5.2}$$

so that

$$L_3 = L_{3c} P_e \tag{5.3}$$

The loop compensator is now designed in a manner similar to Section 3.2. For Case 6, the required loop transmission is

$$L_3 = \frac{3.70 \times 10^8}{s(231, 0.62)(-35.8)(7.91, 0.58)} \tag{5.4}$$

Substitute Eq (3.14) and Eq (5.4) into Eq (5.3) to obtain

$$L_{3c} = \frac{2.454}{s} \tag{5.5}$$

This achieves the Nichols plot shown in Figure 5.2.

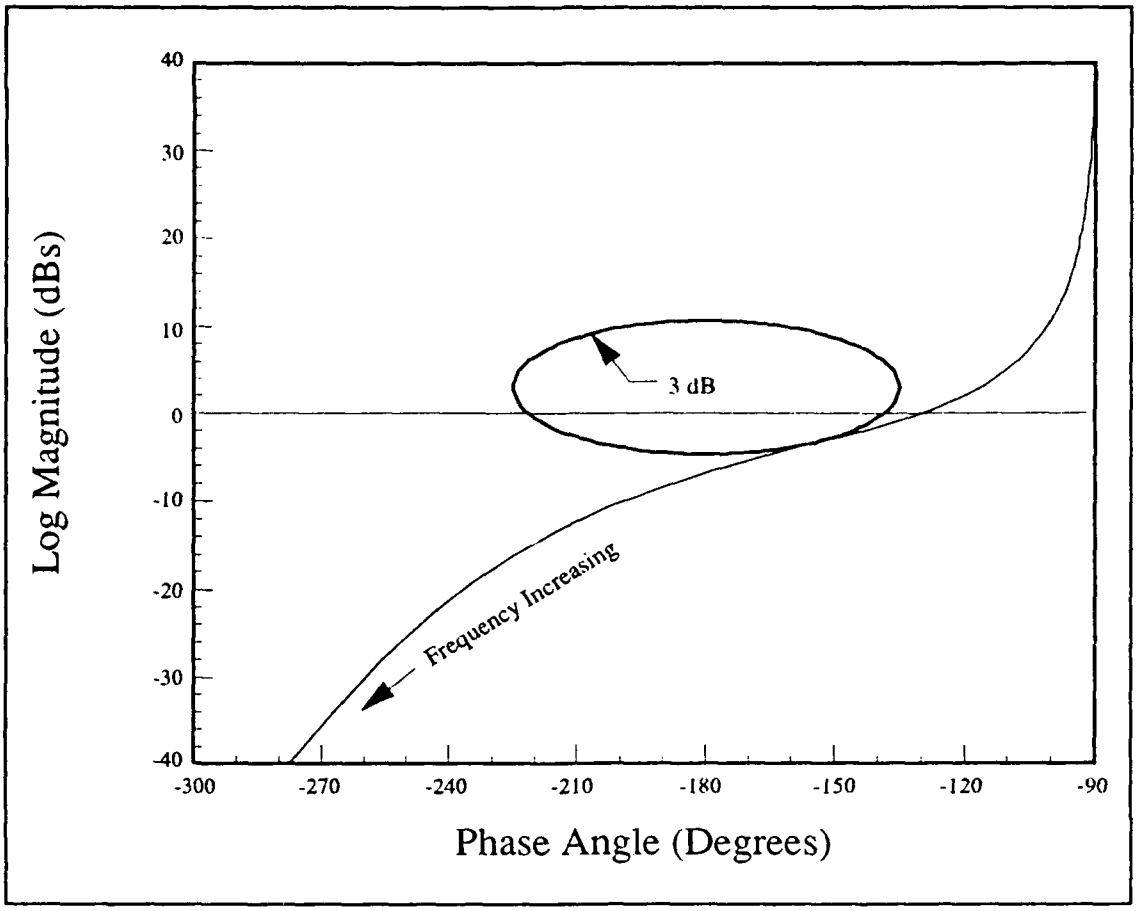

Figure 5.2. Outer Loop Nichols Plot for Case 6

5.2 Command Limiter Minor Loop

Figure 5.3 shows a representative block diagram of the system during command limiter saturation.

In this condition, the signal at the input to the command limiter is governed by

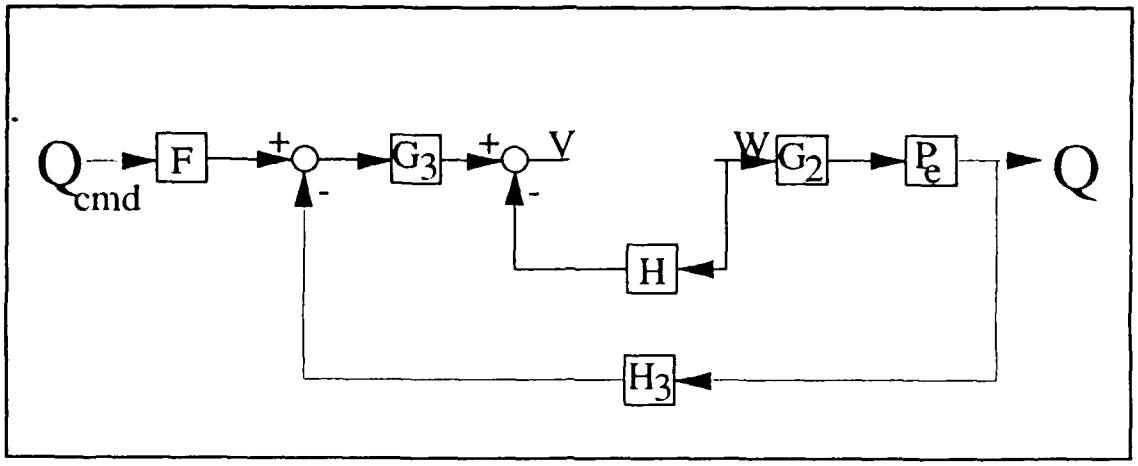

Figure 5.3. Tracking Control Loop with Command Limiting

$$V = FG_3Q_{cmd} - L_N W \tag{5.6}$$

where

$$L_N = H + G_2G_3H_3P_e \tag{5.7}$$

To provide the fastest possible return to linear operation, it is useful for the transfer function L_N to be Type 1 with little overshoot and be very fast with respect to the rest of the system (5:176). Therefore, it is desirable to have

$$L_N = \frac{K}{s} \tag{5.8}$$

From Eq (3.15), obtain

$$G_2G_3H_3 = L_{3c}(1 + H) \tag{5.9}$$

Substituting Eq (5.8) and Eq (5.9) into Eq (5.7) yields

$$\frac{K}{s} = L_{3c}(1+H)P_e + H \tag{5.10}$$

If $H \gg 1$ over the frequency range of interest, then Eq (5.10) simplifies to

$$\frac{K}{s} \approx (L_{3c}P_e + 1)H \tag{5.11}$$

Rearranging and using Eq (5.3) gives

$$H \approx \frac{K}{s}\frac{1}{1+L_{3c}P_e} \approx \frac{K}{s(1+L_3)} \tag{5.12}$$

By Defining

$$P_3 = \frac{L_3}{1+L_3} \tag{5.13}$$

Eq (5.12) becomes

$$H \approx \frac{KP_3}{sL_3} \tag{5.14}$$

Substituting Eq (5.4) into Eq (5.13) gives

$$P_3 = \frac{3.70 \times 10^8}{(231.3, 0.62)(-35.5)(5.9, 0.32)(-5.54)} \tag{5.15}$$

Since the loop shaping process completely determines both the open loop and closed loop transfer functions (L_3 and P_3, respectively), K can be chosen without affecting the loop transmission (although G_2 and G_3 are affected). Letting K=10, substituting Eq (5.4) and Eq (5.15) into Eq (5.14) and removing pole-zero pairs which nearly cancel gives

$$H = \frac{10(7.91, 0.58)}{(5.9, 0.32)(-5.54)} \tag{5.16}$$

Since L_3 is Type 1, the free s cancels, which results in Eq (5.14) and Eq (5.16) being Type 0.

5.3 Compensator Placement

In deciding where to place the various parts of the outer loop compensator, it is important to notice that the input to the command limiter is also a function of Q_{cmd} filtered by F and G_3. If a large enough command is held for a sufficiently long time, the command limiter will saturate and eventually drive the stabilator to a constant value (near maximum). Figure 5.4 qualitatively shows the significant variables as the system responds to a large step command. Since the basic plant transfer function (Q/Y) is Type (-1), Q will approach zero in steady state(because of the constant input to a differentiator). Because the stabilator transfer function (P_y) is Type 1, its input (R_1 from Figure 3.1) must eventually go to zero to achieve constant stabilator deflection angle. Unless G_2 contains a differentiator, its input (W) must also go to zero. Eq (5.6) becomes

$$V = FG_3Q_{cmd} \tag{5.17}$$

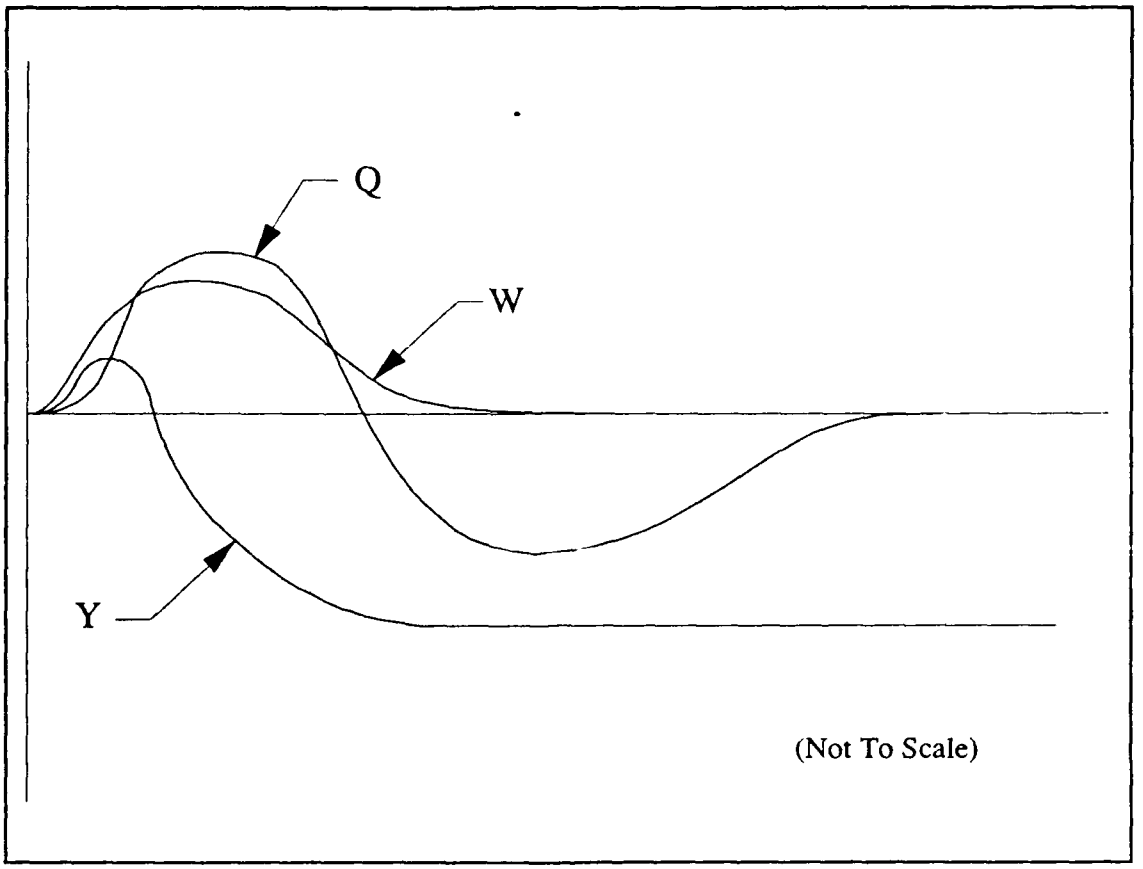

Figure 5.4. Large Command Response

If, for a very large command input, the integrator of the loop compensator is placed in G_3 , then, for the entire time the command limiter is saturated, the input to the limiter will be continually increasing.

At some point in the future, when the pilot commands some sub-maximal pitch rate, the aircraft will not be able to respond to that command reduction until the integral of the negative error returns V to the linear range. The time it takes to unsaturate the command limiter is dependent upon the length of time the limiter is saturated.

The delay between the command and the action would result in an overshoot of the desired pitch angle because the aircraft would continue to pitch at maximum rate

throughout the delay. While some delay is unavoidable, the time it takes to unsaturate the command limiter should be the same no matter how long the limiter was saturated. Therefore, it is undesirable to integrate the input before the command limiter. Thus G_3 should be Type 0. Since H is Type 0, so is $(1+H)^{-1}$. This places the integrator of L_{3c} in G_2.

As before, the feedback compensator H_3 can contain any RHP zeros of L_{3c} to remove them from the closed loop transfer function. For Cases 1 and 5, it is beneficial to add a RHP zero to L_{3c} and $H_3 \neq 1$. See Appendices B and F. For all other cases, $H_3 = 1$.

Substituting Eqs (4.23) and (5.26) into Eq (5.2) and solving for G_3 gives

$$G_3 = \frac{-5.17(7.99, 0.41)(0.12, 0.06)}{(-0.012)(-0.03)(5.9, 0.32)(-5.54)} \tag{5.18}$$

5.4 Prefilter

The prefilter produces the desired closed loop frequency response characteristics over the frequency range of interest. Figure 5.5 shows the log magnitude plot of P_3 for case 6.

The prefilter necessary to obtain the desired characteristics shown in Figure 5.5 over the frequency range 0.1 to 20 rad/sec is

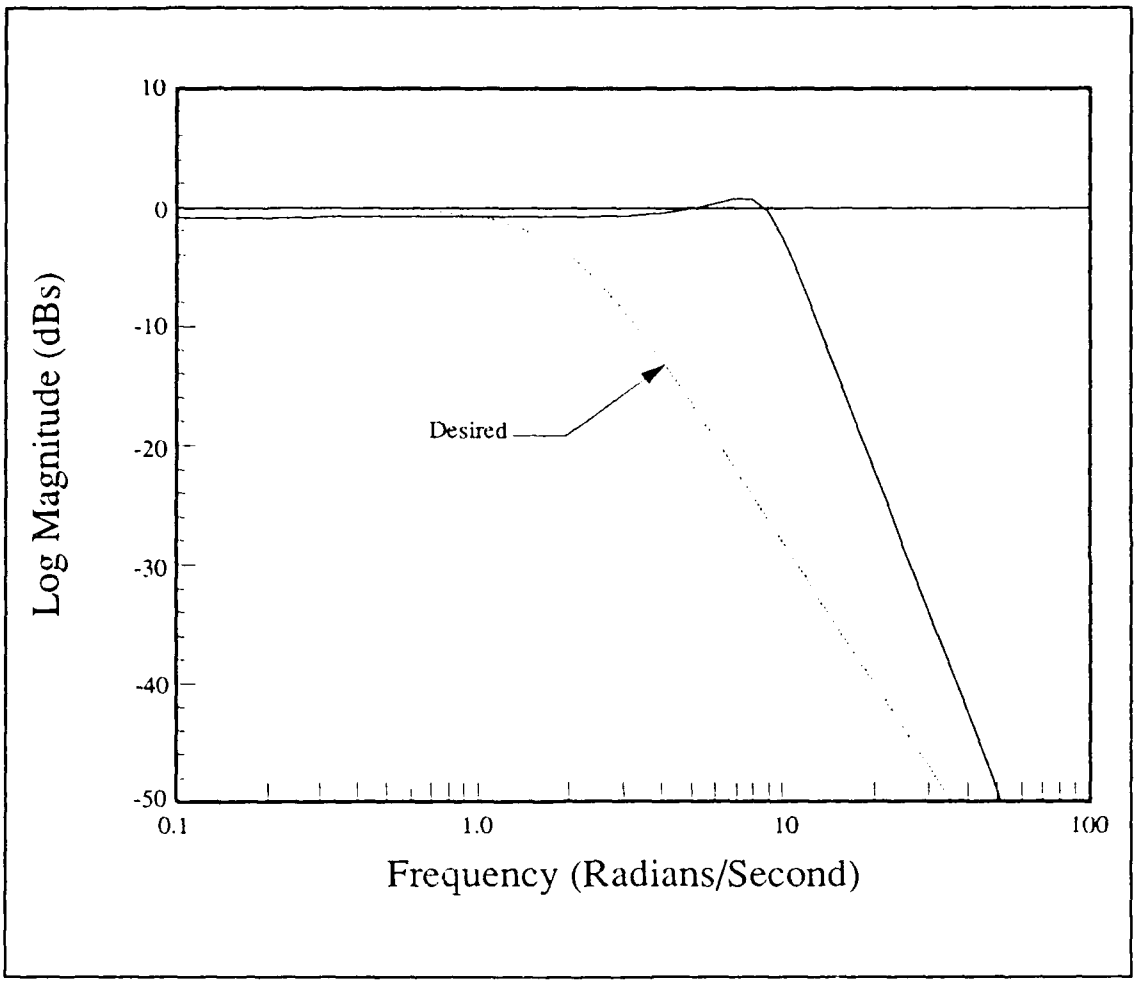

Figure 5.5. Closed Loop Frequency Response Without Prefilter

$$F = \frac{2.20(5.92, 0.32)(-5.2)}{(-1^{\wedge}0)(2, 0.8)} \tag{5.19}$$

and yields the desired frequency response shown in Figure 5.6.

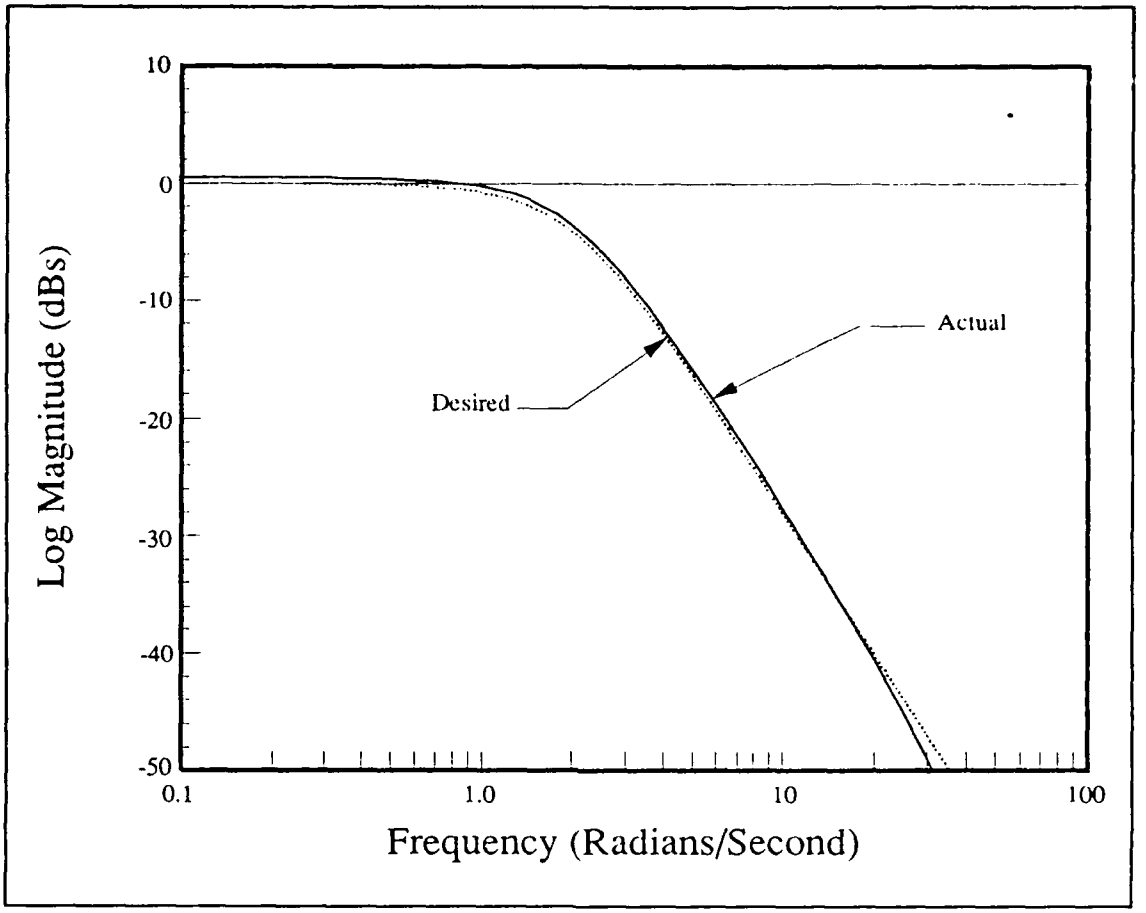

Figure 5.6. Closed Loop Frequency Response with Prefilter

VI. Final Design and Simulation

6.1 Simulation Setup

Figure 6.1 shows the final block diagram to be implemented.

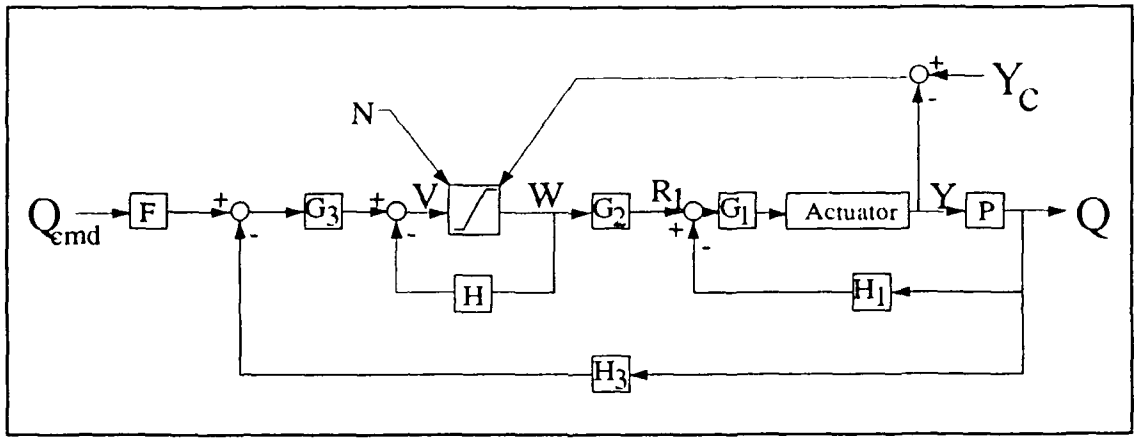

Figure 6.1. Final Block Diagram

Simulations are performed using the System_Build feature of the software package MATRIX$_x$. Each of the component pieces of the block diagram of Figure 6.1 are placed in state space form, connected together, and simulated under the control of System_Build. While MATRIX$_x$ is primarily a linear design tool, System_Build allows non-linear elements to be included in the system to be simulated (13).

System_Build includes several pre-defined non-linear elements which can be added to a system, but it lacks the elements necessary to define the actuator with its limits and the command limiter. Therefore it is necessary to define these elements in FORTRAN and link the new routines with MATRIX$_x$ (13).

6.1.1 Actuator. The actuator has a third order linear model and its state space representation has states representing position, velocity and acceleration. The position and velocity limits are presented in Section 2.3. Acceleration is assumed

unlimited. In creating the non-linear model, there is a great temptation to implement the linear model and then simply limit the output. However, this does not accurately reflect the behavior of a real actuator. If velocity saturates, acceleration must go to zero. Similarly, if position saturates both velocity and acceleration must go to zero. Therefore the linear and nonlinear elements of the model must be blended together into one unit.

To implement such a model as a $MATRIX_x$ user code routine requires defining state and output equations in the following format (13:SB 6-2):

$$\begin{aligned} \dot{x} &= f(t, x, u) \\ y &= h(t, x, u) \end{aligned} \tag{6.1}$$

where

t is the current value of time

x is the current state value

u is the current input value

Figure 6.2 shows the logic flow chart for the actuator model user code routine.

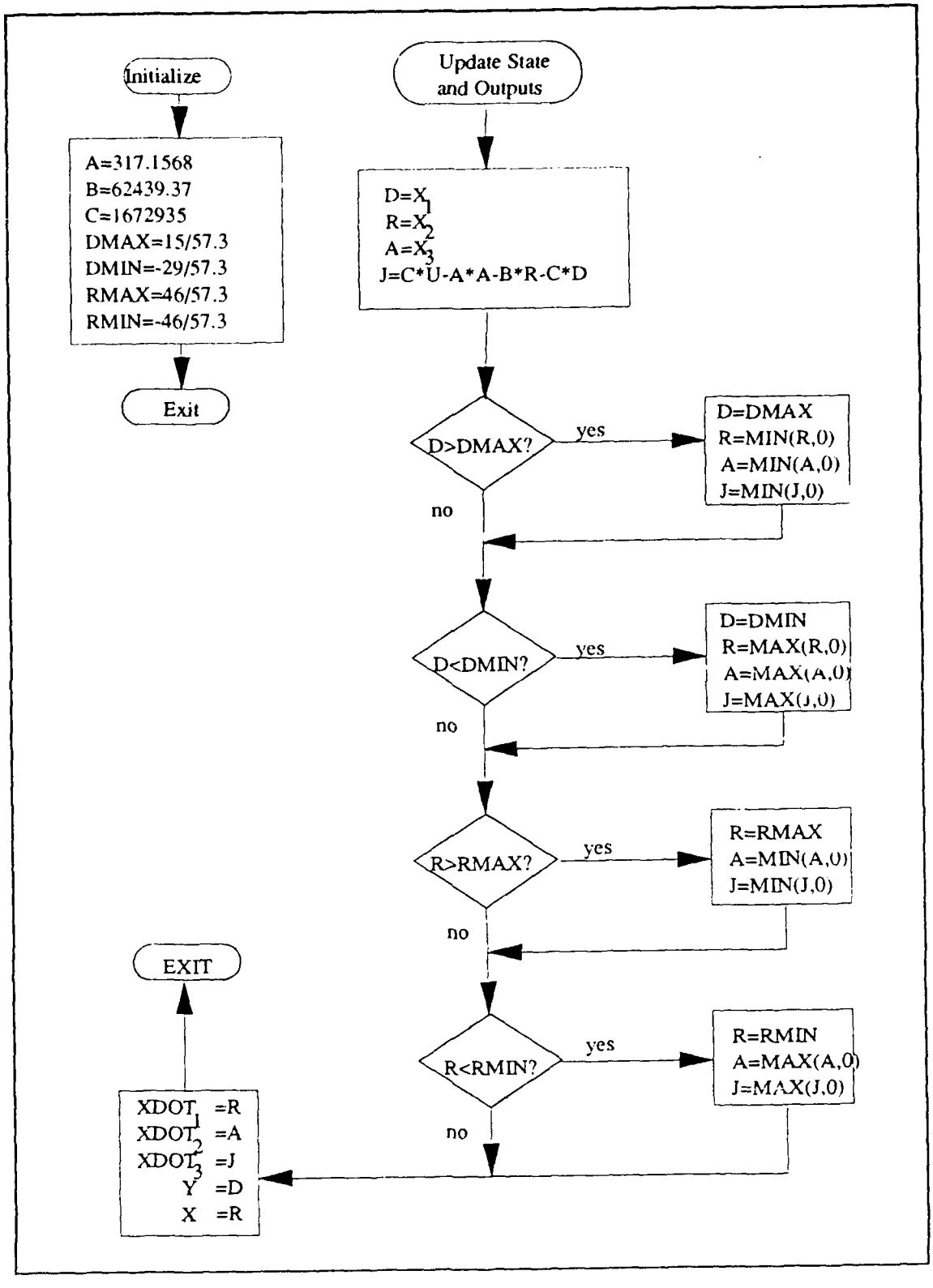

Figure 6.2. Actuator Model User Code Routine Flow Chart

6.1.2 Command Limiter. The command limiter does not contain any dynamic elements and is simply an adjustable limiter. The routine has three inputs. The first is the quantity to be limited (V of Figure 5.1). The second and third inputs are the upper and lower limits respectively. Figure 6.3 shows the logic flow chart for the command limiter.

Since there are both upper and lower limits, there are, in fact, two feedback loops for saturation control. Also, two different values of, Y_c, are input to the system. The upper limit, driven by its respective feedback loop and value of Y_c, attempts to drive the stabilator to its maximum positive value. Conversely, the lower limit, driven by its respective feedback loop and value of Y_c, attempts to drive the stabilator to its maximum negative value. Since the upper and lower values of Y_c are constants, the difference between the upper and lower limits is also a constant. This defines a sliding window of acceptable output values.

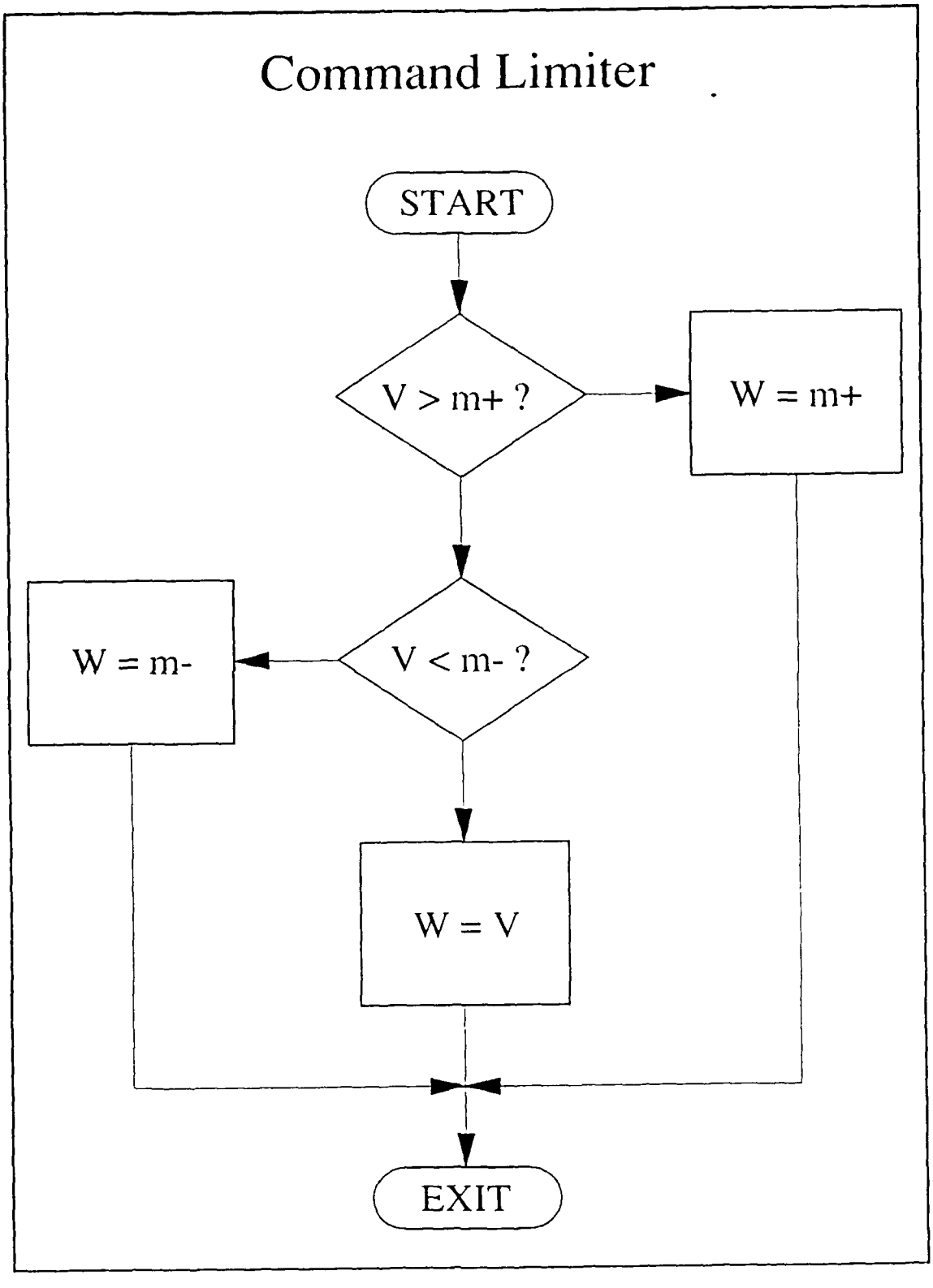

Figure 6.3. Command Limiter User Code Routine Flow Chart

6.2 Simulation Results and Analysis

Several simulations are performed to test the various aspects of the design. The time span for all simulations is 20 seconds.

For each simulation, time response plots of pitch rate, stabilator deflection, and command limiter activity are presented. The pitch rate plots also show the time response of the desired second order model presented in Section 2.4.

6.2.1 Deflection and Rate Cutoff Values. The first simulation must be performed to determine the appropriate value of Y_c. A very large pitch rate is commanded and the actuator is configured to be completely linear. A simulation is performed with Y_c set to the actual stabilator limits. Figure 6.4 shows the deflection control loop time response to a 1000 radian/second pitch rate command for each of the six cases. Y_c^+ is set to +15 degrees and Y_c^- is set to -29 degrees.

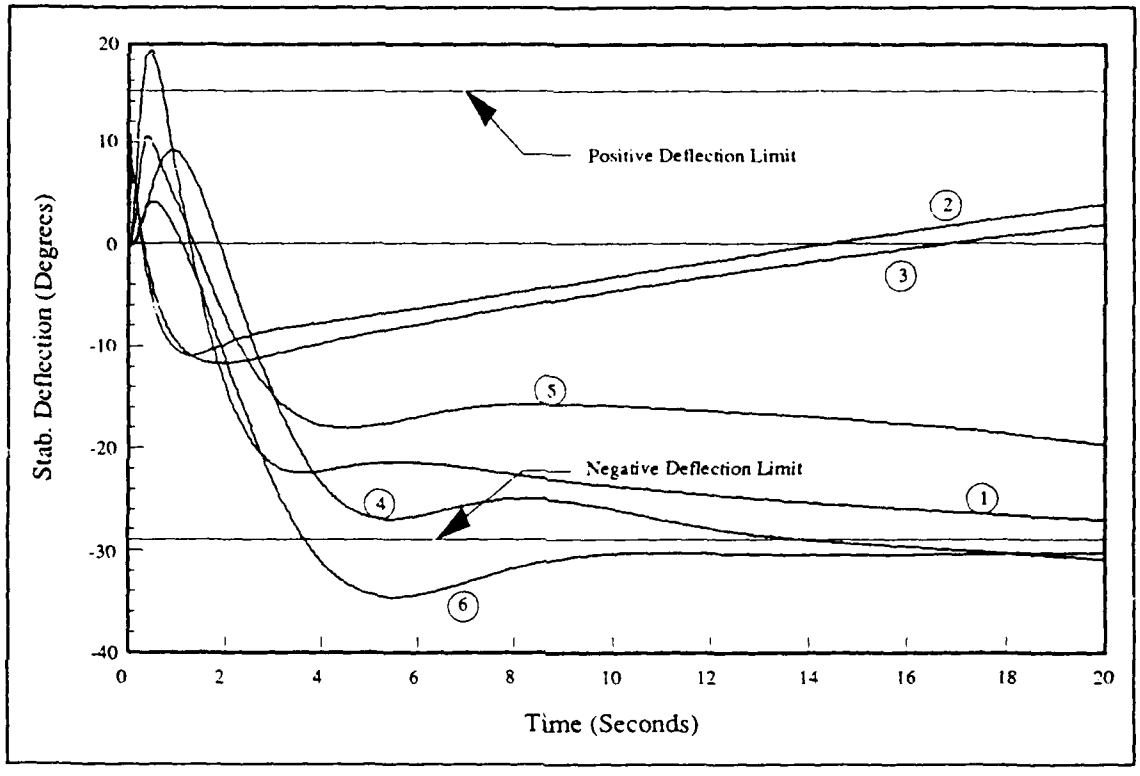

Figure 6.4. Deflection Control Loop Time Response

Case 1 shows an initial spike above the positive limit, then a rapid reversal to near the negative limit where it eventually settles. The initial peak is well below the positive limit for all the other cases. Because the initial saturation does not threaten loss of control, it is ignored. Cases 4 and 6 both show some overshoot of the negative limit. Case 6 is the worst with an approximate 20% overshoot. Cases 2 and 3, which each have a second real RHP zero, have a small initial positive peak and a quick reversal. The second peak is well short of the negative limit. The second reversal is quite slow, and after 20 seconds the deflection angle is still well short of the positive limit.

To accommodate the 20% overshoot of Case 6, Y_c is reduced by about 20% for the subsequent simulations. For Cases 2 and 3, it is obvious that the saturation control loop is constraining the stabilator to about half its full authority, and therefore, it is hampering performance. Considering that both cases occur at high speed (Mach 0.9), it is reasonable to guess that deflection saturation would be a very rare occurrence. So subsequent simulations of Cases 2 and 3 are performed with Y_c^+ set to 100 degrees and Y_c^- set to -100 degrees to test the hypothesis. For all other cases, Y_c^+ is set to 15 degrees and Y_c^- is set to -23 degrees

6.2.2 Small Step Command. The next simulation commands a constant one degree/second pitch rate for the entire time period. This command is small enough that all six cases should be able to follow the command and remain linear. The stabilator should not approach any of its limits and the saturation control loop should not take control. This tests the linear design for the desired time response. Figures 6.5 through 6.8 shows the simulation results for a step one degree/sec pitch rate command.

All cases except 1 and 5 follow the command quite well and have nearly identical responses. The rise of Cases 1 and 5 is also satisfactory but they both begin a gradual fall. This is caused by the RHP zero in their basic plants.

Clearly the linear design is highly successful. The actual time response is nearly indistinguishable from the second order model for the small pitch command. The small stabilator deflection and negligible saturation element activity is reasonable for this small command and flight condition.

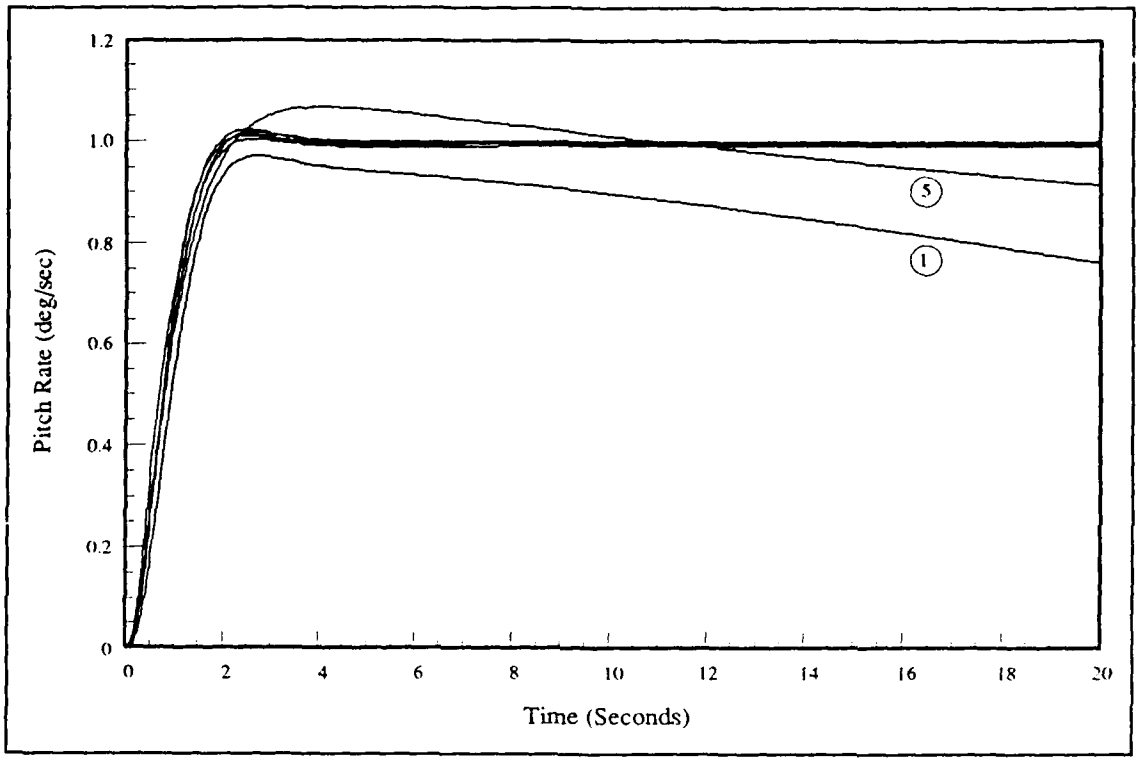

Figure 6.5. Pitch Rate for a Small Step Command

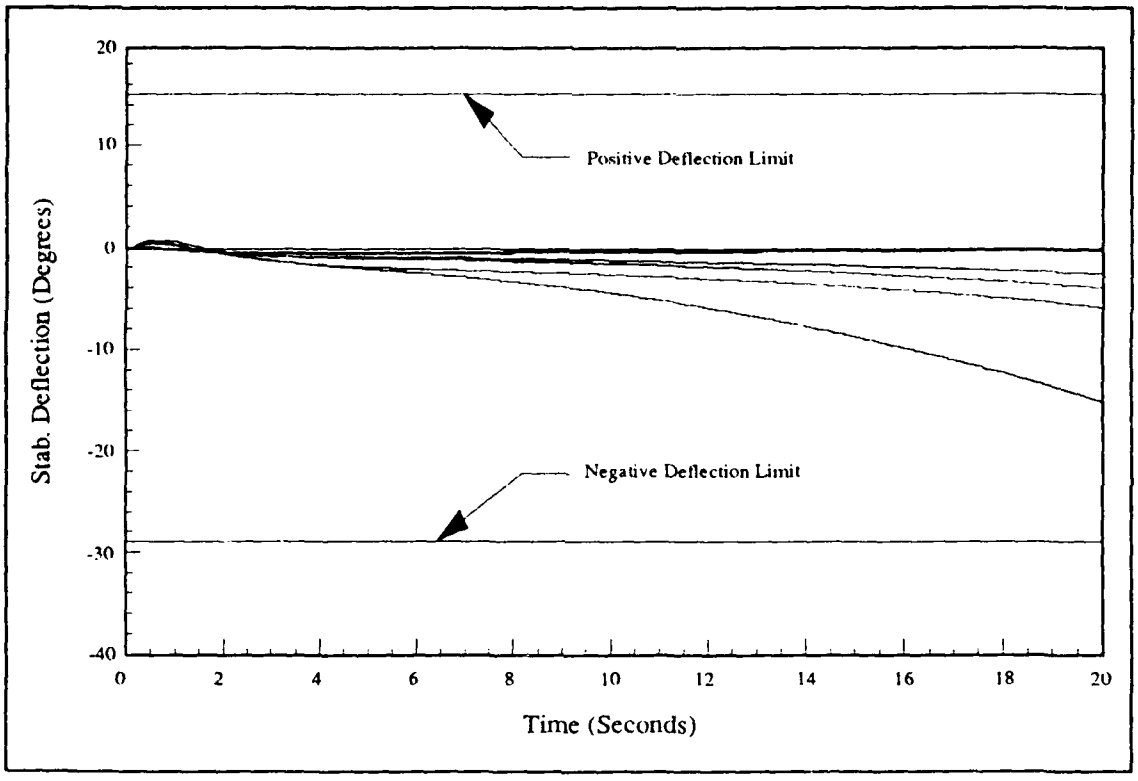

Figure 6.6. Stabilator Deflection for a Small Command

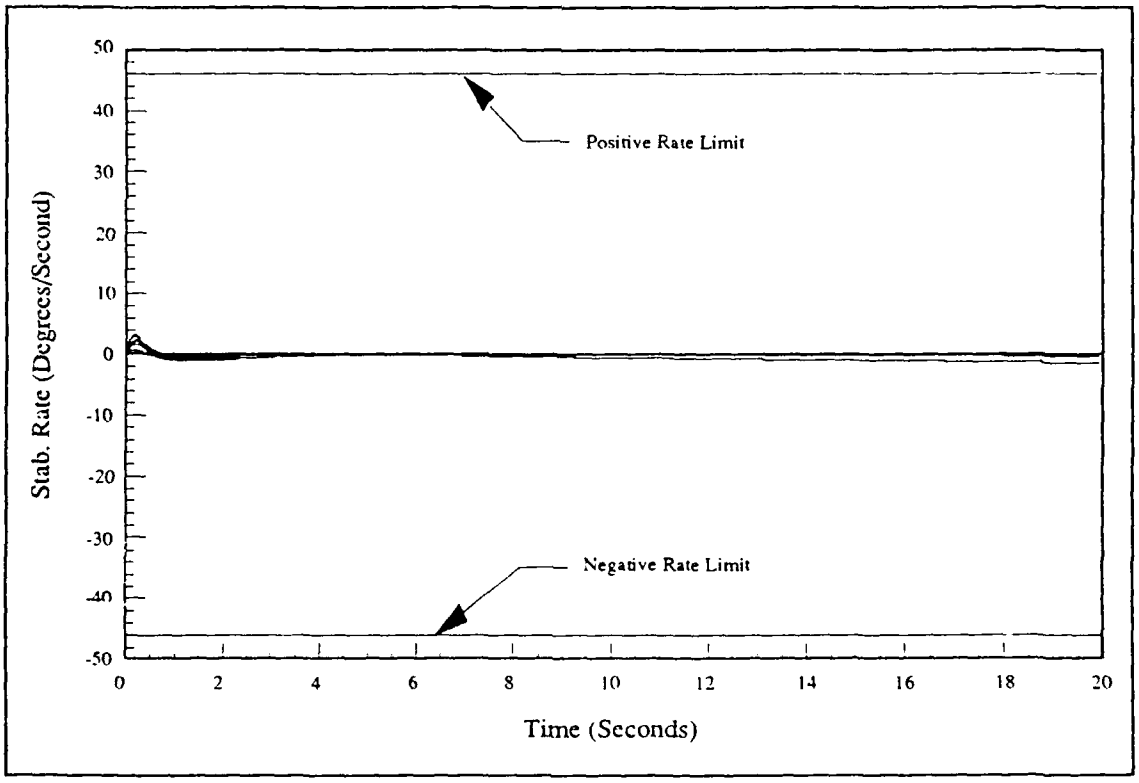

Figure 6.7. Stabilator Rate for a Small Step Command

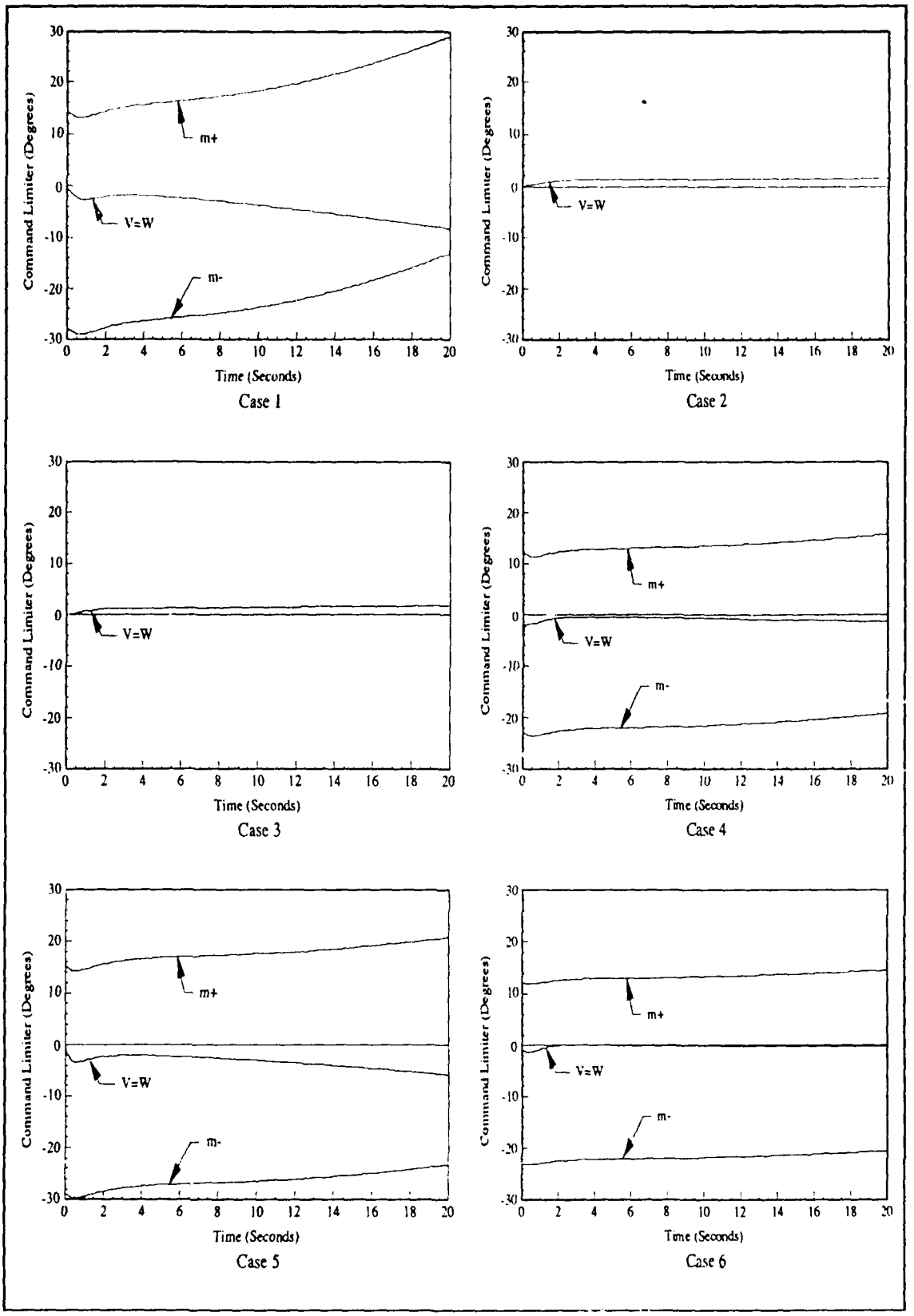

Figure 6.8. Command Limiter Activity for a Small Step Command

6.2.3 Moderate Step Command. This simulation tests the action of the saturation control loop as the stabilator approaches its limit gradually during a moderate pitch up. A 20 degree/second step command is used here except for Cases 1 and 5. Cases 1 and 5 saturate with much smaller commands so a 5 degree/second step command is used. Figures 6.9 through 6.12 show the simulation results.

Initially, all cases follow the command well. Sometime later, the stabilator approaches the limit and the saturation control loop takes over and forces a pitch rate reduction. For Case 4, this happens immediately since 20 degrees/second is slightly beyond its capabilities. Stabilator deflection angles and rates remain within limits. Cases 2 and 3 have no trouble following the command for the entire time and the deflections and rates stay well within limits.

The abrupt command onset causes immediate saturation of the command limiter. All cases except number 4 come out of saturation within 2 seconds. The effects of this is evident in the slightly slower than desired rise of the pitch rate. However, the delay is insignificant and peak time, peak value, and settling time is virtually identical to the model. As the airplane continues to pitch up, the stabilator angle continues to increase. After several seconds the saturation control loop takes over to prevent saturation of the stabilator.

When this happens, the pitch rate begins to decrease and the stabilator deflection angle stabilizes near the negative limit. The pitch rate continues to decrease, until it actually goes negative. This is easily explained by considering an aircraft which has pitched up to an extremely nose high attitude. After some period of time, the airspeed will decrease to a point beyond which the nose must be lowered to maintain aircraft control. It is not enough to simply stop pitching. The aircraft must pitch down.

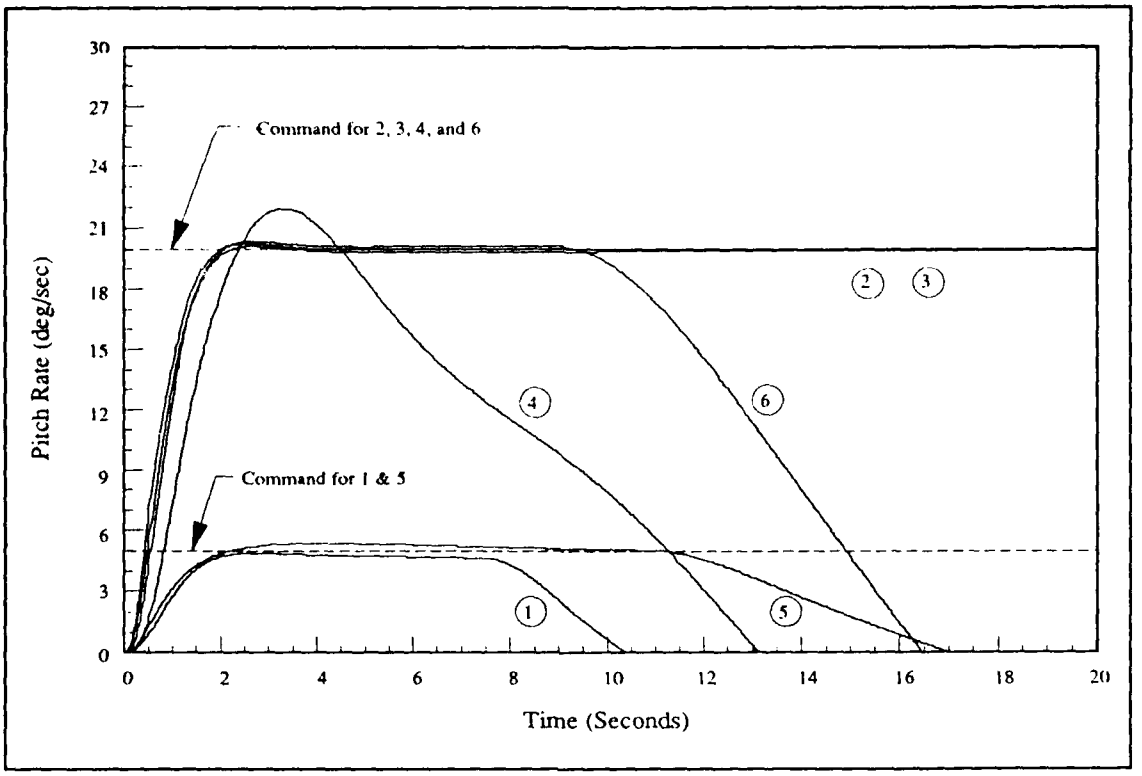

Figure 6.9. Pitch Rate for a Moderate Step Command

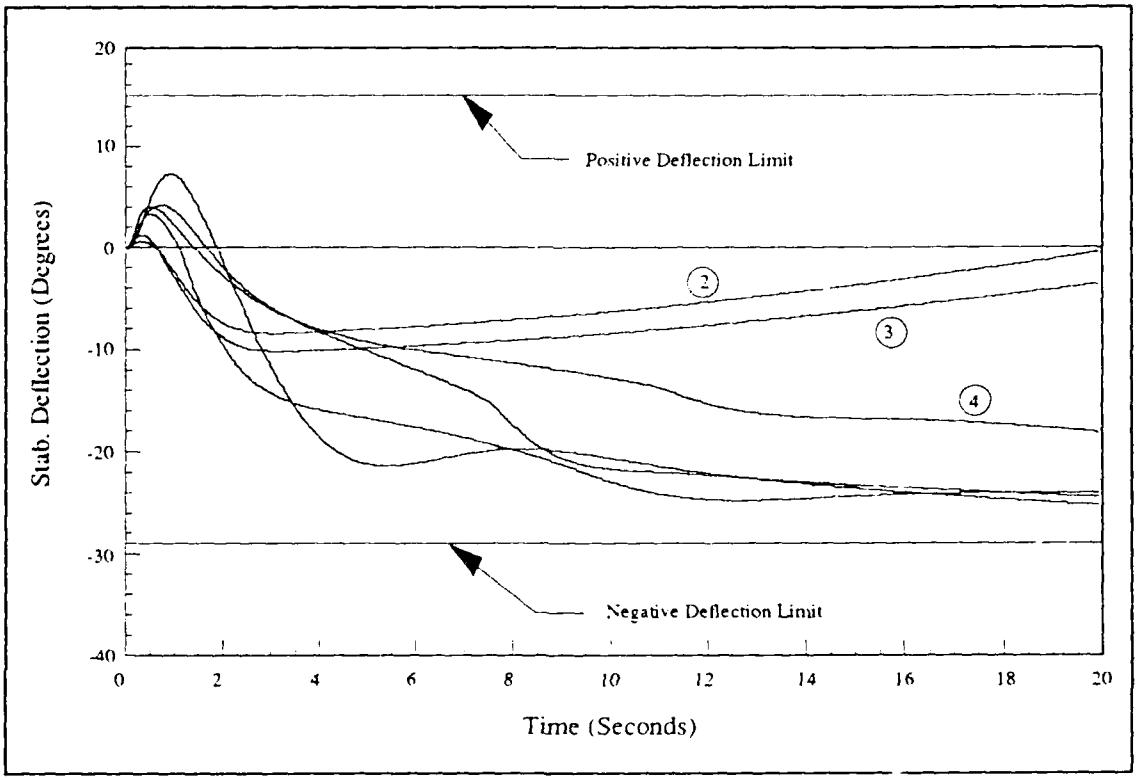

Figure 6.10. Stabilator Deflection for a Moderate Command

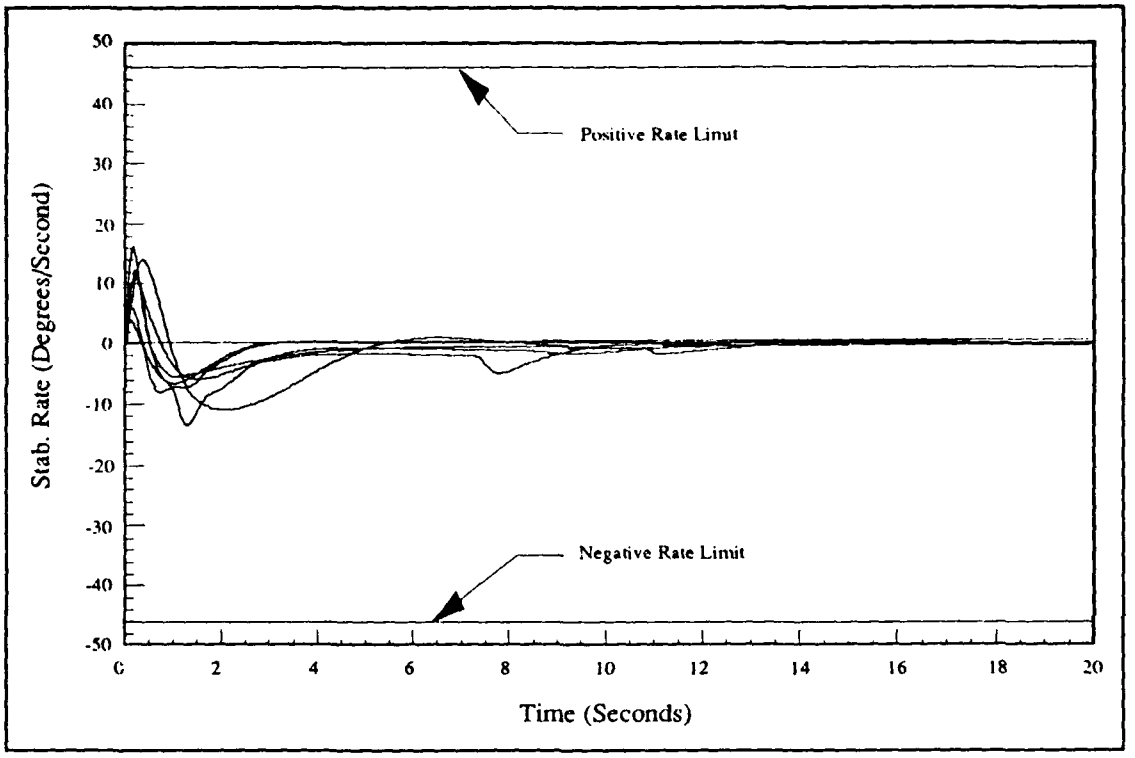

Figure 6.11. Stabilator Rate for a Moderate Step Command

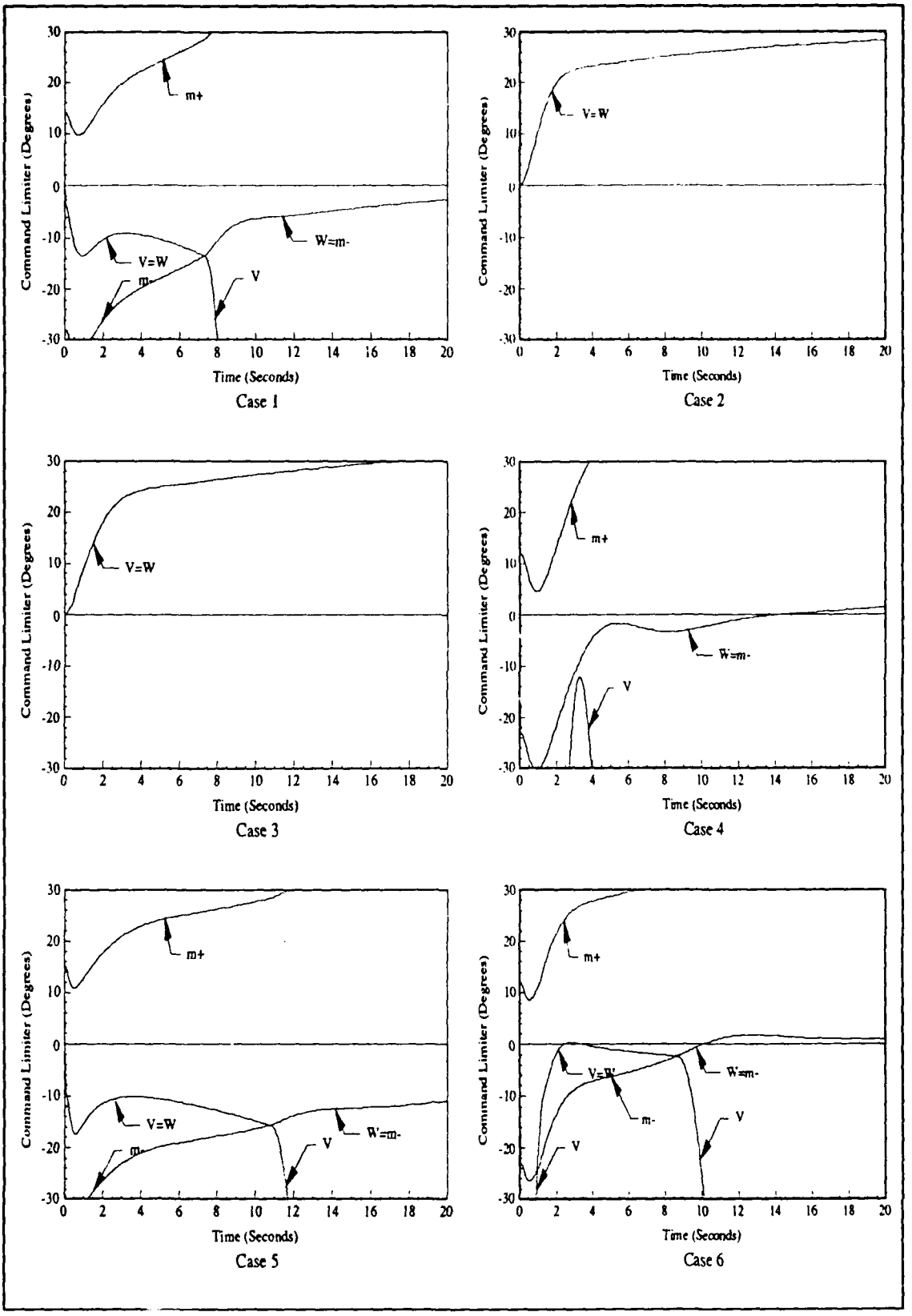

Figure 6.12. Command Limiter Activity for a Moderate Step Command

6.2.4 Large Step Command. The next simulation test the action of the saturation control loop in response to the abrupt application of a very large command input. Figures 6.13 through 6.16 shows the simulation results for a 50 degree/second step command.

Again Cases 2 and 3 have no trouble following the command, but now the stabilator deflections are approaching the limits so this is probably nearly maximum performance. Positive saturation would occur if this command is maintained long enough, but such a command is not a reasonable maneuver for an aircraft at Mach 0.9. All other cases are unable to reach the commanded value and the saturation control loops take over during the rise. Deflections and rates all remain within limits.

In this simulation, the command limiter saturates immediately and remains saturated throughout. Rise rate is slower than desired and the pitch rate reaches a peak value significantly below the desired value. After which, the pitch rate begins to decrease in a manner similar to that shown in Figure 6.9. Figure 6.15 demonstrates that even with extreme commands, stabilator rate remains below the 46 degree/second limit and a rate saturation control loop is not needed. Again the behavior is perfectly reasonable and the design functions as intended.

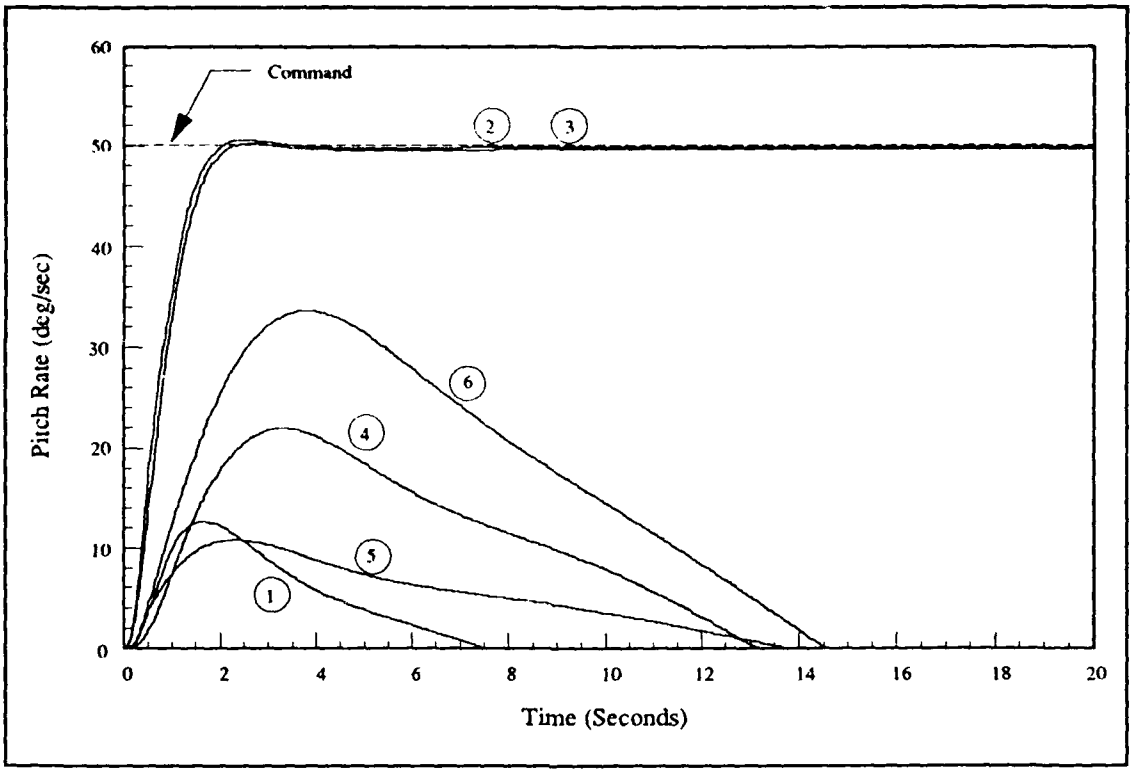

Figure 6.13. Pitch Rate for a Large Step Command

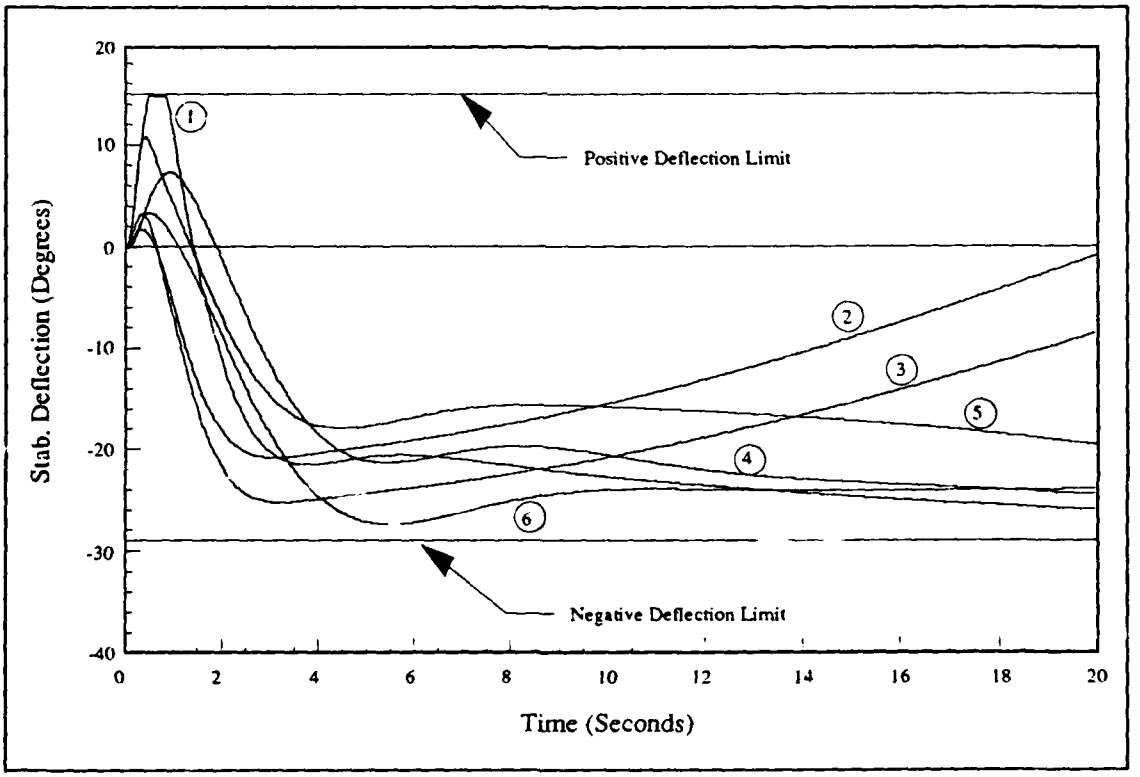

Figure 6.14. Stabilator Deflection for a Large Step Command

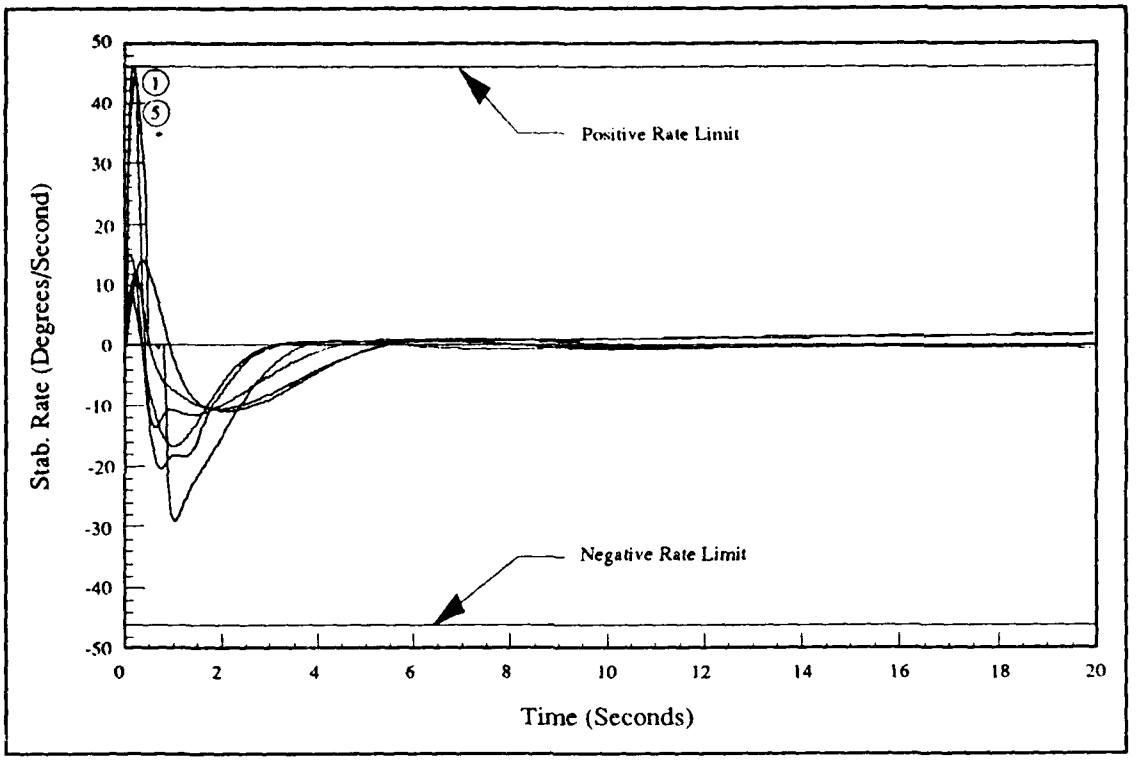

Figure 6.15. Stabilator Rate for a Large Step Command

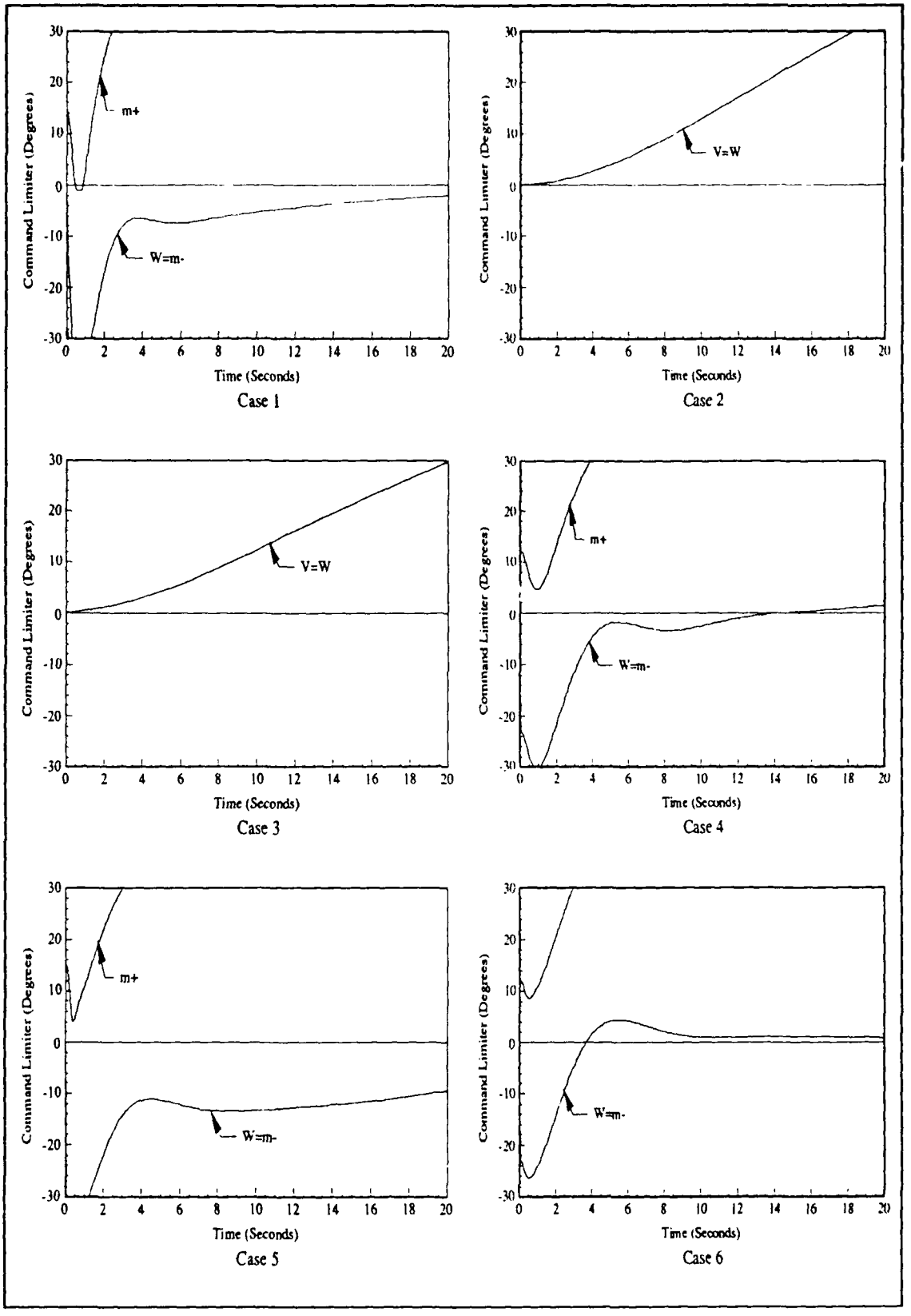

Figure 6.16. Command Limiter Activity for a Large Step Command

6.2.5 Pulse Command. The last simulation tests the ability of the system to respond when the stabilator is already near the limit. A 20 degree/second pulse command is used here. The duration of the pulse is 10 seconds. Again, a 5 degree/second command is used for Cases 1 and 5. The simulation results are shown in Figures 6.17 through 6.20.

Again Cases 2 and 3 have no trouble following the commands. All other cases follow the initial command quite well. For those systems with unsaturated command limiters when the pulse ends, the aircraft responds immediately and the pitch rate reduces as expected. Cases 1 and 4 enter command limiter saturation well before the pulse ends. For these cases, V never falls far enough to unsaturate the limiter and pitch rate continues to decrease under the command of the saturation control loop. For Case 6, the pulse ends just after the command limiter saturates. When the command goes to zero, V falls quite rapidly and unsaturates the limiter returning control to the tracking control loop. Case 6 tracks the return to zero and maintains the value until the deflection again approaches the limit and then the saturation control loop takes over again and forces a pitch down.

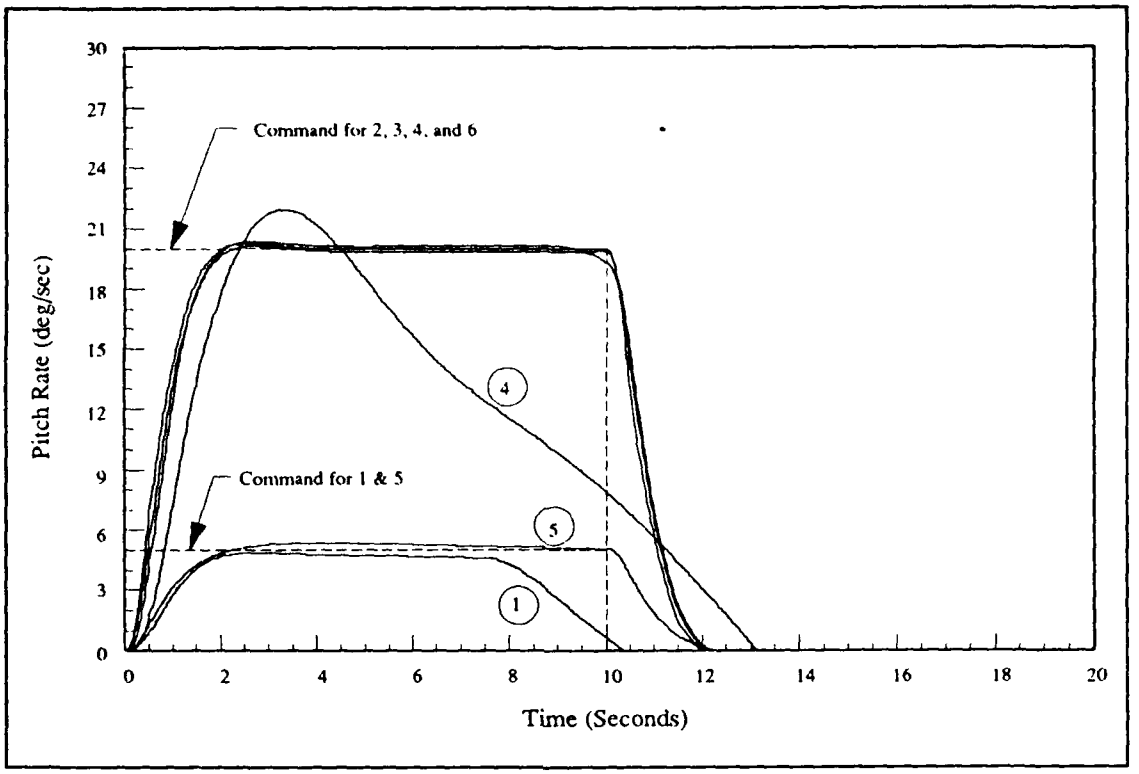

Figure 6.17. Pitch Rate for a Pulse Command

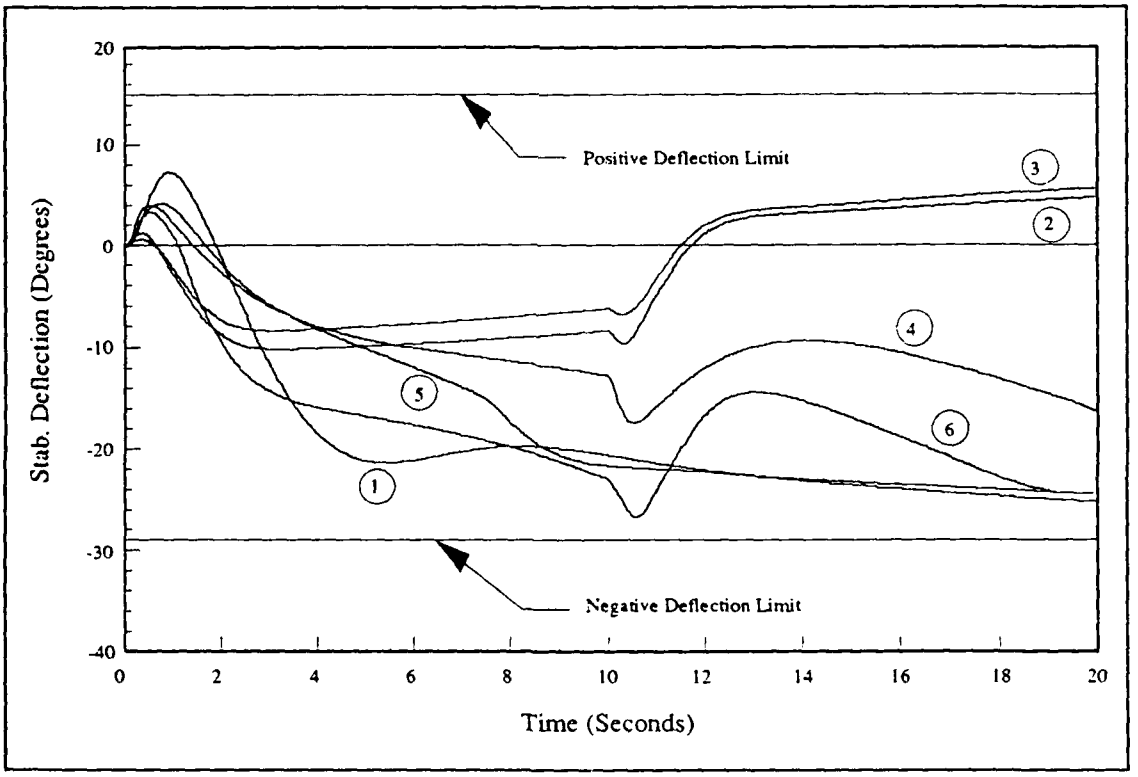

Figure 6.18. Stabilator Deflection for a Pulse Command

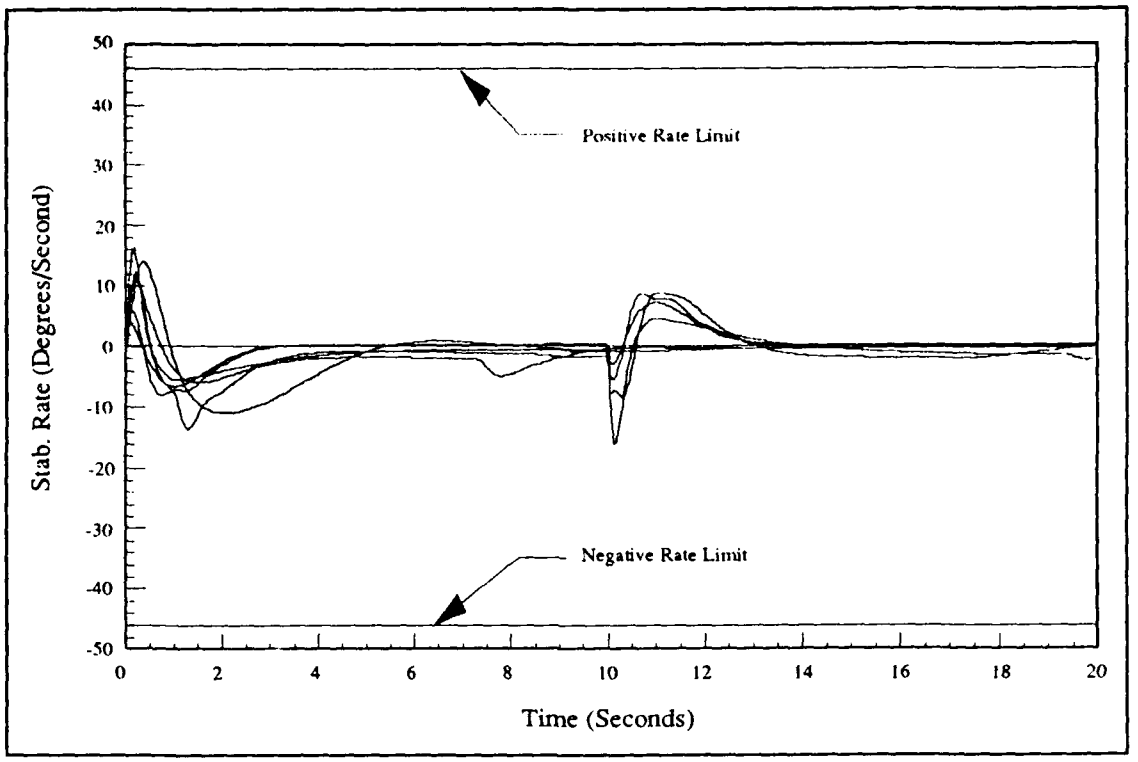

Figure 6.19. Stabilator Rate for a Pulse Command

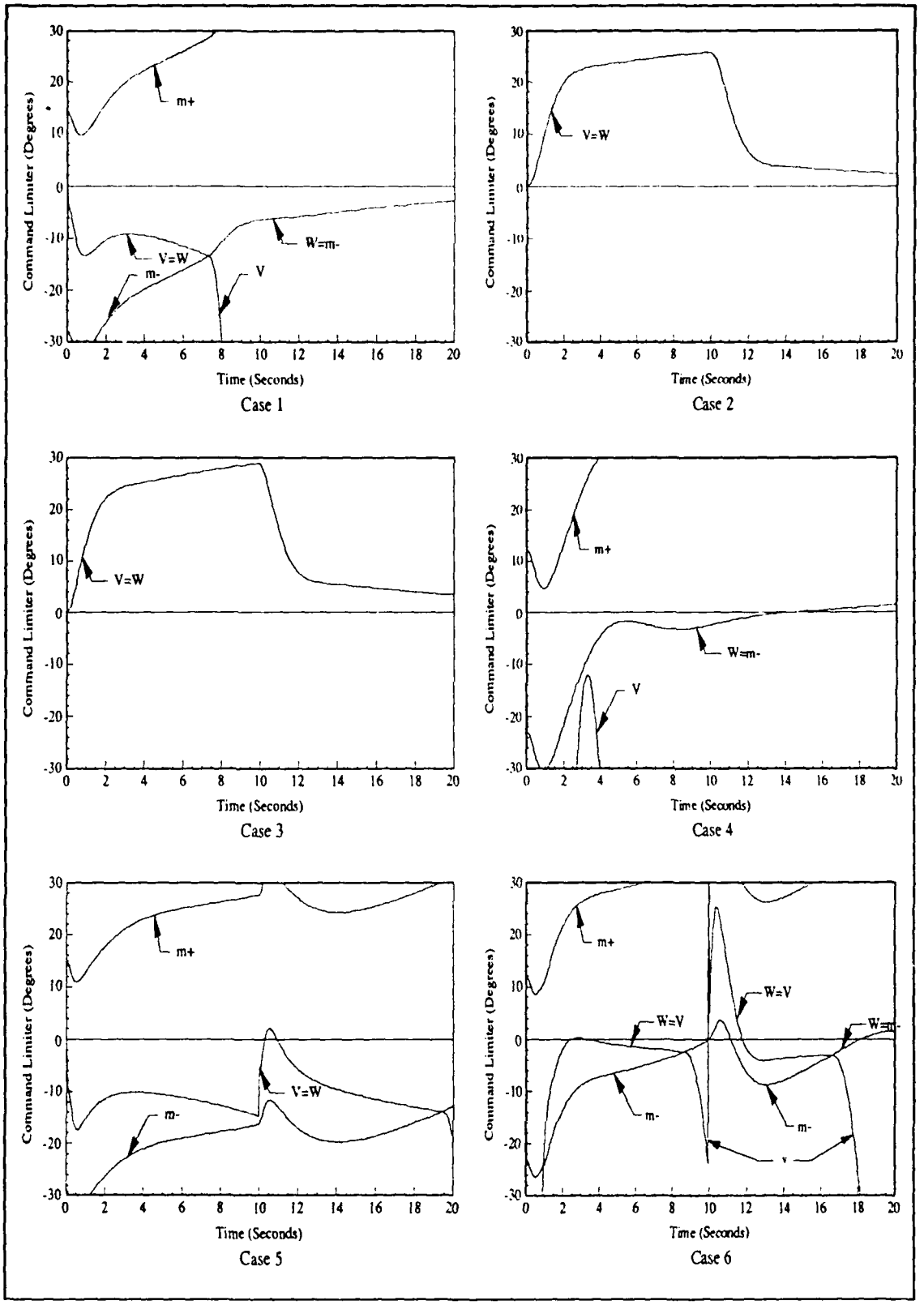

Figure 6.20. Command Limiter Activity for a Pulse Command

VII. Conclusions and Recommendations

7.1 Discussion

This thesis demonstrates the application of relatively straightforward linear design techniques to a problem containing highly nonlinear elements. It also attempts to create a single set of compensators which produce satisfactory responses over the entire subsonic flight envelope using a QFT approach.

While it is certainly true that an unstable airplane requires protection from control surface saturation, it is not clear that this protection is needed in all regions of the flight envelope. Consider an aircraft beginning a steady pitch up at the bottom of a circular vertical loop flight path. The airplane generates an angular velocity Ω as it travels in a circular path of radius r with a forward velocity U.

A particle in circular motion generates radial acceleration equal to the product of its angular velocity and its tangential velocity (3:255). Thus, the normal acceleration needed to hold the aircraft in its loop is (including gravity)

$$a_n = \Omega U + g \tag{7.1}$$

Since the forward velocity vector is always approximately at right angles to the radius of the circle, the angular velocity equals the angular rate of change of the velocity direction ($\Omega \approx Q$) . Dividing both sides by g, Eq (7.1) becomes

$$N_z = \frac{QU}{g} + 1 \tag{7.2}$$

where

N_z = Normal acceleration at Center of Mass (g's)

Table 7.1 lists the calculated "g" forces for each of the six cases for a 20 degree/second pitch rate command. The 20 degree/second pitch rate command necessary to well saturate the command limiter for Cases 2 and 3 produces very large "g" forces even though the stabilator could be allowed closer to its limit. These "g" forces are already near or beyond the structural limits of the aircraft and further increases would be pointless or even destructive. Thus, it is obvious that, in certain regions of the flight envelope, it would be very unlikely to encounter the stabilator deflection limit without first encountering some other operational constraint.

Table 7.1. Normal Acceleration for a 20 deg/sec Pitch Rate

Case	U (ft/sec)	N_z(g's)
1	222.73	3.42
2	1002.34	11.87
3	831.22	10.02
4	302.00	4.28
5	239.56	3.60
6	431.22	5.68

7.2 Conclusions

1. It is possible to stabilize the aircraft over all six flight conditions presented here with a single compensator designed with the aid of QFT techniques. However, the effective plants, P_e and P_y, contain varying numbers of RHP zeros. Additionally the variation in the location of the RHP zeros covered a fairly large frequency range. These factors make a single compensator set for the saturation control loop and the tracking control loop impossible if at least Type 1 open loop transfer functions are maintained.
2. Stabilization of all six conditions is only possible if Regions B and D are sufficiently "far apart" in the low frequency templates. This is assumed true for this

aircraft. Further investigation of many more points in the flight envelope between Cases 2 and 5 may prove the assumption false. But the analysis process is valid whether the assumption is true or false. If false, it only proves that a single compensator will not stabilize this airplane over the entire flight envelope. It says nothing about any other aircraft. If the assumption is true, then this thesis directly demonstrates QFT's ability to stabilize extremely varied plants under certain circumstances.

3. Even though a single compensator set cannot handle the entire design problem for these flight conditions, the major portion of this thesis is quite successful. Each portion of the design process is a fairly simple linear design problem and can be accomplished by any of a number of conventional techniques. The potential pitfalls in the process are documented with each design step and are largely a matter of carefully considering the locations of the integrators in the problem.

4. Although not a limitation, the approach works best when the basic plant contains only one RHP zero. A second RHP pole becomes a second RHP zero in the saturation control loop, causing an additional reversal in its time response which, in turn, makes maximum performance difficult to produce. Protection from saturation is still achieved.

5. A more complicated nonlinear approach may produce better performance. However, for Cases 2 and 3, which exhibit the second reversal, it is doubtful whether improved performance would be either beneficial or desired.

6. Using these methods, a control system can be designed for a practical problem involving a modern, unstable, jet fighter aircraft. By dealing with the stabilator limits as a known quantity at the beginning of the design instead of deliberately ignoring the non-linearities which normally make linear design techniques difficult or impossible, a control system can be fashioned which provides satisfactory

performance. This avoids much of the trial and error of other techniques and increases the probability that the design will give satisfactory results with a minimum of "tweaking".

7. The primary advantage of this approach is that the solution is a "closed loop" solution. It is more insensitive to modelling inaccuracies than an approach which limits the command at the prefilter. This allows the designer to add less "safety factor", giving the system potential for higher performance. In other words, the system can operate closer to the limits more of the time.
8. The success of this design suggests the approach may be useful for controlling other factors which limit the aircraft's performance such as angle of attack or normal acceleration.

7.3 Recommendations

1. The primary hindrance to the goal of a QFT design for this problem is the extreme variation of the plant parameters. This problem should be reworked with a much smaller region of the flight envelope containing many more sample points. An alternative is to use an aircraft with more benign characteristics.
2. This thesis uses only one of the available longitudinal controls for both stabilization and tracking control. This design should be reworked making use of the extra controls available.
3. Sensor delays, added sensor noise, and external disturbances are assumed negligible. These added complexities should be included in any further design study
4. The lateral and longitudinal modes were assumed decoupled to simplify the design. Another likely flight maneuver which might produce stabilator saturation is an extended high "g" steady turn. This maneuver should be examined.

Appendix A: Frequency Response Templates

Table 1. Frequency Template for 1.0000D-04 r/s

Case	Gain (dB)	Phase(deg)
1	-3.2351D+01	-2.3921D+00
2	2.5244D+01	-3.5985D+02
3	2.5248D+01	-3.5981D+02
4	-1.1086D+01	-1.7897D+02
5	-1.4913D+01	-3.6102D+02
6	8.9536D-01	-1.7953D+02

Table 2. Frequency Template for 1.7783D-04 r/s

Case	Gain (dB)	Phase(deg)
1	-3.2334D+01	-4.2484D+00
2	2.5244D+01	-3.5974D+02
3	2.5248D+01	-3.5966D+02
4	-1.1083D+01	-1.7817D+02
5	-1.4910D+01	-3.6181D+02
6	8.9601D-01	-1.7916D+02

Table 3. Frequency Template for 3.1623D-04 r/s

Case	Gain (dB)	Phase(deg)
1	-3.2282D+01	-7.5246D+00
2	2.5244D+01	-3.5953D+02
3	2.5248D+01	-3.5940D+02
4	-1.1074D+01	-1.7675D+02
5	-1.4900D+01	-3.6322D+02
6	8.9807D-01	-1.7850D+02

Table 4. Frequency Template for 5.6234D-04 r/s

Case	Gain (dB)	Phase(deg)
1	-3.2122D+01	-1.3216D+01
2	2.5244D+01	-3.5917D+02
3	2.5248D+01	-3.5893D+02
4	-1.1044D+01	-1.7423D+02
5	-1.4869D+01	-3.6572D+02
6	9.0458D-01	-1.7734D+02

Table 5. Frequency Template for 1.0000D-03 r/s

Case	Gain (dB)	Phase(deg)
1	-3.1652D+01	-2.2653D+01
2	2.5244D+01	-3.5852D+02
3	2.5248D+01	-3.5810D+02
4	-1.0952D+01	-1.6982D+02
5	-1.4772D+01	-3.7009D+02
6	9.2510D-01	-1.7527D+02

Table 6. Frequency Template for 1.7783D-03 r/s

Case	Gain (dB)	Phase(deg)
1	-3.0432D+01	-3.6524D+01
2	2.5245D+01	-3.5737D+02
3	2.5249D+01	-3.5662D+02
4	-1.0673D+01	-1.6227D+02
5	-1.4479D+01	-3.7754D+02
6	9.8938D-01	-1.7164D+02

Table 7. Frequency Template for 3.1623D-03 r/s

Case	Gain (dB)	Phase(deg)
1	-2.7940D+01	-5.2609D+01
2	2.5245D+01	-3.5533D+02
3	2.5251D+01	-3.5400D+02
4	-9.8917D+00	-1.5033D+02
5	-1.3663D+01	-3.8921D+02
6	1.1868D+00	-1.6535D+02

Table 8. Frequency Template for 5.6234D-03 r/s

Case	Gain (dB)	Phase(deg)
1	-2.4170D+01	-6.6313D+01
2	2.5245D+01	-3.5172D+02
3	2.5259D+01	-3.4938D+02
4	-8.0676D+00	-1.3442D+02
5	-1.1779D+01	-4.0439D+02
6	1.7602D+00	-1.5506D+02

Table 9. Frequency Template for 1.0000D-02 r/s

Case	Gain (dB)	Phase(deg)
1	-1.9632D+01	-7.5291D+01
2	2.5247D+01	-3.4540D+02
3	2.5279D+01	-3.4138D+02
4	-4.8577D+00	-1.1829D+02
5	-8.5024D+00	-4.1891D+02
6	3.2096D+00	-1.4038D+02

Table 10. Frequency Template for 1.7783D-02 r/s

Case	Gain (dB)	Phase(deg)
1	-1.4750D+01	-8.0034D+01
2	2.5247D+01	-3.3468D+02
3	2.5324D+01	-3.2823D+02
4	-5.4644D-01	-1.0565D+02
5	-4.1263D+00	-4.2868D+02
6	6.0758D+00	-1.2410D+02

Table 11. Frequency Template for 3.1623D-02 r/s

Case	Gain (dB)	Phase(deg)
1	-9.6598D+00	-8.1555D+01
2	2.5204D+01	-3.1810D+02
3	2.5326D+01	-3.0943D+02
4	4.4711D+00	-9.6706D+01
5	1.0126D+00	-4.3261D+02
6	1.0458D+01	-1.1074D+02

Table 12. Frequency Template for 5.6234D-02 r/s

Case	Gain (dB)	Phase(deg)
1	-4.2103D+00	-8.0345D+01
2	2.4881D+01	-2.9746D+02
3	2.4855D+01	-2.8930D+02
4	1.0391D+01	-8.9847D+01
5	7.3380D+00	-4.3015D+02
6	1.6636D+01	-1.0246D+02

Table 13. Frequency Template for 1.0000D-01 r/s

Case	Gain (dB)	Phase(deg)
1	2.4327D+00	-7.6669D+01
2	2.3624D+01	-2.7969D+02
3	2.3094D+01	-2.7482D+02
4	1.9676D+01	-8.4317D+01
5	1.8990D+01	-4.0911D+02
6	2.9774D+01	-1.1028D+02

Table 14. Frequency Template for 1.7783D-01 r/s

Case	Gain (dB)	Phase(deg)
1	1.6128D+01	-8.2492D+01
2	2.0868D+01	-2.6888D+02
3	1.9777D+01	-2.6633D+02
4	2.4094D+01	-2.4342D+02
5	1.4506D+01	-2.5561D+02
6	2.2034D+01	-2.5269D+02

Table 15. Frequency Template for 3.1623D-01 r/s

Case	Gain (dB)	Phase(deg)
1	8.0150D+00	-2.1442D+02
2	1.6861D+01	-2.6140D+02
3	1.5451D+01	-2.5905D+02
4	1.1870D+01	-2.3188D+02
5	5.6750D+00	-2.3054D+02
6	1.3409D+01	-2.4663D+02

Table 16. Frequency Template for 5.6234D-01 r/s

Case	Gain (dB)	Phase(deg)
1	-2.1543D-01	-1.9652D+02
2	1.2221D+01	-2.5245D+02
3	1.0694D+01	-2.4902D+02
4	5.0184D+00	-2.1068D+02
5	2.9602D-02	-2.0661D+02
6	7.5777D+00	-2.3169D+02

Table 17. Frequency Template for 1. r/s

Case	Gain (dB)	Phase(deg)
1	-6.2724D+00	-1.7876D+02
2	7.3292D+00	-2.3872D+02
3	5.7918D+00	-2.3346D+02
4	-1.3023D+00	-1.8904D+02
5	-5.5451D+00	-1.8655D+02
6	2.3639D+00	-2.1075D+02

Table 18. Frequency Template for 1.7783D+00 r/s

Case	Gain (dB)	Phase(deg)
1	-1.3021D+01	-1.7113D+02
2	2.3076D+00	-2.1857D+02
3	8.0152D-01	-2.1187D+02
4	-8.1724D+00	-1.7631D+02
5	-1.2225D+01	-1.7690D+02
6	-3.0957D+00	-1.9048D+02

Table 19. Frequency Template for 3.1623D+00 r/s

Case	Gain (dB)	Phase(deg)
1	-2.1175D+01	-1.7165D+02
2	-2.9662D+00	-1.9536D+02
3	-4.5303D+00	-1.8986D+02
4	-1.6186D+01	-1.7359D+02
5	-2.0445D+01	-1.7551D+02
6	-9.6896D+00	-1.7916D+02

Table 20. Frequency Template for 5.6234D+00 r/s

Case	Gain (dB)	Phase(deg)
1	-3.0393D+01	-1.7441D+02
2	-8.9395D+00	-1.7845D+02
3	-1.0820D+01	-1.7665D+02
4	-2.5268D+01	-1.7511D+02
5	-2.9716D+01	-1.7676D+02
6	-1.7800D+01	-1.7654D+02

Table 21. Frequency Template for 10. r/s

Case	Gain (dB)	Phase(deg)
1	-4.0115D+01	-1.7667D+02
2	-1.6186D+01	-1.7273D+02
3	-1.8554D+01	-1.7363D+02
4	-3.4927D+01	-1.7697D+02
5	-3.9461D+01	-1.7803D+02
6	-2.7006D+01	-1.7724D+02

Table 22. Frequency Template for 1.7783D+01 r/s

Case	Gain (dB)	Phase(deg)
1	-5.0024D+01	-1.7809D+02
2	-2.4786D+01	-1.7366D+02
3	-2.7522D+01	-1.7507D+02
4	-4.4813D+01	-1.7824D+02
5	-4.9378D+01	-1.7886D+02
6	-3.6725D+01	-1.7828D+02

Table 23. Frequency Template for 3.1623D+01 r/s

Case	Gain (dB)	Phase(deg)
1	-5.9994D+01	-1.7892D+02
2	-3.4233D+01	-1.7589D+02
3	-3.7141D+01	-1.7693D+02
4	-5.4776D+01	-1.7900D+02
5	-5.9351D+01	-1.7936D+02
6	-4.6632D+01	-1.7900D+02

Table 24. Frequency Template for 5.6234D+01 r/s

Case	Gain (dB)	Phase(deg)
1	-6.9985D+01	-1.7939D+02
2	-4.4042D+01	-1.7758D+02
3	-4.7013D+01	-1.7822D+02
4	-6.4764D+01	-1.7944D+02
5	-6.9343D+01	-1.7964D+02
6	-5.6603D+01	-1.7943D+02

Table 25. Frequency Template for 100. r/s

Case	Gain (dB)	Phase(deg)
1	-7.9982D+01	-1.7966D+02
2	-5.3981D+01	-1.7862D+02
3	-5.6972D+01	-1.7899D+02
4	-7.4761D+01	-1.7968D+02
5	-7.9340D+01	-1.7980D+02
6	-6.6593D+01	-1.7968D+02

Table 26. Frequency Template for 1.7783D+02 r/s

Case	Gain (dB)	Phase(deg)
1	-8.9981D+01	-1.7981D+02
2	-6.3961D+01	-1.7922D+02
3	-6.6959D+01	-1.7943D+02
4	-8.4760D+01	-1.7982D+02
5	-8.9339D+01	-1.7989D+02
6	-7.6590D+01	-1.7982D+02

Table 27. Frequency Template for 3.1623D+02 r/s

Case	Gain (dB)	Phase(deg)
1	-9.9981D+01	-1.7989D+02
2	-7.3954D+01	-1.7956D+02
3	-7.6955D+01	-1.7968D+02
4	-9.4759D+01	-1.7990D+02
5	-9.9339D+01	-1.7994D+02
6	-8.6589D+01	-1.7990D+02

Table 28. Frequency Template for 5.6234D+02 r/s

Case	Gain (dB)	Phase(deg)
1	-1.0998D+02	-1.7994D+02
2	-8.3953D+01	-1.7975D+02
3	-8.6953D+01	-1.7982D+02
4	-1.0476D+02	-1.7994D+02
5	-1.0934D+02	-1.7996D+02
6	-9.6589D+01	-1.7994D+02

Appendix B: Controller Design Summary for Case 1

Case 1 has the following Category C basic plant

$$P = \frac{1.00s(-0.507)(0.0024)}{(-1.74)(0.67)(0.21, 0.062)} \tag{B.1}$$

Because the RHP zero is closer to the origin than the RHP pole, it is easier to stabilize the plant with an extra RHP pole following the development of Section 3.1.4. A stable loop transmission is

$$L_1 = \frac{3.23 \times 10^8(-5)(-.507)(0.0024)}{(0.02)(-4)(-25)(-1.74)(0.67)(-31.27)(231.3, 0.618)} \tag{B.2}$$

which has the frequency response shown in Figure B.1 and yields the following stabilization compensator G_1:

$$G_1 = \frac{L_1}{AP} = \frac{192.9(-5)(0.21, 0.062)}{s(0.02)(-4)(-25)} \tag{B.3}$$

and the following effective plants P_e and P_y

$$P_e = \frac{L_1}{(1+L_1)} = \frac{3.23 \times 10^8(-5)(-.507)(0.0024)}{(-0.0032)(-0.36)(-5.62)(11.64, 0.58)(-41.8)(231.3, 0.618)} \tag{B.4}$$

$$P_y = \frac{L_1}{P(1+L_1)} = \frac{3.23 \times 10^8(-5)(-1.74)(0.67)(0.21, 0.062)}{s(-0.0032)(-0.36)(-5.62)(11.64, 0.58)(-41.8)(231.3, 0.618)} \tag{B.5}$$

A satisfactory saturation control loop transmission is

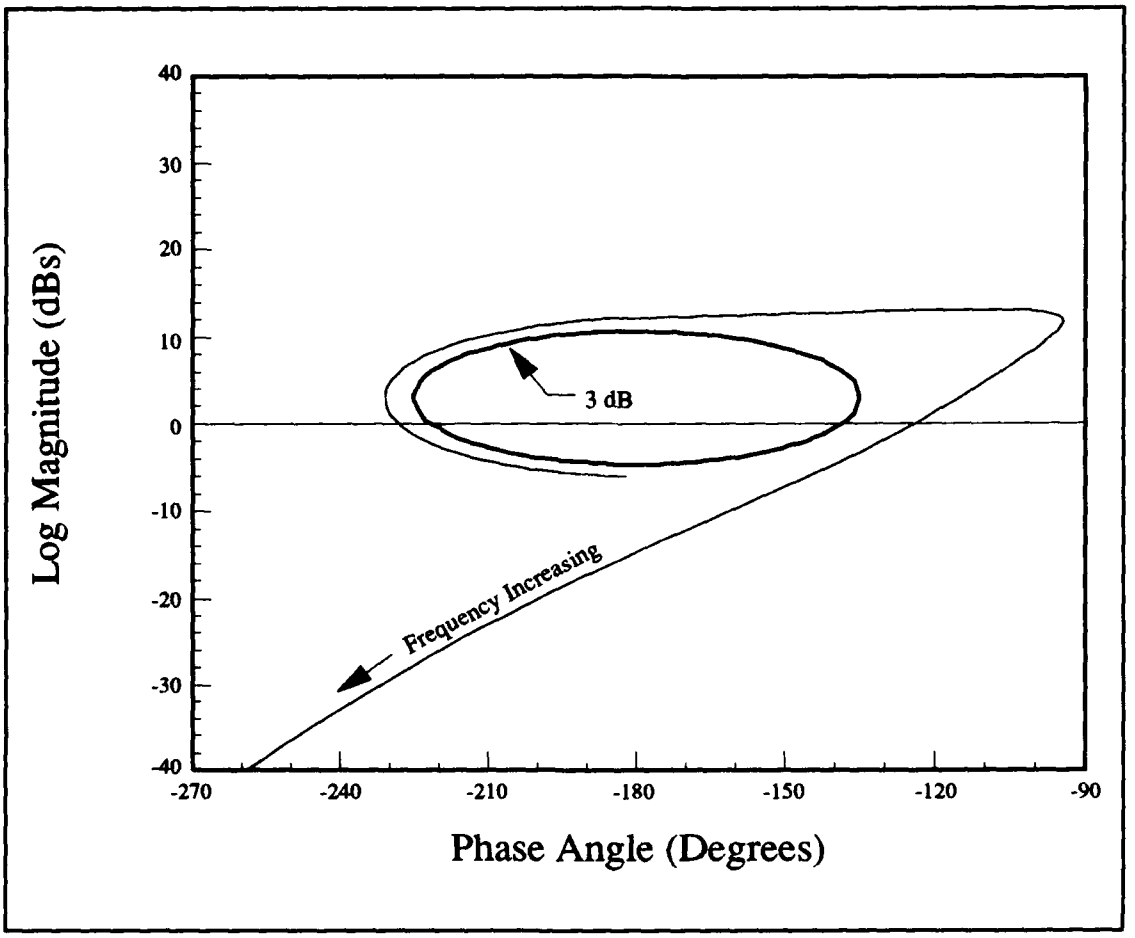

Figure B.1. Stabilization Loop Nichols Plot for Case 1

$$L_2 = \frac{-1.49 \times 10^8(-5)(-.12)(-1.74)(0.67)(-0.005)}{s^2(-0.36)(-5.62)(11.64, 0.58)(-41.8)(231.3, 0.618)} \tag{B.6}$$

which has the frequency response shown in Figure B.2 and gives the following saturation control loop compensator G_2

$$G_2 = \frac{L_2}{P_y} = \frac{-0.462(-0.12)(-0.005)(-0.0032)}{s(0.21, 0.062)(-1.2)} \tag{B.7}$$

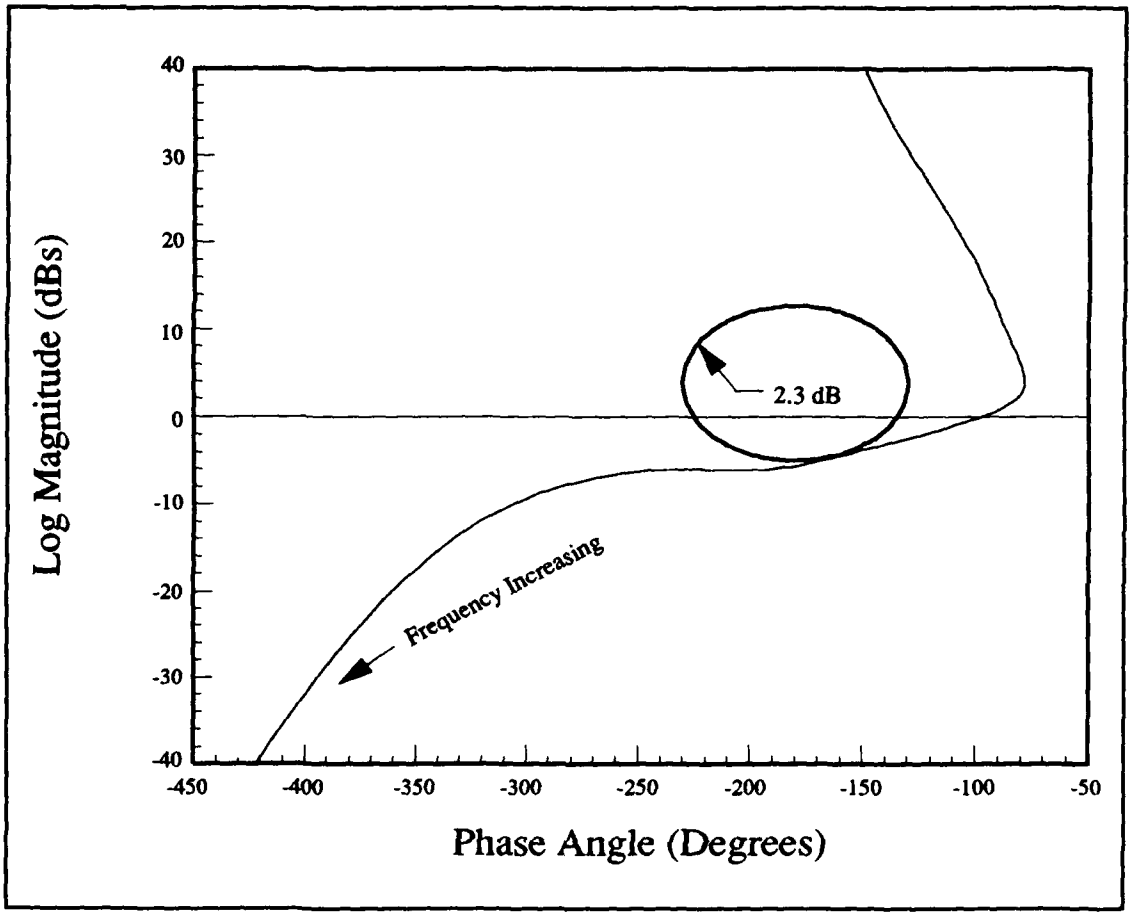

Figure B.2. Saturation Control Loop Nichols Plot for Case 1

The fact that the RHP zero in P_e is very near the origin severely limits the bandwidth of the tracking control loop. In order to provide increased loop gain over a wider range of frequency, a second RHP zero is added. A satisfactory tracking control loop transmission is

$$L_3 = \frac{1.44 \times 10^9 (-5)(-.507)(0.0024)(0.003)}{s(-0.3)(-0.2)(-0.36)(-5.62)(11.64, 0.58)(-41.8)(231.3, 0.618)} \qquad \text{(B.8)}$$

which has the frequency response shown in Figure B.3 and gives the following tracking control loop compensator L_{3c}

$$L_{3c} = \frac{L_3}{P_e} = \frac{4.44(0.003)(-0.0032)}{s(-0.3)(-0.2)} \tag{B.9}$$

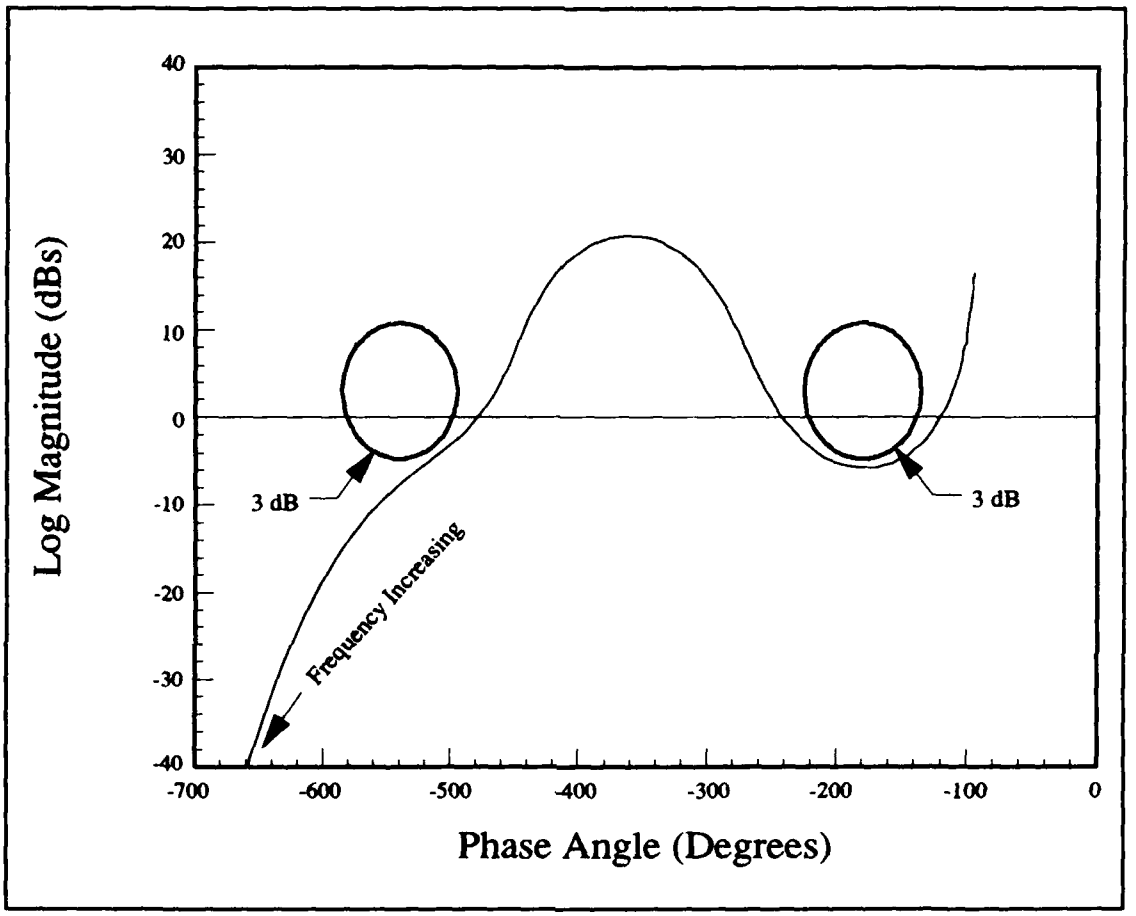

Figure B.3. Tracking Control Loop Nichols Plot for Case 1

The RHP zero in L_{3c}, along with the pole farthest from the origin, is placed in the feedback compensator H_3. This "hides" the RHP zero from the closed loop transfer function. Therefore, the feedback compensator H_3 is

$$H_3 = \frac{100(0.003)}{(-0.3)} \tag{B.10}$$

and the closed loop transfer function P_3 is

$$P_3 = \frac{L_3}{H_3(1+L_3)}$$

$$= \frac{1.44\times 10^7(-.3)(-5)(-.507)(0.0024)}{(0.0026,0.84)(-0.511)(-4.34)(8.88,0.31)(-10.4)(-41.1)(231.3,0.618)} \tag{B.11}$$

The command limiter minor loop compensator H is calculated as in Section 5.2:

$$H = \frac{10P_3}{sL_3} \approx \frac{10(-.3)(-.2)(-0.36)(11.64,0.58)}{(0.0026,0.84)(-4.34)(8.88,0.31)(-10.4)} \tag{B.12}$$

The compensator G_3 is

$$G_3 = \frac{L_{3c}(1+H)}{G_2H_3}$$

$$= \frac{-9.62(0.21,0.062)(-1.2)(0.08,0.45)(-2.00)(10.9,0.41)}{(-0.2)(-1.2)(-0.005)(-10.4)(-4.34)(8.88,0.31)(-4.34)(0.0026,0.84)} \tag{B.13}$$

The closed loop transfer function P_3 has the frequency response shown in Figure B.4.

To obtain the desired frequency response, the following prefilter is used:

$$F = \frac{63.78(-0.003)(11.1,0.36)(-8)}{(-.3)(-100)(2,0.8)} \tag{B.14}$$

The final closed loop frequency response is nearly indistinguishable from that shown in Figure 5.5 for Case 6.

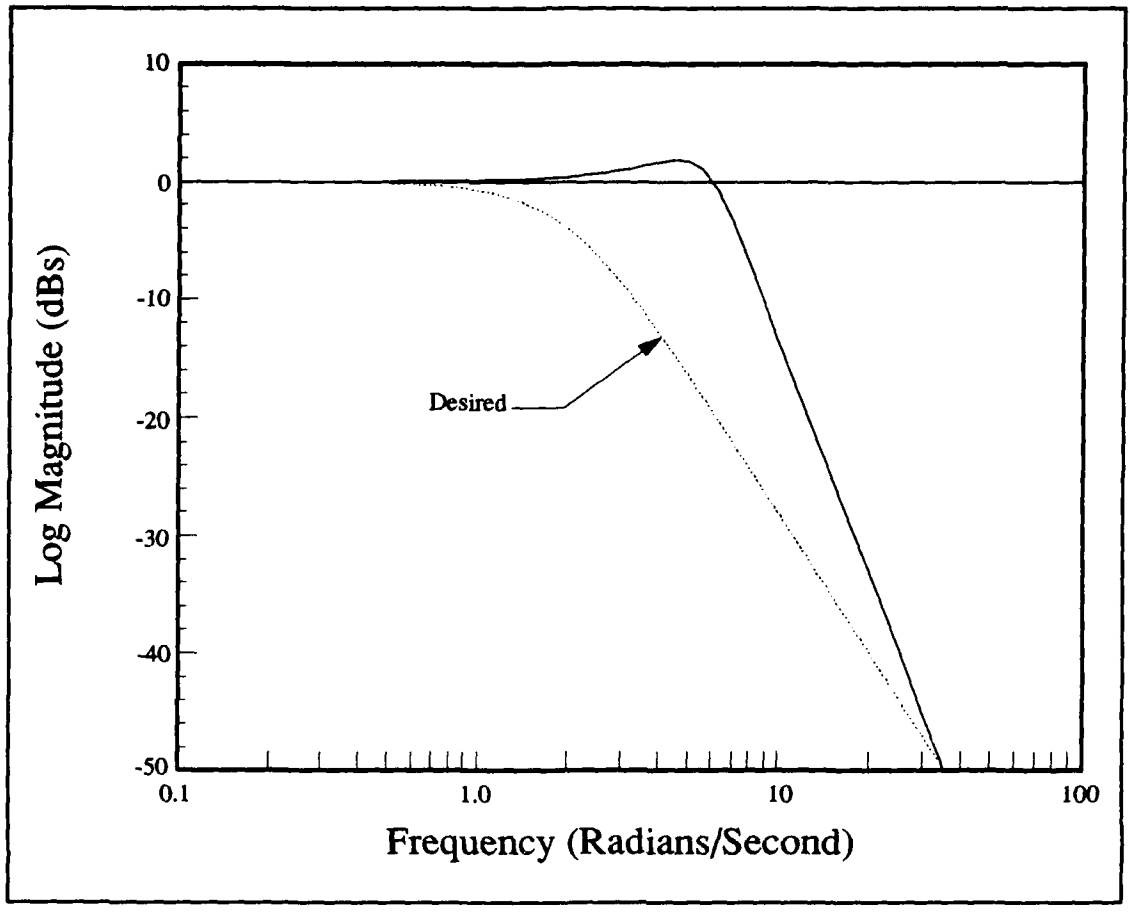

Figure B.4. Closed Loop Frequency Response without Prefilter for Case 1

Appendix C: Controller Design Summary for Case 2

Case 2 has the following Category B basic plant

$$P = \frac{20.06s(-2.77)(-0.054)}{(-8.12)(2.92)(-0.11)(0.063)} \tag{C.1}$$

A stable loop transmission is

$$L_1 = \frac{9.86\times 10^8(-2.77)(-0.054)(-5.5)(-2.8)}{(-2)(-3.2)(-40)(-8.12)(2.92)(0.063)(-31.27)(231.3, 0.618)} \tag{C.2}$$

which has the frequency response shown in Figure C.1 and yields the following stabilization compensator G_1

$$G_1 = \frac{L_1}{AP} = \frac{2.94(-5.5)(-2.8)(-0.11)}{s(-2)(-40)(-3.2)} \tag{C.3}$$

and the following effective plants P_e and P_y

$$P_e = \frac{L_1}{(1+L_1)} = \frac{9.86\times 10^8(-5.5)(-2.8)(-2.77)(-0.054)}{(-0.092)(2.99, 0.96)(-3.83)(17.4, 0.44)(-56.7)(231.3, 0.618)} \tag{C.4}$$

$$P_y = \frac{L_1}{P(1+L_1)} = \frac{4.91\times 10^7(-5.5)(-0.11)(-2.8)(-8.12)(2.92)(0.063)}{s(-0.092)(2.99, 0.96)(-3.83)(17.4, 0.44)(-56.7)(231.3, 0.618)} \tag{C.5}$$

A satisfactory saturation control loop transmission is

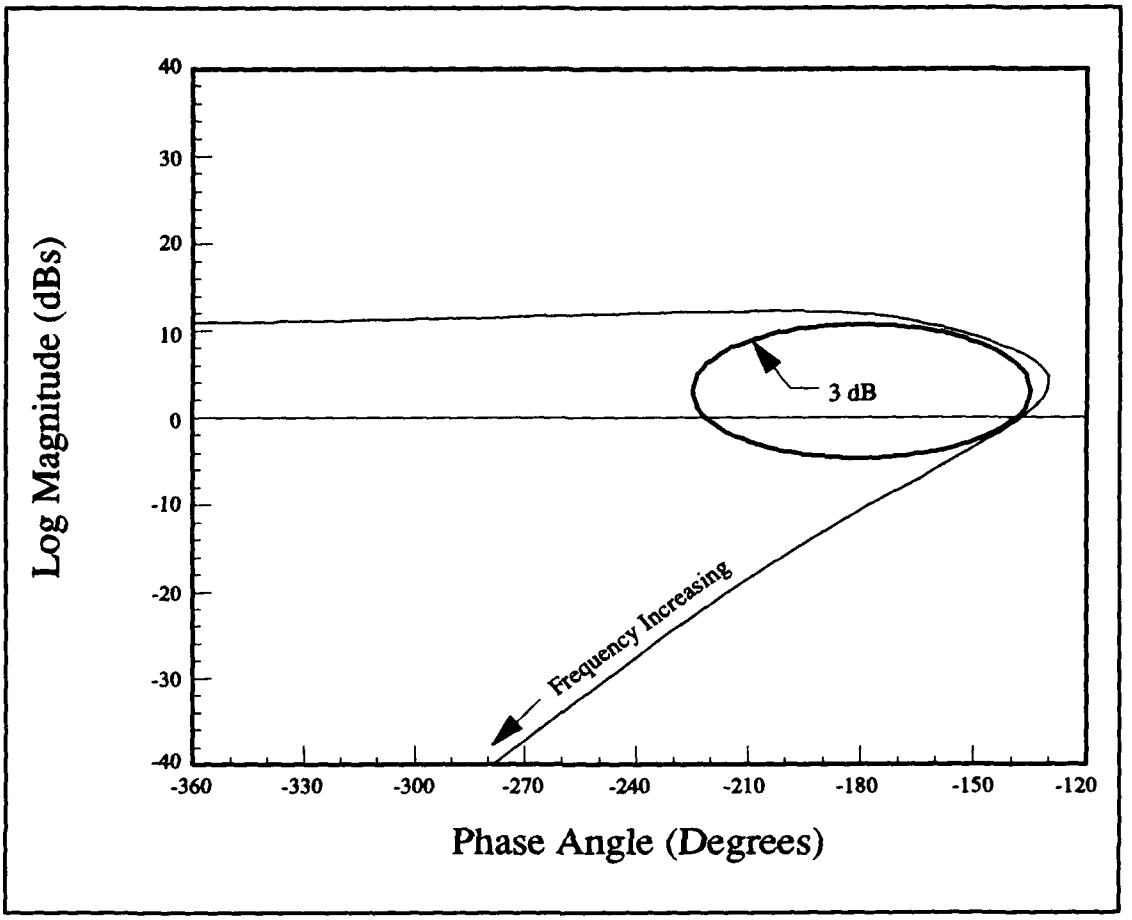

Figure C.1. Stabilization Loop Nichols Plot for Case 2

$$L_2 = \frac{1.21 \times 10^{10}(-5.5)(-0.005)(-2.8)(-1.7)(-8.12)(2.92)(-0.11)(0.063)}{s^2(-5)(-100)(17.4, 0.44)(-3.83)(2.99, 0.96)(-.092)(-56.7)(231.3, 0.618)} \quad \text{(C.6)}$$

which has the frequency response shown in Figure C.2 and gives the following saturation control loop compensator G_2

$$G_2 = \frac{L_2}{P_y} = \frac{245(-1.7)(-0.005)}{s(-5)(-100)} \quad \text{(C.7)}$$

A satisfactory tracking control loop transmission is

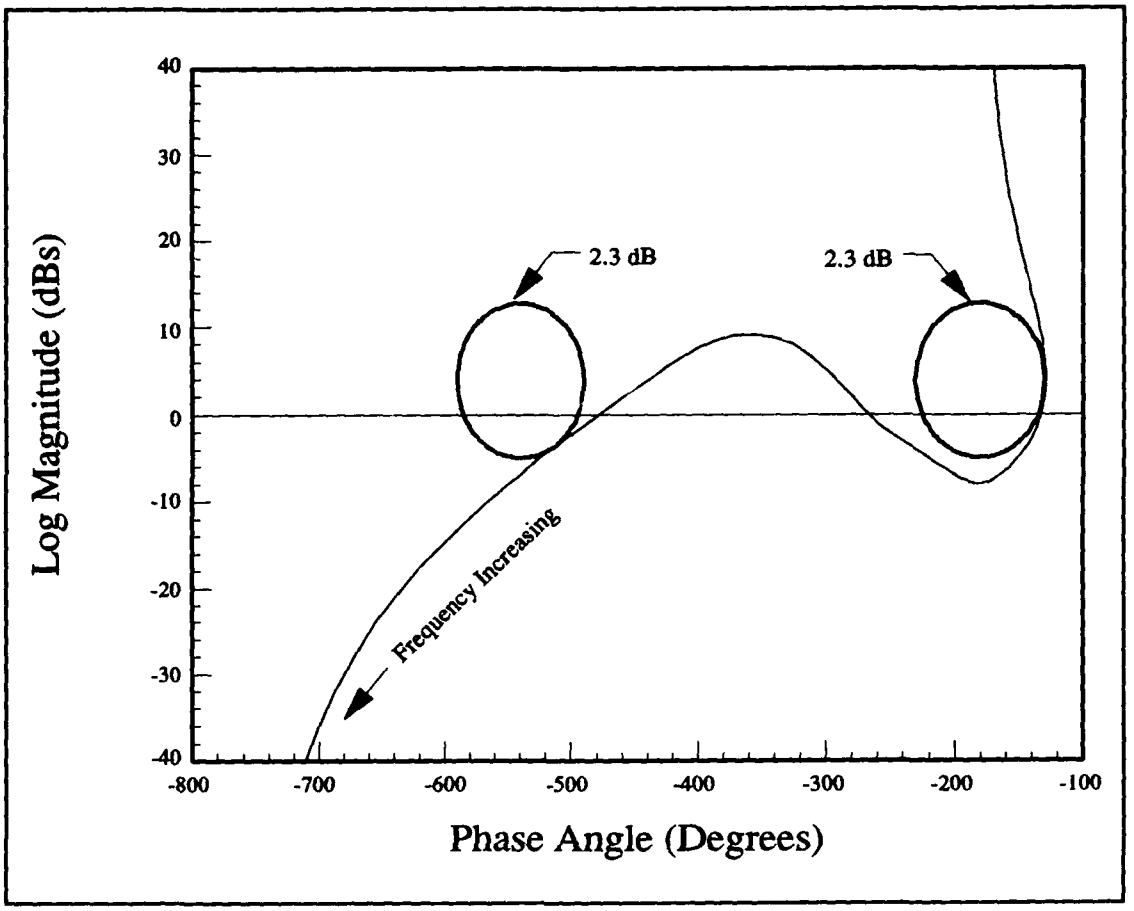

Figure C.2. Saturation Control Loop Nichols Plot for Case 2

$$L_3 = \frac{5.03 \times 10^9 (-5.5)(-2.8)(0.0024)(-2.77)(0.054)}{s(-0.092)(2.99, 0.96)(-3.83)(17.4, 0.44)(-56.7)(231.3, 0.618)} \qquad \text{(C.8)}$$

which has the frequency response shown in Figure C.3 and gives the following tracking control loop compensator L_{3c}

$$L_{3c} = \frac{L_3}{P_e} = \frac{5.10}{s} \qquad \text{(C.9)}$$

There are no RHP poles in the loop transmission. Therefore, the feedback compensator H_3 is

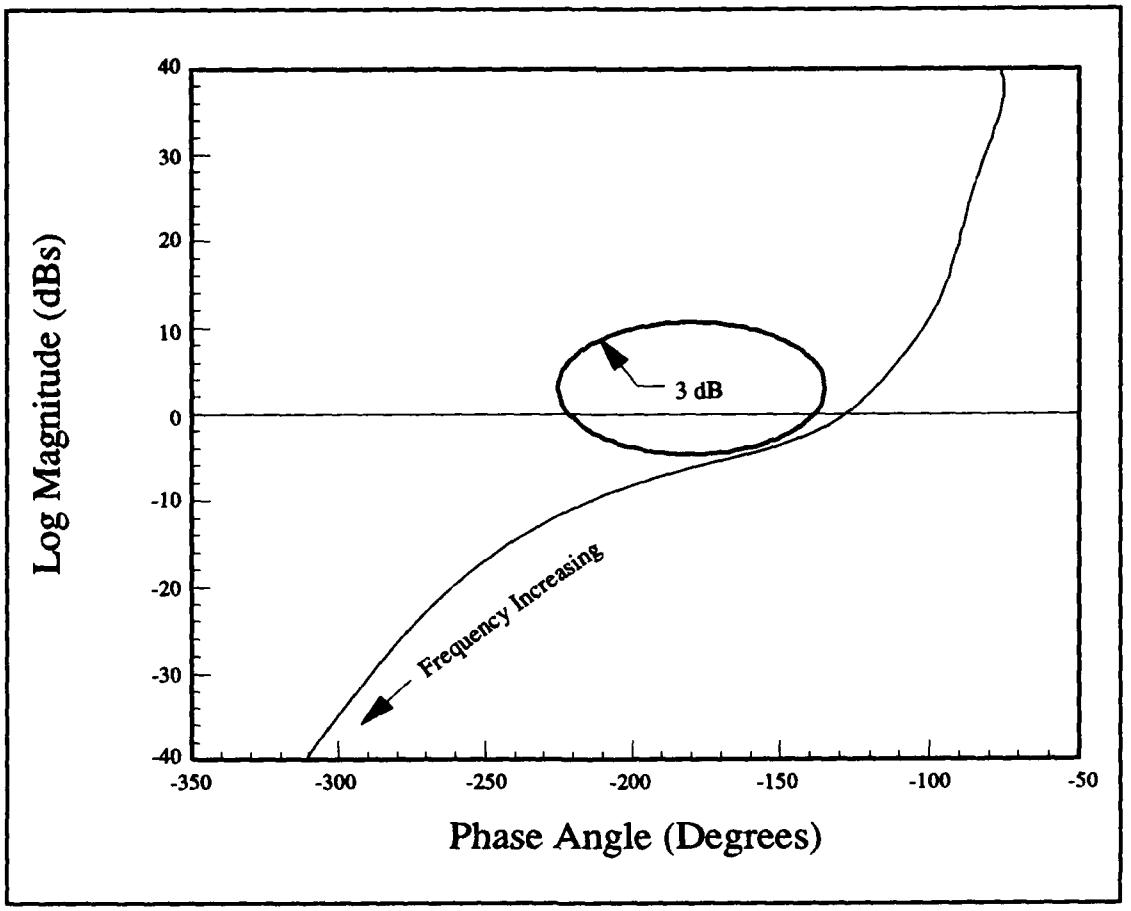

Figure C.3. Tracking Control Loop Nichols Plot for Case 2

$$H_3 = 1 \tag{C.10}$$

and the closed loop transfer function P_3 is

$$P_3 = \frac{L_3}{H_3(1+L_3)}$$

$$= \frac{5.03 \times 10^9(-.054)(-2.77)(-5.5)(-2.8)}{(-0.054)(-2.38)(-3.115)(7.19, 0.87)(13.7, 0.284)(-55.904)(231.3, 0.618)} \tag{C.11}$$

The command limiter minor loop compensator H is calculated as in Section 5.2:

$$H = \frac{10P_3}{sL_3} \approx \frac{10(-0.092)(2.99, 0.96)(-3.83)(17.4, 0.44)}{(-0.054)(-2.38)(-3.12)(7.82, 0.87)(13.7, 0.28)} \tag{C.12}$$

The compensator G_3 is

$$\begin{aligned} G_3 &= \frac{L_{3c}(1+H)}{G_2 H_3} \\ &= \frac{0.021(-5)(-100)(-0.057)(2.90, 0.99)(-4.79)(16.1, 0.26)(-16.7)}{(-0.005)(-1.7)(-3.12)(2.38)(13.7, 0.28)(7.82, 0.87)(-0.054)} \end{aligned} \tag{C.13}$$

The closed loop transfer function P_3 has the frequency response shown in Figure C.4.

To obtain the desired frequency response, the following prefilter is used:

$$F = \frac{0.25(13.7, 0.28)(7.17, 0.86)}{(-6)(-100)(2, 0.8)} \tag{C.14}$$

The final closed loop frequency response is nearly indistinguishable from that shown in Figure 5.5 for Case 6.

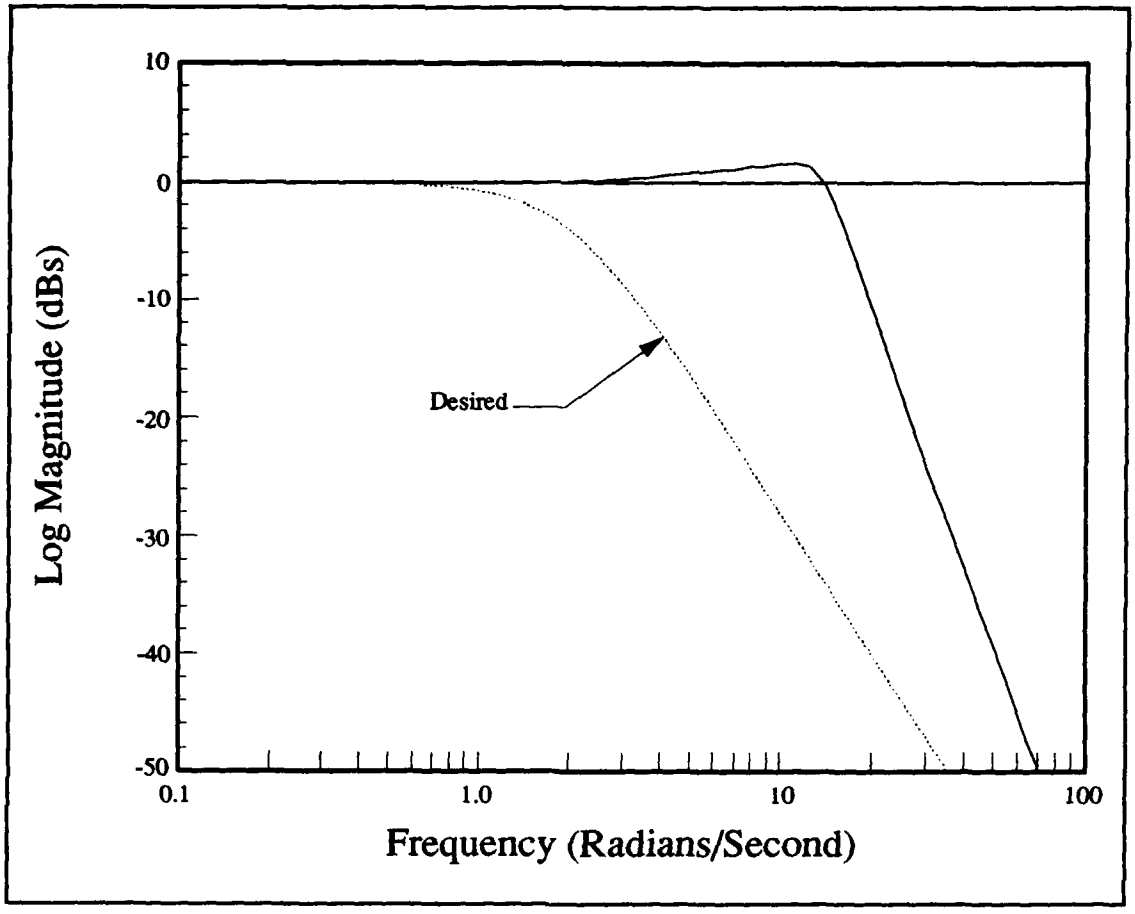

Figure C.4. Closed Loop Frequency Response without Prefilter for Case 2

Appendix D: Controller Design Summary for Case 3

Case 3 has the following Category B basic plant

$$P = \frac{14.2s(-2.26)(-0.041)}{(-6.55)(2.51)(-0.085)(0.051)} \tag{D.1}$$

A stable loop transmission is

$$L_1 = \frac{9.07\times 10^8(-5.5)(-2.8)(-0.041)}{(-3.2)(-40)(-6.55)(2.51)(0.51)(-31.27)(231.3, 0.618)} \tag{D.2}$$

which has the frequency response shown in Figure D.1 and yields the following stabilization compensator G_1

$$G_1 = \frac{L_1}{AP} = \frac{38.2(-5.5)(-2.8)(-0.085)}{s(-2.26)(-3.2)(-40)} \tag{D.3}$$

and the following effective plants P_e and P_y

$$P_e = \frac{L_1}{(1+L_1)} = \frac{9.07\times 10^8(-5.5)(-2.8)(-0.041)}{(-0.073)(-2.49)(-4.98)(16.6, 0.45)(-55.9)(231.3, 0.618)} \tag{D.4}$$

$$P_y = \frac{L_1}{P(1+L_1)} = \frac{6.39\times 10^7(-5.5)(-2.8)(-6.55)(2.51)(-0.085)(0.051)}{s(-0.073)(-2.49)(-4.98)(-2.26)(16.6, 0.45)(-55.9)(231.3, 0.618)} \tag{D.5}$$

A satisfactory saturation control loop transmission is

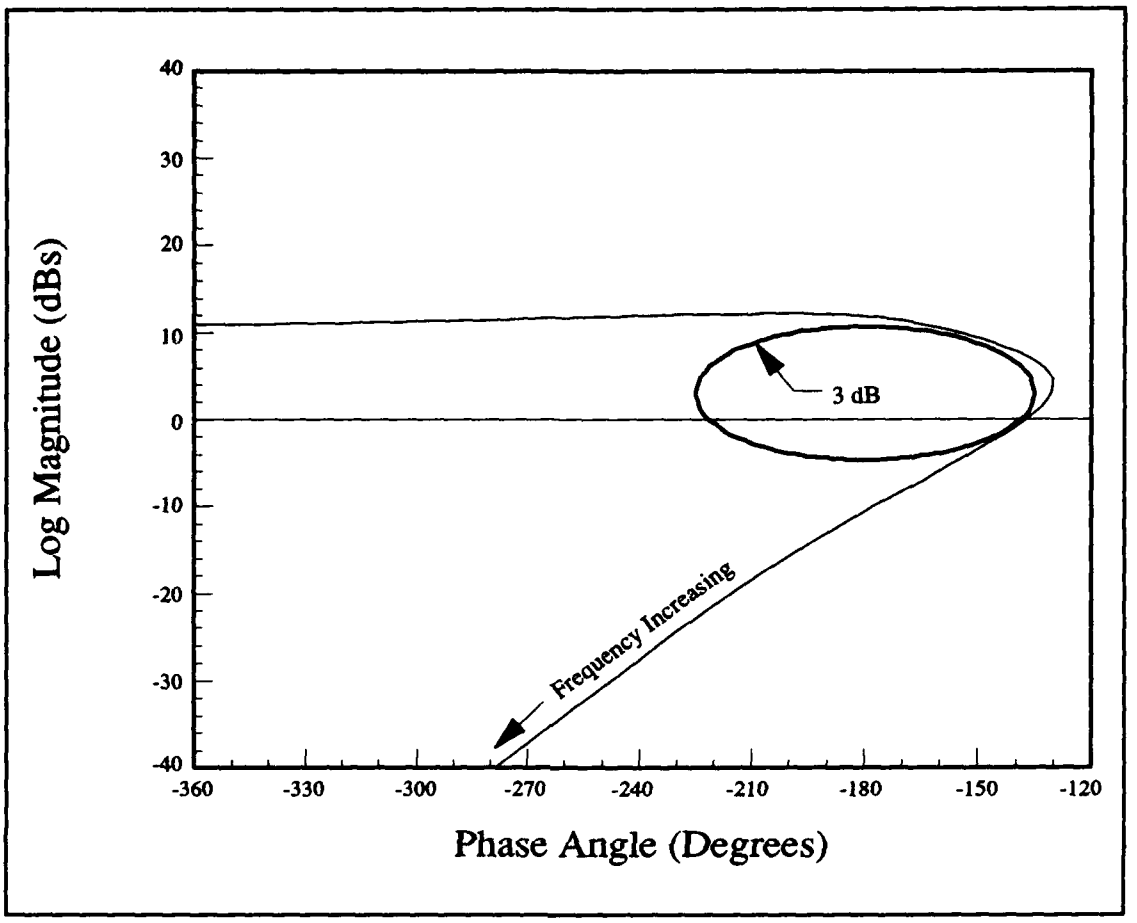

Figure D.1. Stabilization Loop Nichols Plot for Case 3

$$L_2 = \frac{2.23 \times 10^{10}(-0.002)(-0.04)(-.085)(-5.5)(2.8)(-6.551)(2.51)}{s^2(-6)(-100)(-4.98)(-2.49)(-2.26)(-0.073)(16.6, 0.45)(-55.9)(231.3, 0.618)} \quad \text{(D.6)}$$

which has the frequency response shown in Figure D.2 and gives the following saturation control loop compensator G_2

$$G_2 = \frac{L_2}{P_y} = \frac{350(-0.002)(-0.04)}{s(-6)(-100)} \quad \text{(D.7)}$$

A satisfactory tracking control loop transmission is

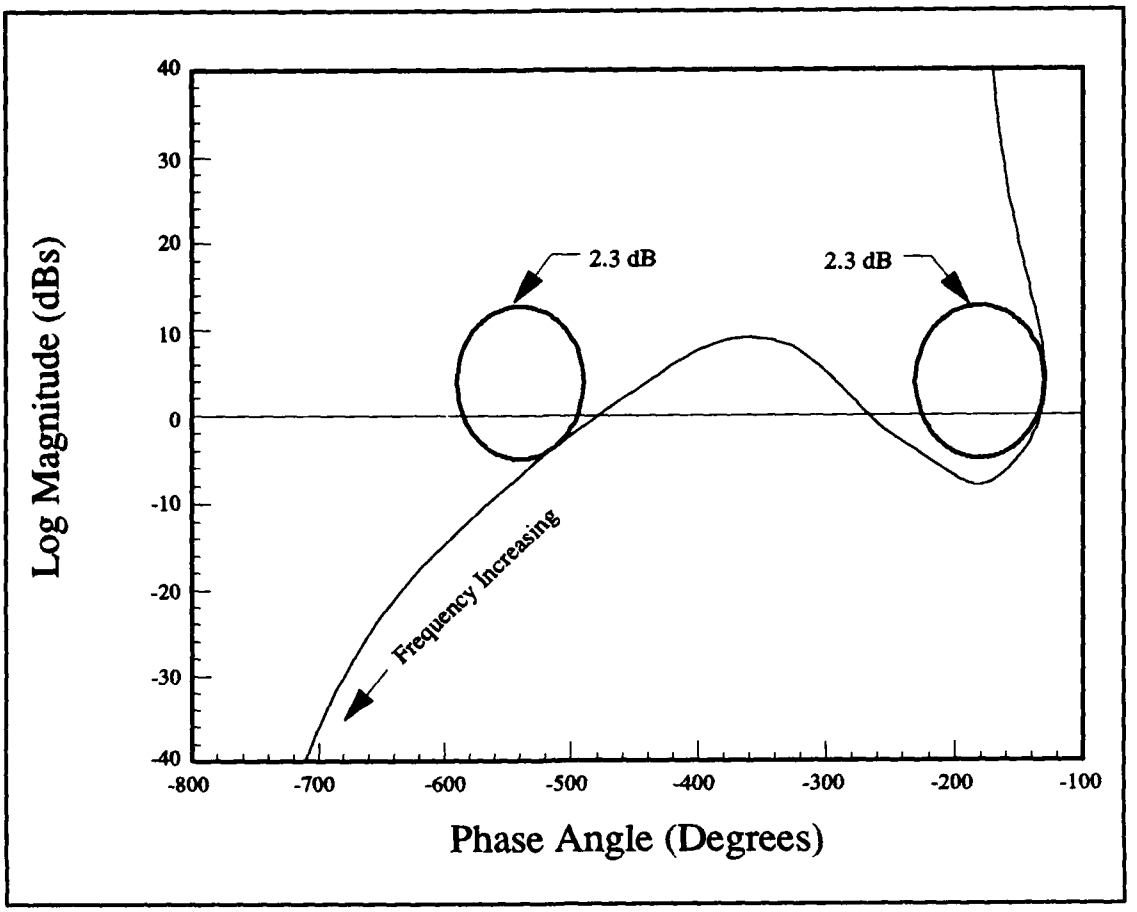

Figure D.2. Saturation Control Loop Nichols Plot for Case 3

$$L_3 = \frac{4.23 \times 10^9 (-5.5)(-2.8)(-0.041)}{s(-0.073)(-2.49)(-4.98)(16.6, 0.45)(-55.9)(231.3, 0.618)} \tag{D.8}$$

which has the frequency response shown in Figure D.3 and gives the following tracking control loop compensator L_{3c}

$$L_{3c} = \frac{L_3}{P_e} = \frac{4.67}{s} \tag{D.9}$$

There are no RHP zeros in the loop transmission. Therefore, the feedback compensator H_3 is

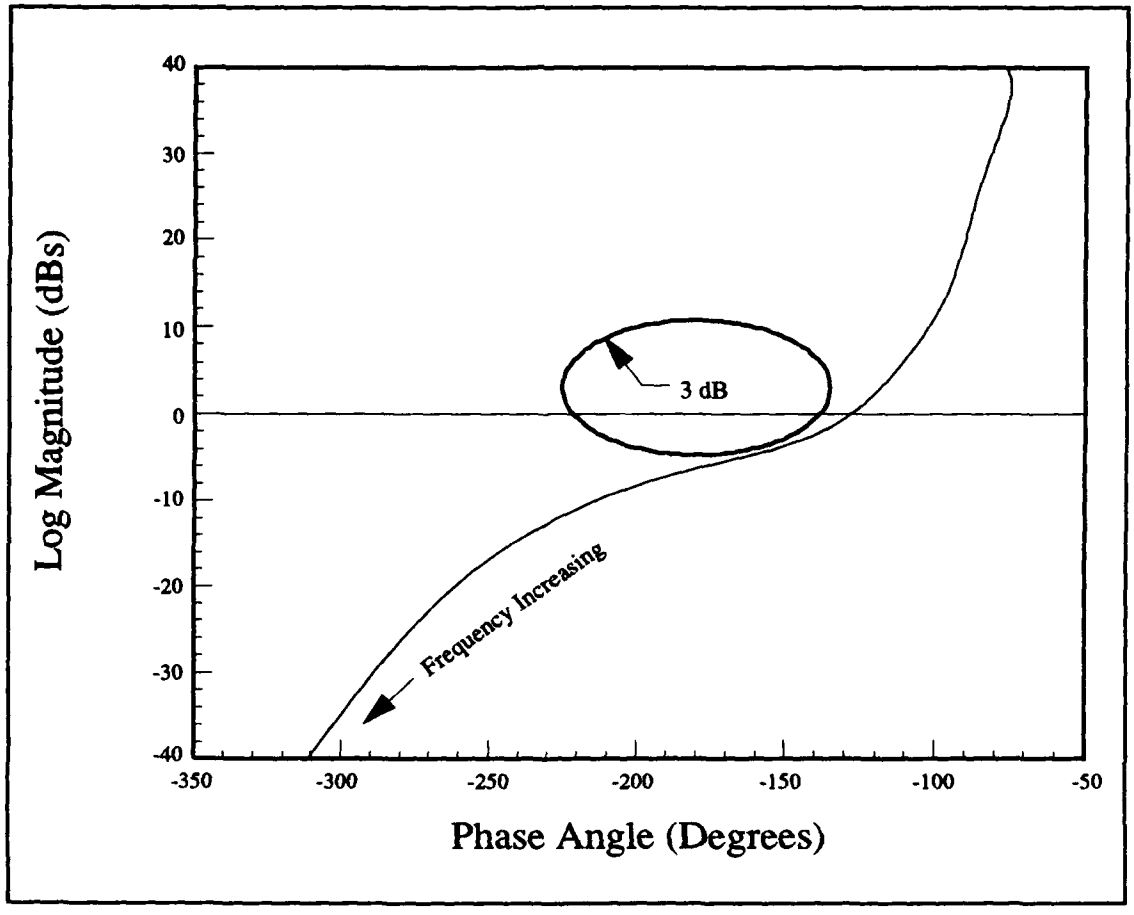

Figure D.3. Tracking Control Loop Nichols Plot for Case 3

$$H_3 = 1 \tag{D.10}$$

and the closed loop transfer function P_3 is

$$P_3 = \frac{L_3}{H_3(1+L_3)}$$
$$= \frac{4.23\times 10^9(-5.5)(-2.8)(-0.041)}{(-0.041)(-2.99)(6.5,0.95)(13.3,0.30)(-55.2)(231,0.62)} \tag{D.11}$$

The command limiter minor loop compensator H is calculated as in Section 5.2:

$$H = \frac{10P_3}{sL_3} \approx \frac{10(16.6, 0.45)(-4.98)(-0.085)}{(-0.04)(6.5, 0.95)(13.3, 0.30)} \tag{D.12}$$

The compensator G_3 is

$$\begin{aligned} G_3 &= \frac{L_{3c}(1+H)}{G_2 H_3} \\ &= \frac{0.013(-6)(-100)(-0.69)(-5.34)(-16.3)(15.6, 0.28)}{(-0.002)(-0.04)(-0.04)(13.3, 0.30)(6.5, 0.95)} \end{aligned} \tag{D.13}$$

The closed loop transfer function P_3 has the frequency response shown in Figure D.4.

To obtain the desired frequency response, the following prefilter is used:

$$F = \frac{0.302(6.45, 0.95)(13.2, 0.30)}{(-5.5)(-100)(2, 0.8)} \tag{D.14}$$

The final closed loop frequency response is nearly indistinguishable from that shown in Figure 5.5 for Case 6.

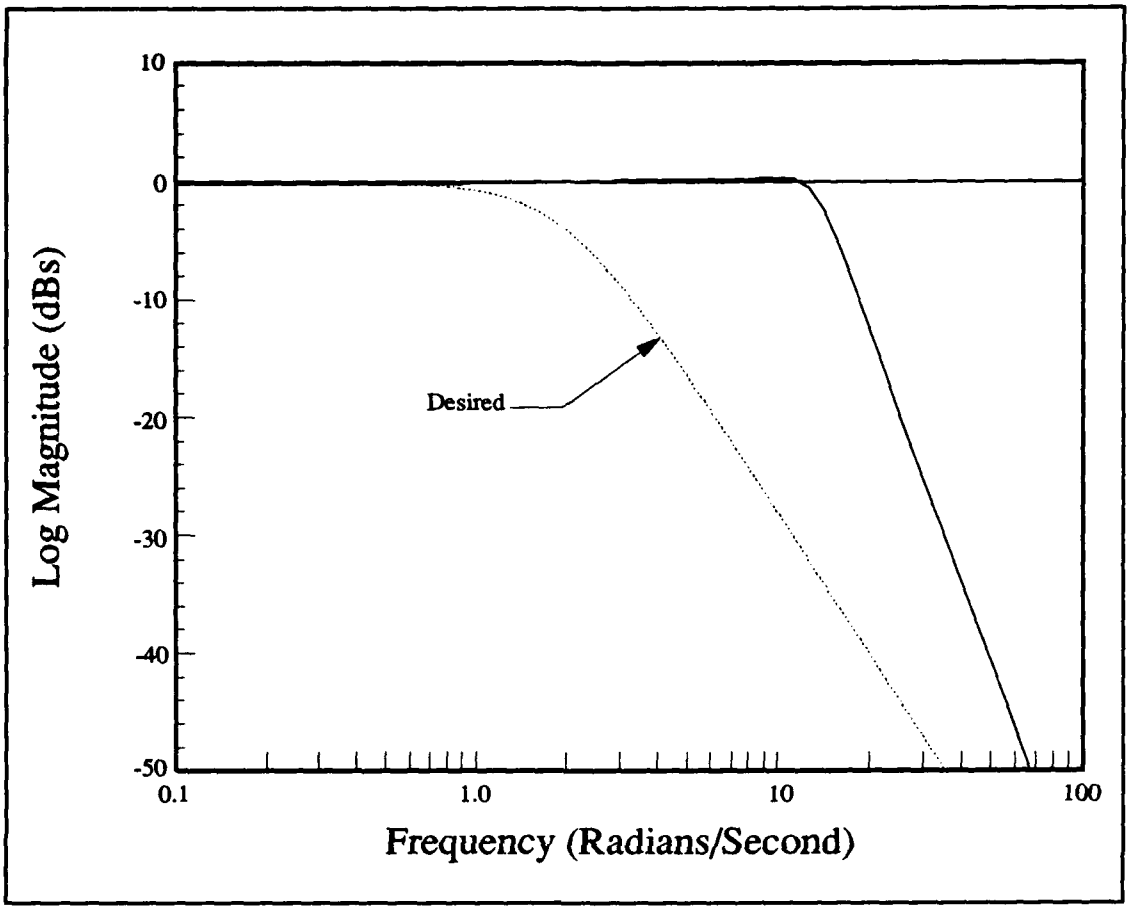

Figure D.4. Closed Loop Frequency Response without Prefilter for Case 3

Appendix E: Controller Design Summary for Case 4

Case 4 has the following Category A basic plant

$$P = \frac{1.83s(-0.78)(-0.0056)}{(-2.03)(0.69)(0.14, 0.024)} \tag{E.1}$$

A stable loop transmission is

$$L_1 = \frac{3.28 \times 10^7}{(-6)(0.69)(-31.27)(231.3, 0.618)} \tag{E.2}$$

which has the frequency response shown in Figure E.1 and yields the following stabilization compensator G_1

$$G_1 = \frac{L_1}{AP} = \frac{10.7(-2.03)(0.14, 0.024)}{s(-0.78)(-0.0056)(-6)} \tag{E.3}$$

and the following effective plants P_e and P_y

$$P_e = \frac{L_1}{(1+L_1)} = \frac{3.28 \times 10^7}{(3.88, 0.58)(-32.1)(231.3, 0.618)} \tag{E.4}$$

$$P_y = \frac{L_1}{P(1+L_1)} = \frac{1.79 \times 10^7(-2.03)(0.69)(0.14, 0.24)}{s(3.88, 0.58)(-32.1)(-0.78)(-0.0056)(231.3, 0.618)} \tag{E.5}$$

A satisfactory saturation control loop transmission is

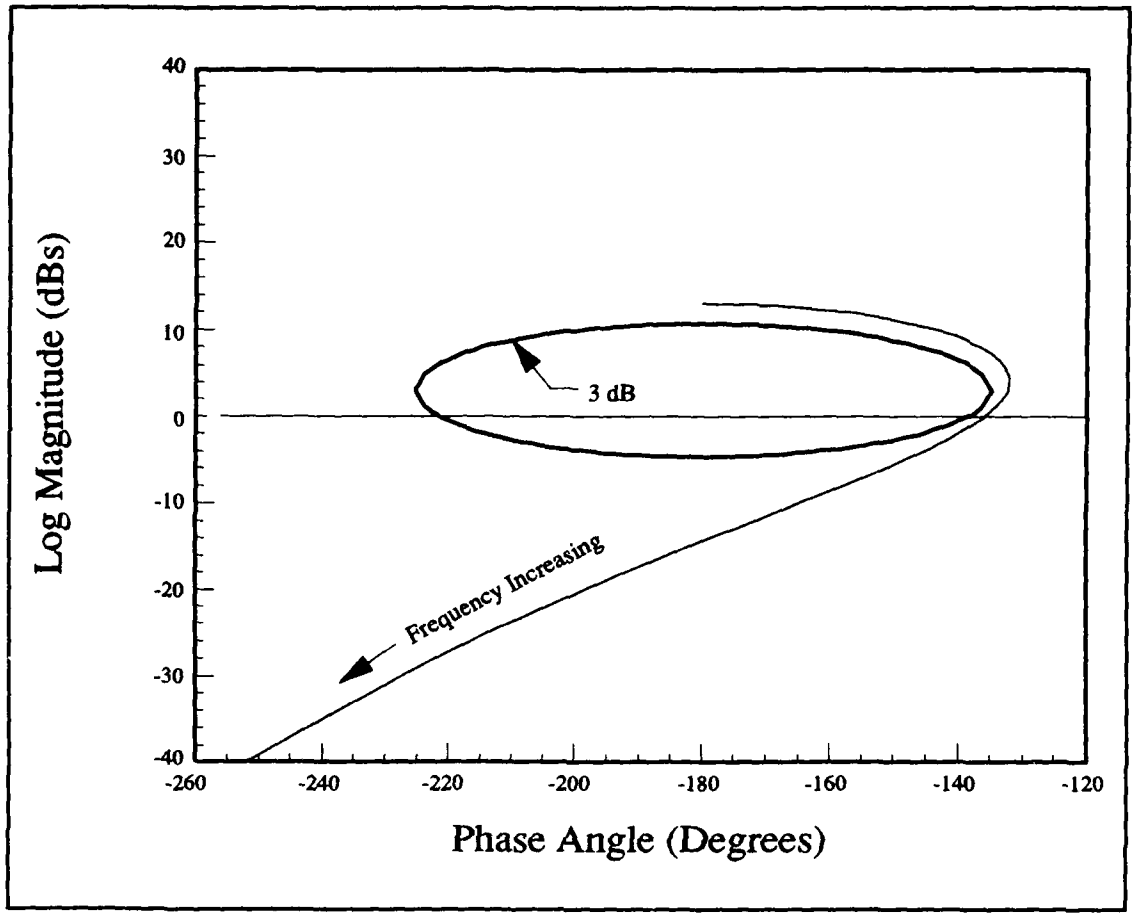

Figure E.1. Stabilization Loop Nichols Plot for Case 4

$$L_2 = \frac{-2.50 \times 10^7 (-2.03)(0.69)(-0.003)}{s^2(-0.78)(3.88, 0.58)(-32.1)(231, 0.62)} \tag{E.6}$$

which has the frequency response shown in Figure E.2 and gives the following saturation control loop compensator G_2

$$G_2 = \frac{L_2}{P_y} = \frac{-1.39(-0.0056)(-0.003)}{s(0.14, 0.024)} \tag{E.7}$$

A satisfactory tracking control loop transmission is

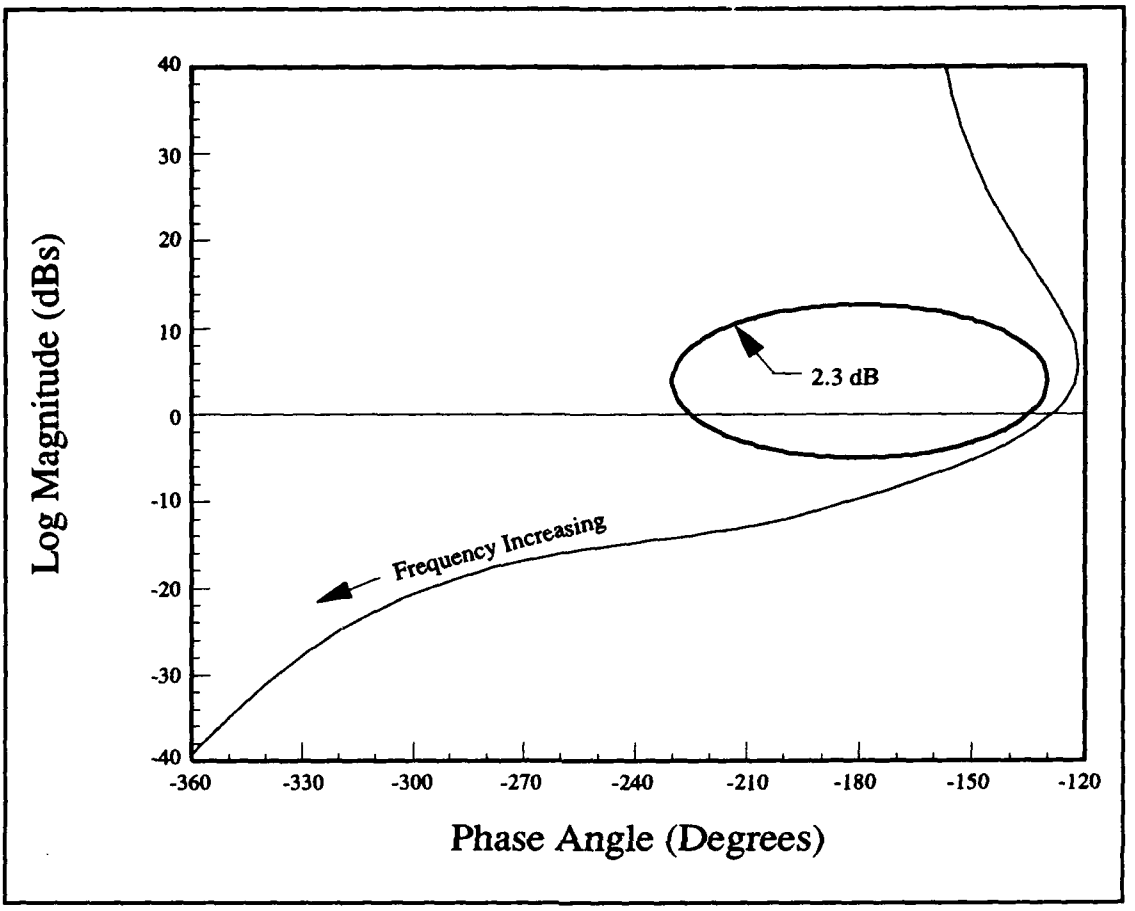

Figure E.2. Saturation Control Loop Nichols Plot for Case 4

$$L_3 = \frac{4.59 \times 10^7}{s(3.88, 0.58)(-32.1)(231, 0.62)} \tag{E.8}$$

which has the frequency response shown in Figure E.3 and gives the following tracking control loop compensator L_{3c}

$$L_{3c} = \frac{L_3}{P_e} = \frac{1.4}{s} \tag{E.9}$$

There are no RHP zeros in the loop transmission. Therefore, the feedback compensator H_3 is

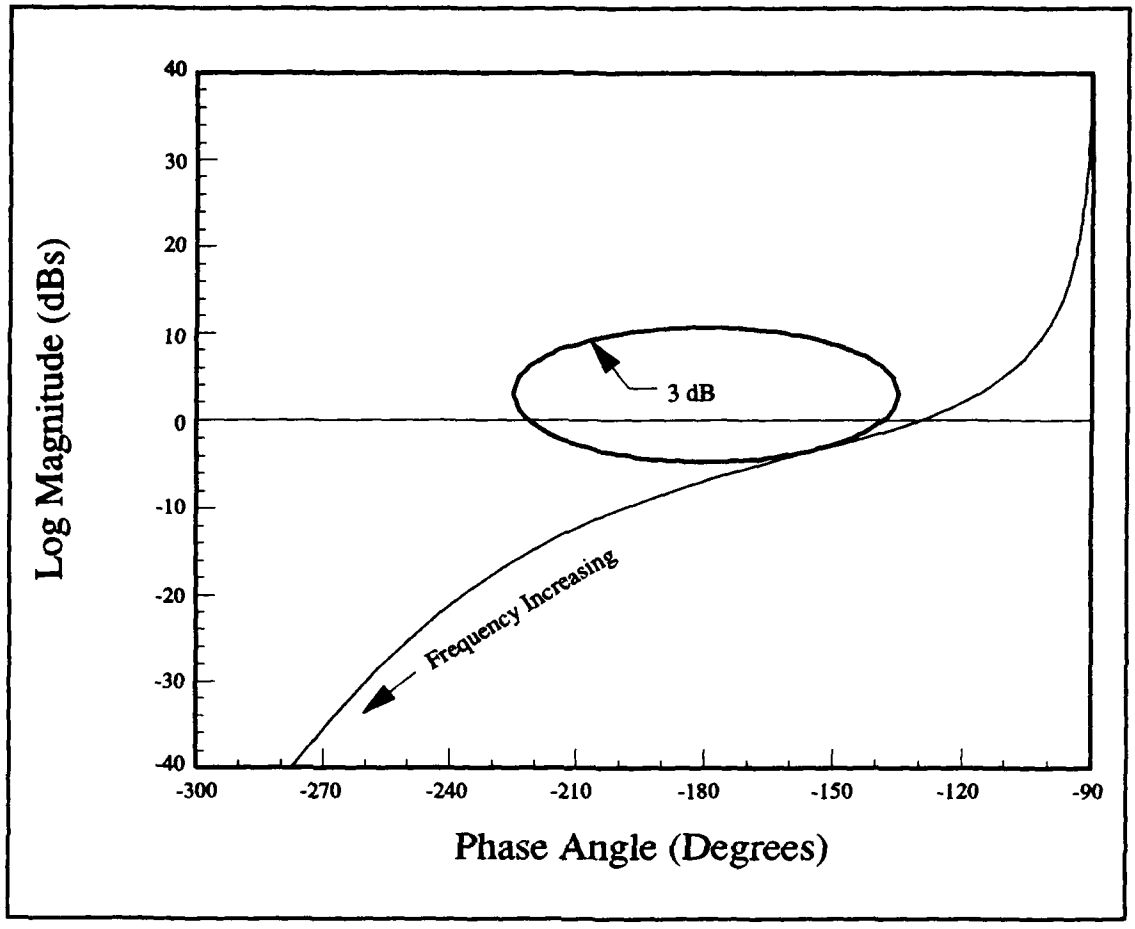

Figure E.3. Tracking Control Loop Nichols Plot for Case 4

$$H_3 = 1 \tag{E.10}$$

and the closed loop transfer function P_3 is

$$P_3 = \frac{L_3}{H_3(1+L_3)} = \frac{4.59\times 10^7}{(-2.86)(3.06, 0.27)(-32.1)(231.3, 0.618)} \tag{E.11}$$

The command limiter minor loop compensator H is calculated as in Section 5.2 :

$$H = \frac{10P_3}{sL_3} \approx \frac{10(3.88, 0.58)}{(-2.86)(3.06, 0.27)} \tag{E.12}$$

The compensator G_3 is

$$G_3 = \frac{L_{3c}(1+H)}{G_2H_3} = \frac{-1.00(0.14, 0.024)(4.10, 0.48)(-10.529)}{(-5.63)(-0.003)(-2.86)(3.06, 0.27)} \tag{E.13}$$

The closed loop transfer function P_3 has the frequency response shown in Figure E.4.

To obtain the desired frequency response, the following prefilter is used:

$$F = \frac{17.68(-2.5)(3.01, 0.27)}{(-100)(2, 0.8)} \tag{E.14}$$

The final closed loop frequency response is nearly indistinguishable from that shown in Figure 5.5 for Case 6.

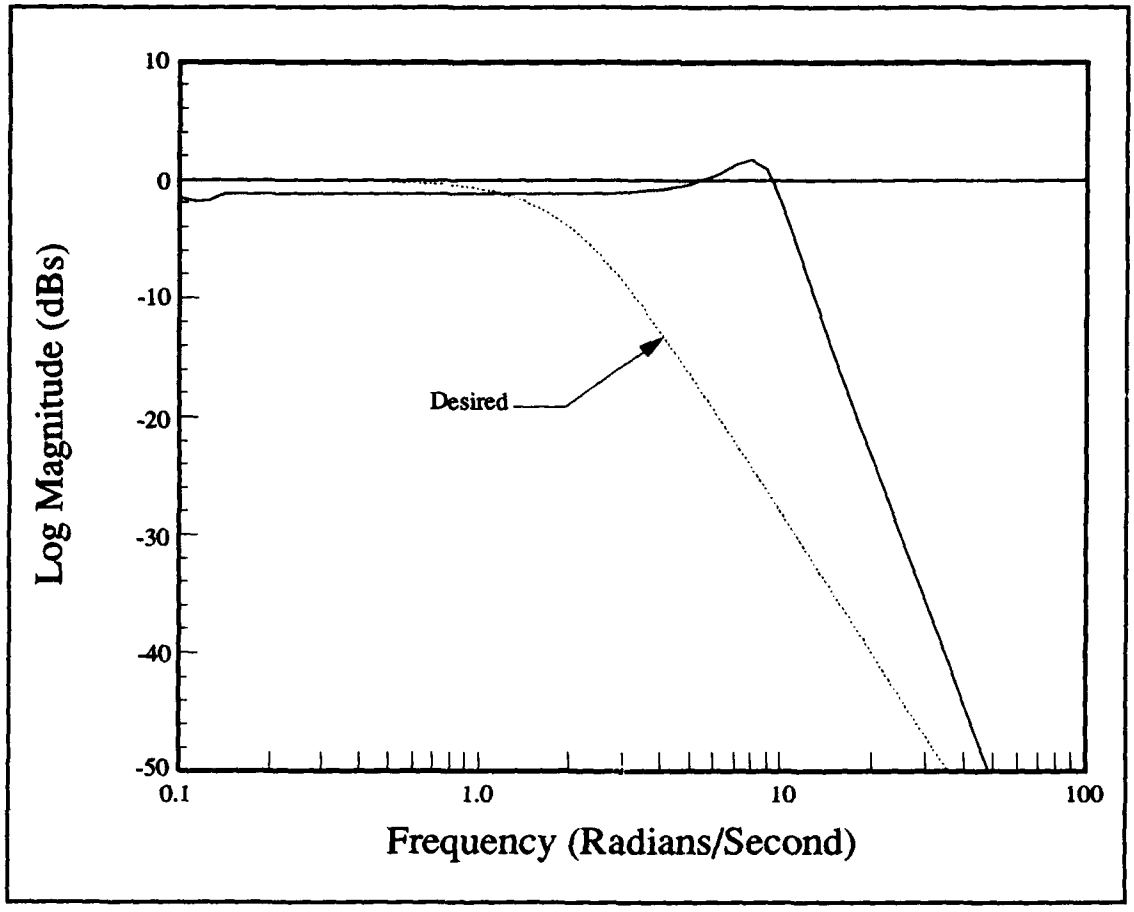

Figure E.4. Closed Loop Frequency Response without Prefilter for Case 4

Appendix F: Controller Design Summary for Case 5

Case 5 has the following Category D basic plant

$$P = \frac{1.08s(-0.54)(0.0055)}{(-1.63)(0.72)(0.12,-0.088)} \tag{F.1}$$

Because the RHP zero is closer to the origin than the real RHP pole, it is easier to stabilize the plant with an extra RHP pole following the development of Section 3.1.4. A stable loop transmission is

$$L_1 = \frac{2.65\times10^8(-5)(-.54)(0.0055)(0.12,0.088)}{(0.05)(-4)(-20)(-1.63)(0.72)(0.12,-0.088)(-31.27)(231.3,0.618)} \tag{F.2}$$

which has the frequency response shown in Figure F.1 and yields the following stabilization compensator G_1

$$G_1 = \frac{L_1}{AP} = \frac{147.0(-5)(0.12,0.088)}{s(0.05)(-4)(-20)} \tag{F.3}$$

and the following effective plants P_e and P_y

$$P_e = \frac{L_1}{(1+L_1)} = \frac{2.65\times10^8(-5)(-0.54)(0.0055)(0.12,0.088)}{(-0.0077)(0.12,0.15)(-0.38)(-5.57)(10.8,0.51)(-39.2)(231.3,0.618)} \tag{F.4}$$

$$P_y = \frac{L_1}{P(1+L_1)} = \frac{2.46\times10^8(-5)(-1.63)(0.72)(0.12,0.088)(0.12,-0.088)}{s(-0.0077)(0.12,0.15)(-0.38)(-5.57)(10.8,0.51)(-39.2)(231.3,0.618)} \tag{F.5}$$

A satisfactory saturation control loop transmission is

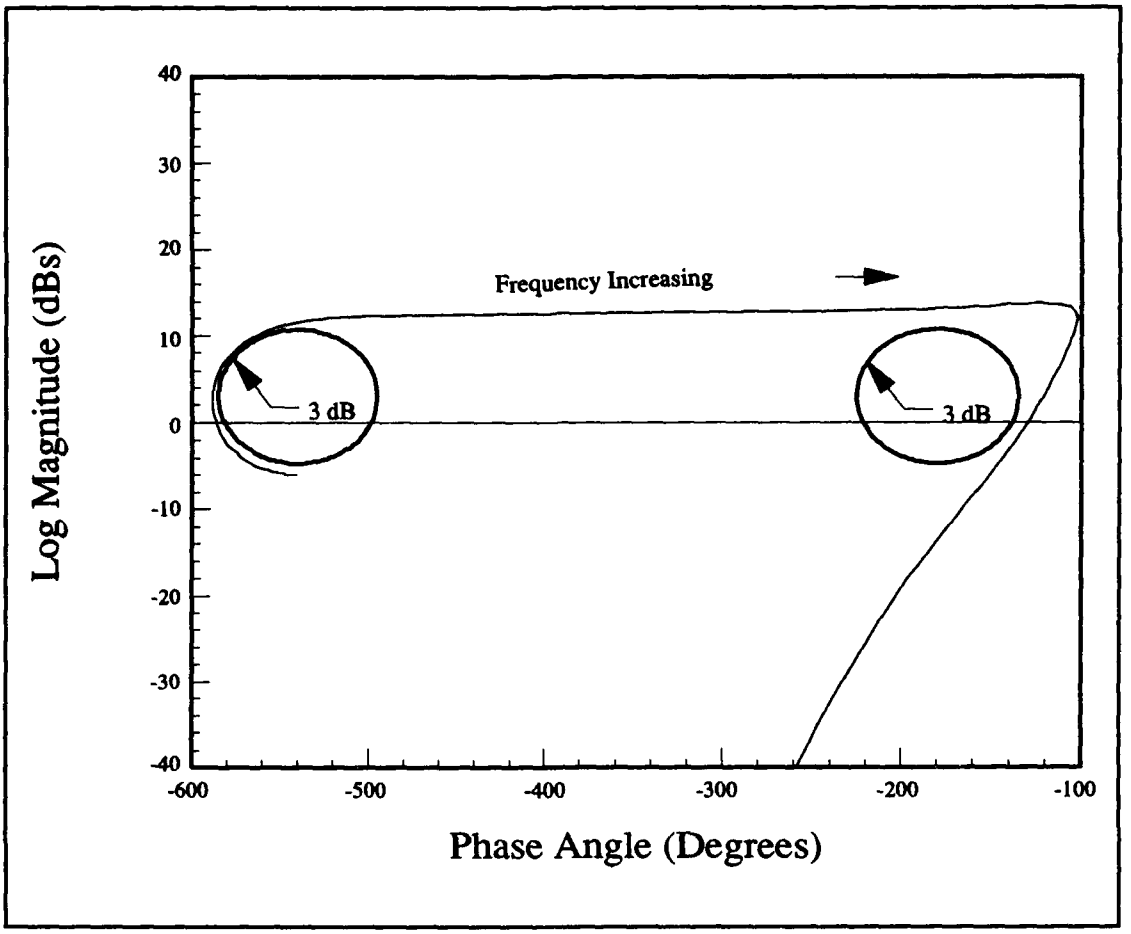

Figure F.1. Stabilization Loop Nichols Plot for Case 5

$$L_2 = \frac{1.25\times 10^8(-0.001)(-0.01)(-5)(-1.63)(0.72)(0.12,0.089)(0.12,-0.089)}{s^2(-3.77)(0.12,0.15)(-5.57)(10.8,0.51)(-0.9)(0.12,0.34)(-39.2)(231,0.62)} \quad \text{(F.6)}$$

which has the frequency response shown in Figure F.2 and gives the following saturation control loop compensator G_2

$$G_2 = \frac{L_2}{P_y} = \frac{-0.507(-0.001)(-0.0076)(-0.01)}{s(0.12,0.34)(-0.9)} \quad \text{(F.7)}$$

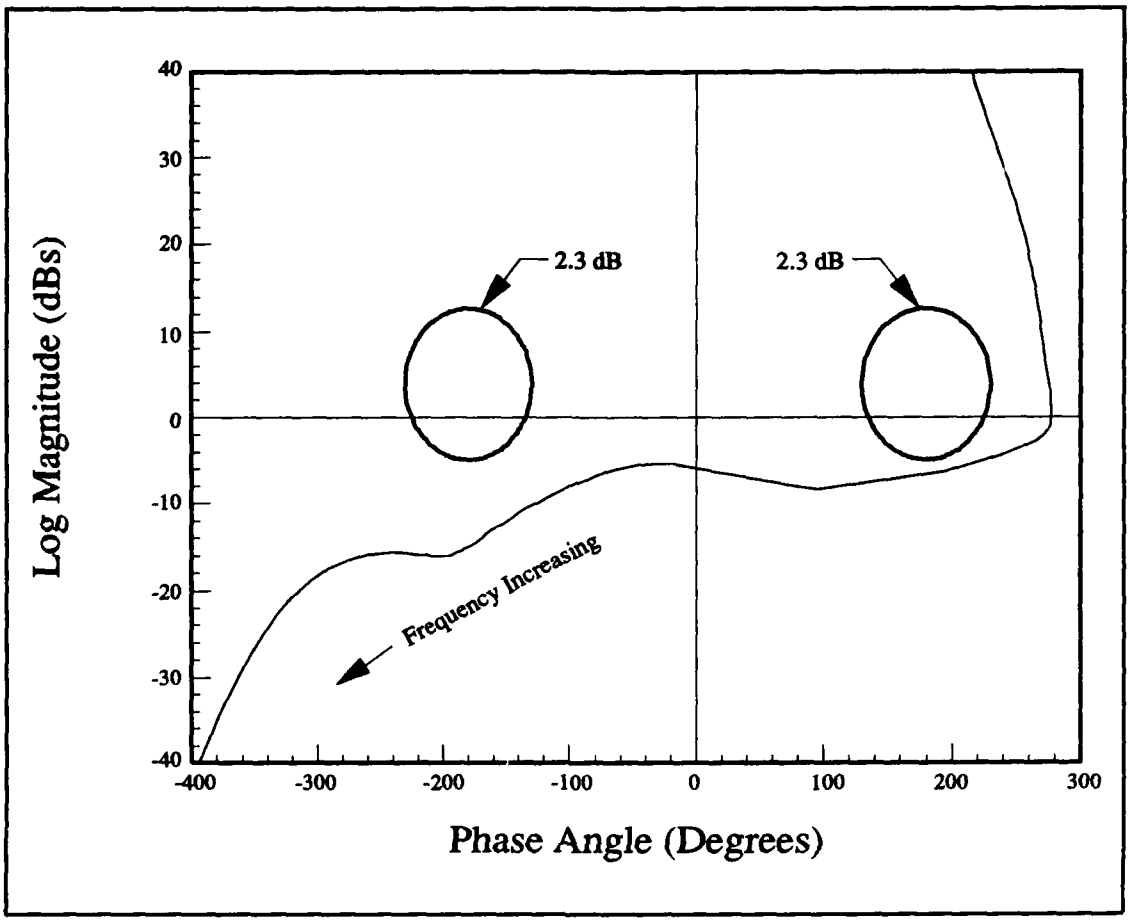

Figure F.2. Saturation Control Loop Nichols Plot for Case 5

The fact that the RHP zero in P_e is very near the origin severely limits the bandwidth of the tracking control loop. In order to provide increased loop gain over a wider range of frequency, a second RHP zero is added. A satisfactory tracking control loop transmission is

$$L_3 = \frac{1.12\times 10^9(-5)(.005)(0.12,0.089)(0.54)(-0.007)(0.0055)}{s(-0.35)(-0.3)(-.0077)(0.12,0.15)(-0.38)(-5.57)(10.8,0.51)(-39.2)(231,0.62)} \quad \text{(F.8)}$$

which has the frequency response shown in Figure F.3 and gives the following tracking control loop compensator L_{3c}

$$L_{3c} = \frac{L_3}{P_e} = \frac{4.22(0.005)(-0.007)}{s(-0.3)(-0.35)} \tag{F.9}$$

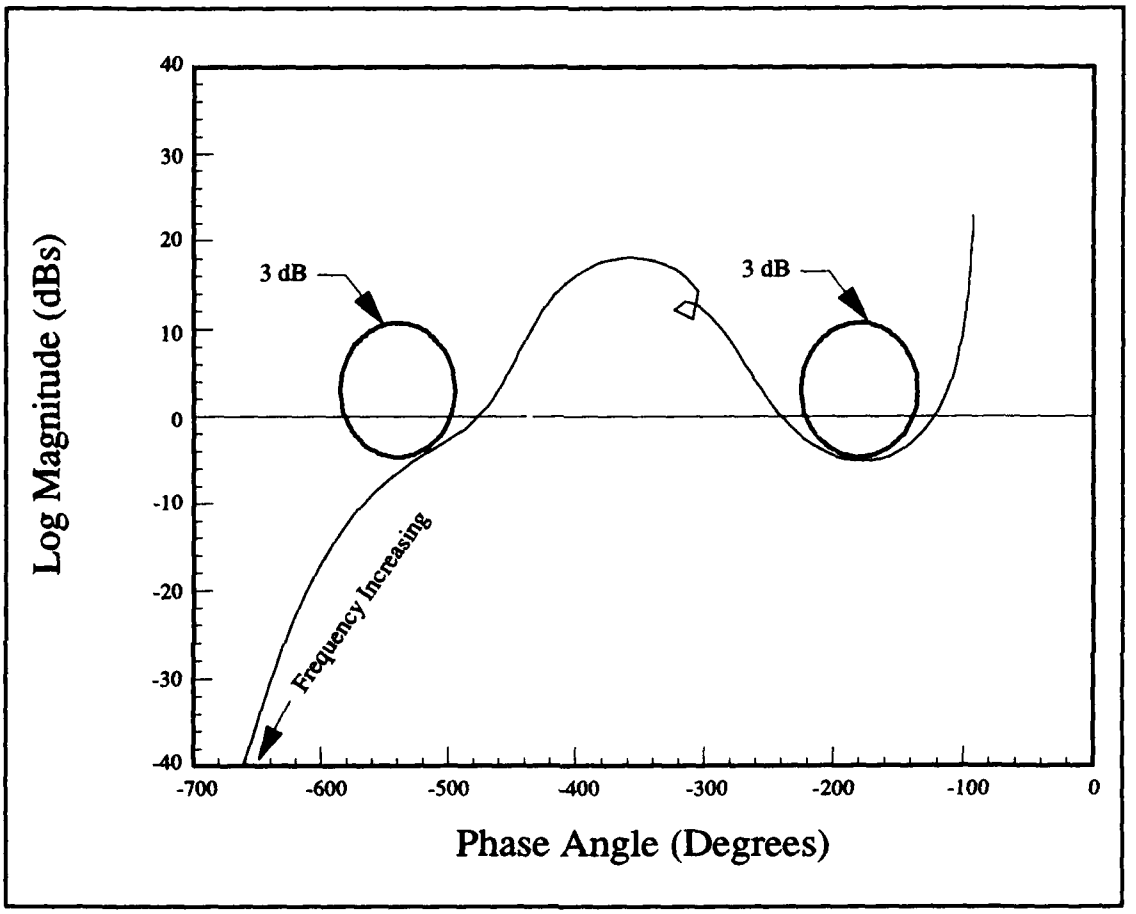

Figure F.3. Tracking Control Loop Nichols Plot for Case 5

The RHP zero in L_{3c}, along with the pole farthest from the origin, is placed in the feedback compensator H_3. This "hides" the RHP zero from the closed loop transfer function. Therefore, the feedback compensator H_3 is

$$H_3 = \frac{70(0.005)}{(-0.35)} \tag{F.10}$$

and the closed loop transfer function P_3 is

$$P_3 = \frac{L_3}{H_3(1+L_3)}$$
$$= \frac{1.60\times 10^7(-.35)(-0.007)(-5)(0.12,0.089)(-.54)(0.0055)}{(-0.0042)(0.12,0.095)(0.0064,0.72)(-0.543)(-4.32)(8.81,0.24)(-9.08)(-38.6)(231,0.62)} \quad \text{(F.11)}$$

The command limiter minor loop compensator H is calculated as in Section 5.2:

$$H = \frac{10P_3}{sL_3} \approx \frac{10(-0.3)(-0.35)(-.377)(10.8,0.51)}{(0.0064,0.72)(-0.54)(8.81,0.24)(-9.08)} \quad \text{(F.12)}$$

The compensator G_3 is

$$G_3 = \frac{L_{3c}(1+H)}{G_2H_3}$$
$$= \frac{-0.119(-0.007)(-0.9)(0.12,0.34)(0.221,0.76)(-0.51)(10.7,0.32)(-16.26)}{(-0.3)(-0.001)(-0.0076)(-0.01)(-9.08)(-0.54)(8.8,0.24)(0.0064,0.72)} \quad \text{(F.13)}$$

The closed loop transfer function P_3 has the frequency response shown in Figure F.4.

To obtain the desired frequency response, the following prefilter is used:

$$F = \frac{10.39(-0.004)(8.76,0.24)}{(-.35)(-1.3)(-7)} \quad \text{(F.14)}$$

The final closed loop frequency response is nearly indistinguishable from that shown in Figure 5.5 for Case 6.

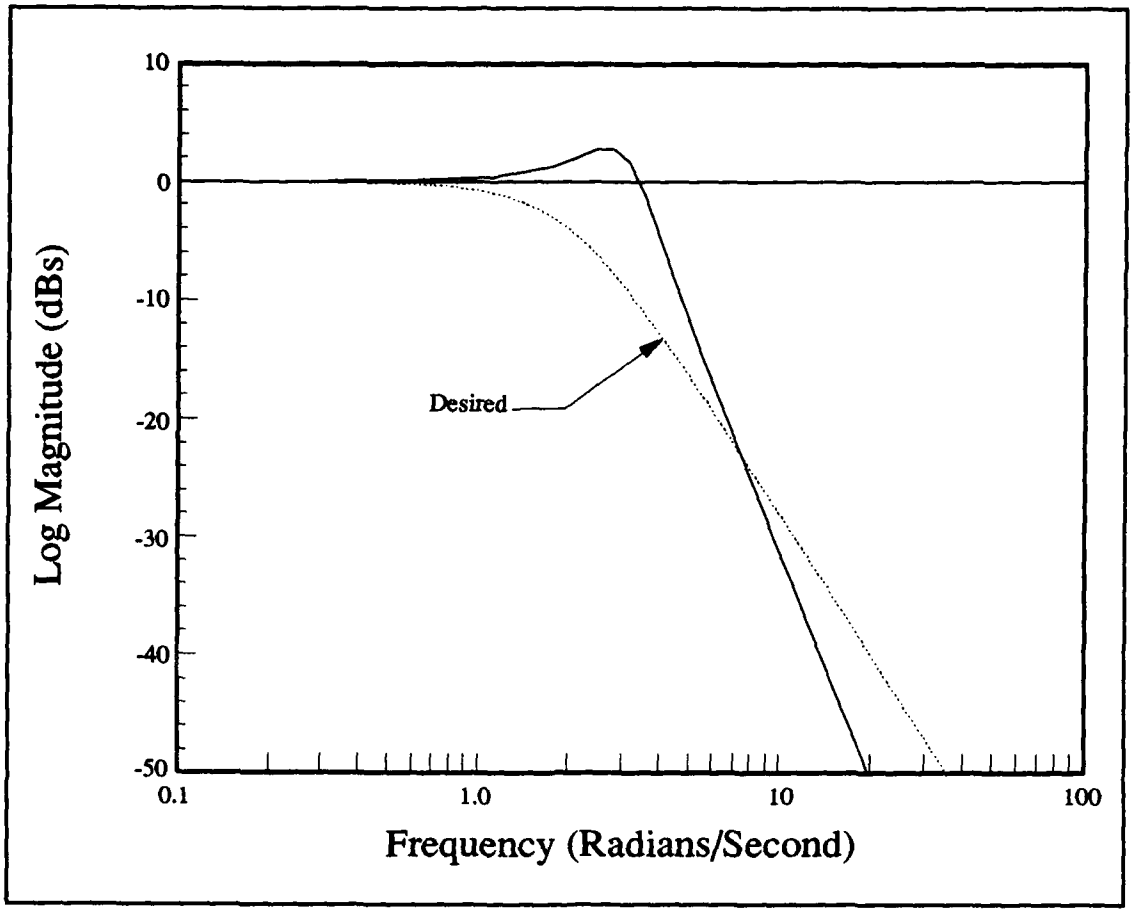

Figure F.4. Closed Loop Frequency Response without Prefilter for Case 5

Appendix G: Controller Design Summary for Case 6

Case 6 has the following Category A basic plant

$$P = \frac{4.68s(-1.15)(-0.012)}{(-3.08)(1.38)(0.12, 0.062)} \tag{G.1}$$

A stable loop transmission is

$$L_1 = \frac{1.54 \times 10^8}{(-31.27)(231, 0.62)(-15)(1.38)} \tag{G.2}$$

which has the frequency response shown in Figure G.1 and yields the following stabilization compensator G_1

$$G_1 = \frac{L_1}{AP} = \frac{19.68(-3.08)(0.12, 0.062)}{s(-15)(-1.15)(-0.012)} \tag{G.3}$$

and the following effective plants P_e and P_y

$$P_e = \frac{L_1}{(1 + L_1)} = \frac{1.54 \times 10^8}{(231, 0.62)(-35.8)(7.91, 0.58)} \tag{G.4}$$

$$P_y = \frac{L_1}{P(1 + L_1)} = \frac{3.29 \times 10^7(-3.08)(1.38)(0.12, 0.062)}{s(231, 0.62)(-35.8)(7.91, 0.58)(-1.15)(0.012)} \tag{G.5}$$

A satisfactory saturation control loop transmission is

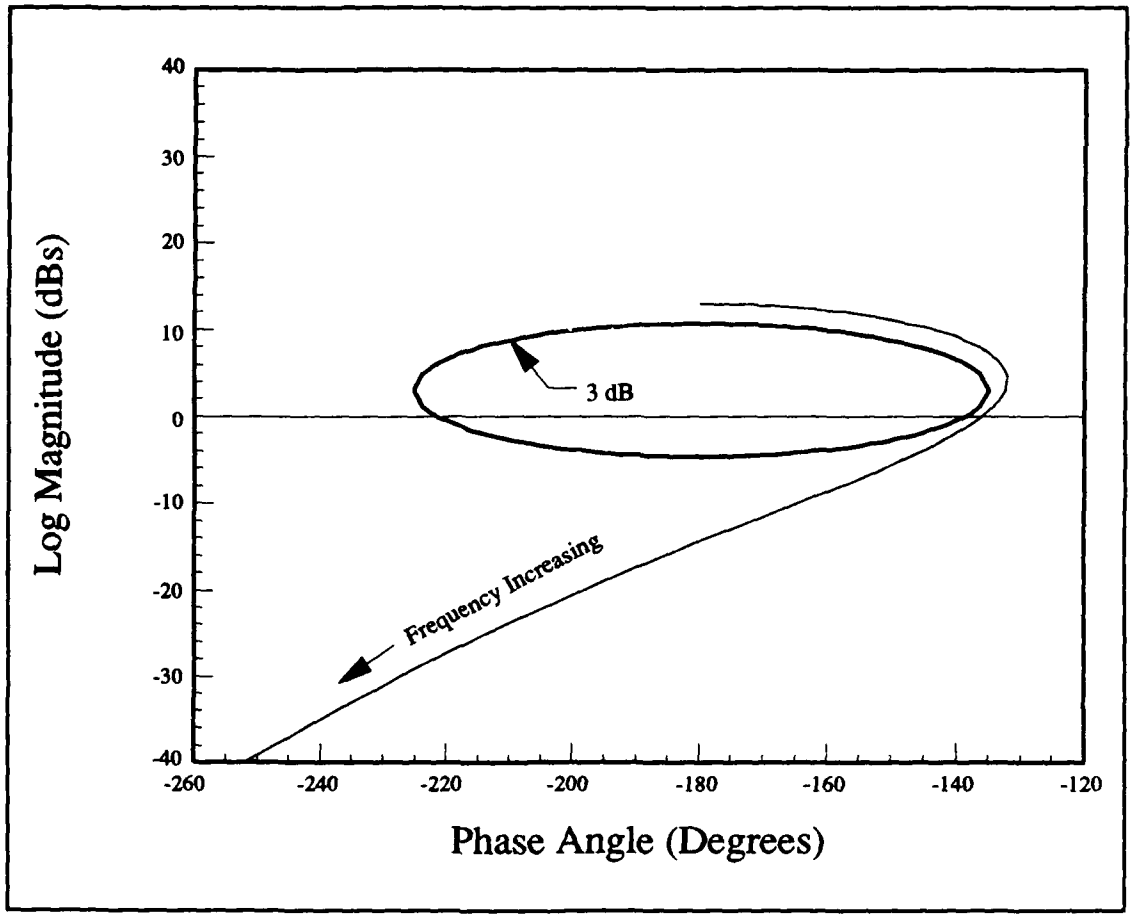

Figure G.1. Stabilization Loop Nichols Plot for Case 6

$$L_2 = \frac{1.53 \times 10^7 (-0.03)(-3.08)(1.38)}{s^2(-1.15)(7.91, 0.58)(-35.8)(231, 0.62)} \tag{G.6}$$

which has the frequency response shown in Figure G.2 and gives the following saturation control loop compensator G_2

$$G_2 = \frac{L_2}{P_y} = \frac{0.464(-0.012)(-0.03)}{s(0.12, 0.062)} \tag{G.7}$$

A satisfactory tracking control loop transmission is

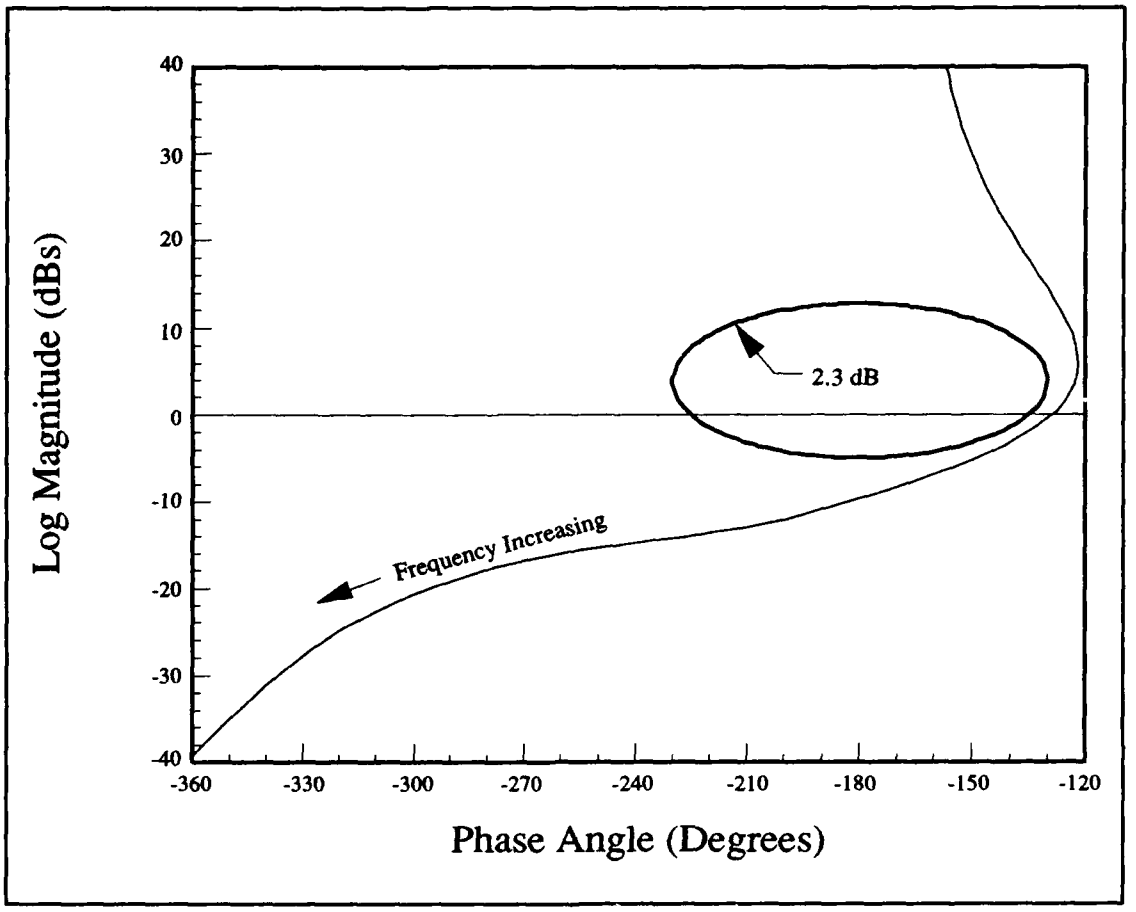

Figure G.2. Saturation Control Loop Nichols Plot for Case 6

$$L_3 = \frac{3.70 \times 10^8}{s(7.91, 0.58)(-35.8)(231, 0.62)} \tag{G.8}$$

which has the frequency response shown in Figure G.3 and gives the following tracking control loop compensator L_{3c}

$$L_{3c} = \frac{L_3}{P_e} = \frac{2.398}{s} \tag{G.9}$$

There are no RHP zeros in the loop transmission. Therefore, the feedback compensator H_3 is

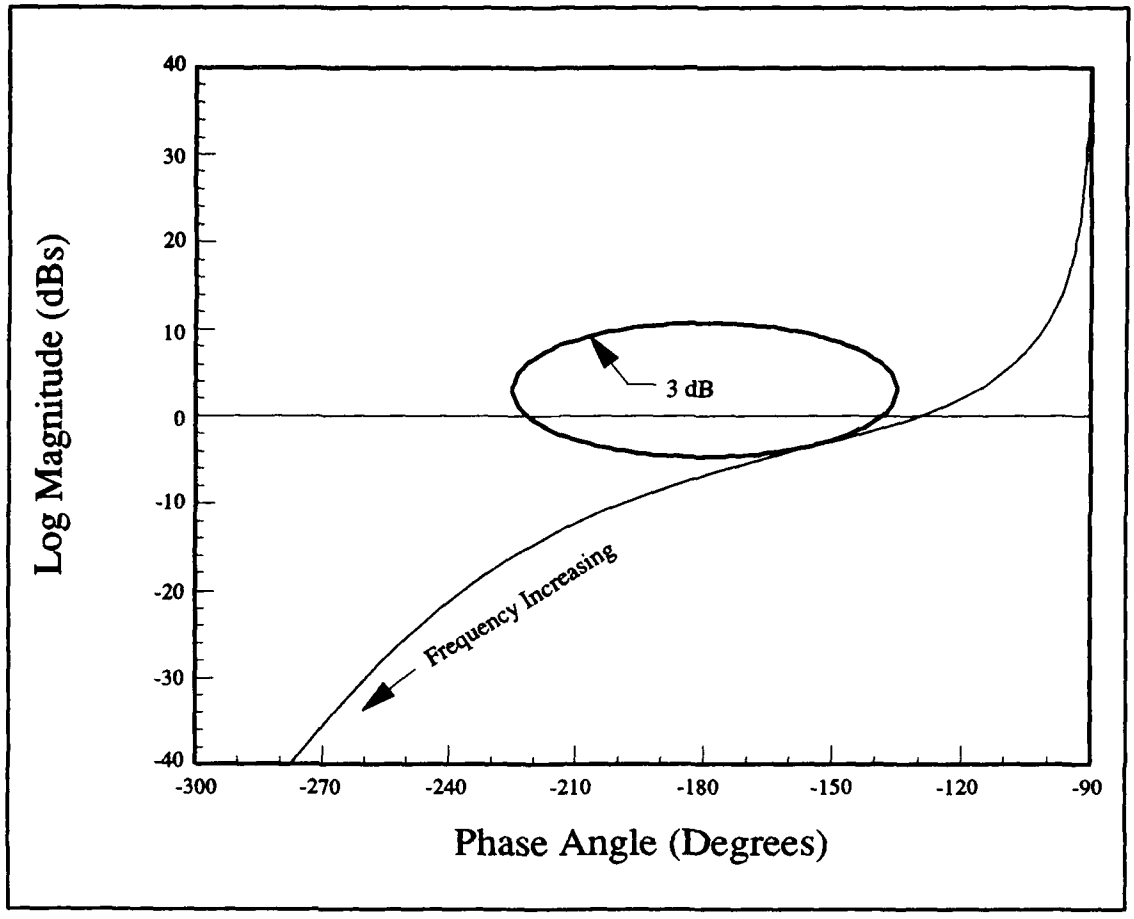

Figure G.3. Tracking Control Loop Nichols Plot for Case 6

$$H_3 = 1 \tag{G.10}$$

and the closed loop transfer function P_3 is

$$\begin{aligned} P_3 &= \frac{L_3}{H_3(1+L_3)} \\ &= \frac{3.70\times 10^8}{(-5.54)(5.9,0.32)(-35.5)(231,0.62)} \end{aligned} \tag{G.11}$$

The command limiter minor loop compensator H is calculated as in Section 5.2.

$$H = \frac{10P_3}{sL_3} \approx \frac{10(7.91, 0.58)}{(-5.54)(5.9, 0.32)} \tag{G.12}$$

The compensator G_3 is

$$G_3 = \frac{L_{3c}(1+H)}{G_2H_3} = \frac{-5.17(0.12, 0.062)(7.99, 0.41)}{(-0.03)(-0.012)(-5.54)(5.9, 0.32)} \tag{G.13}$$

The closed loop transfer function P_3 has the frequency response shown in Figure G.4.

To obtain the desired frequency response, the following prefilter is used giving the frequency response shown in Figure G.5:

$$F = \frac{2.20(-5.2)(5.92, 0.32)}{(-100)(2, 0.8)} \tag{G.14}$$

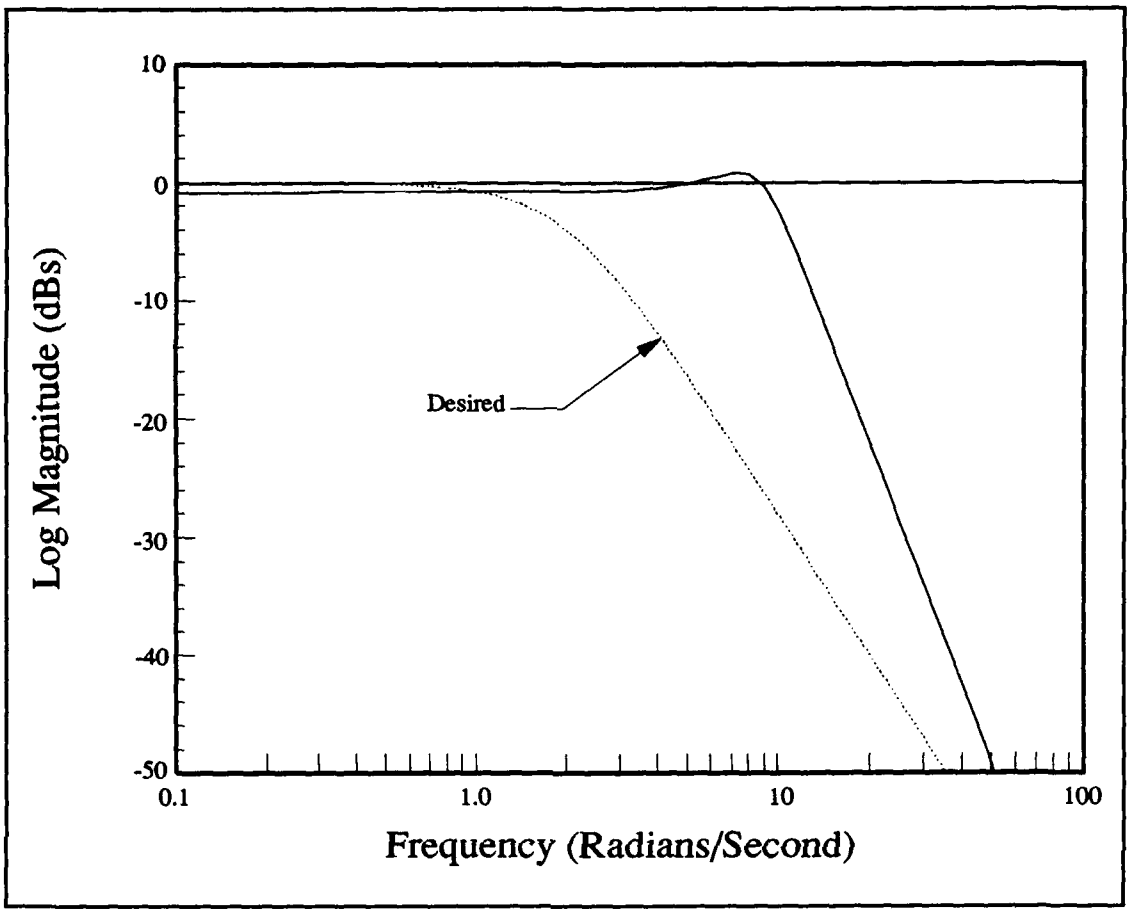

Figure G.4. Closed Loop Frequency Response without Prefilter for Case 6

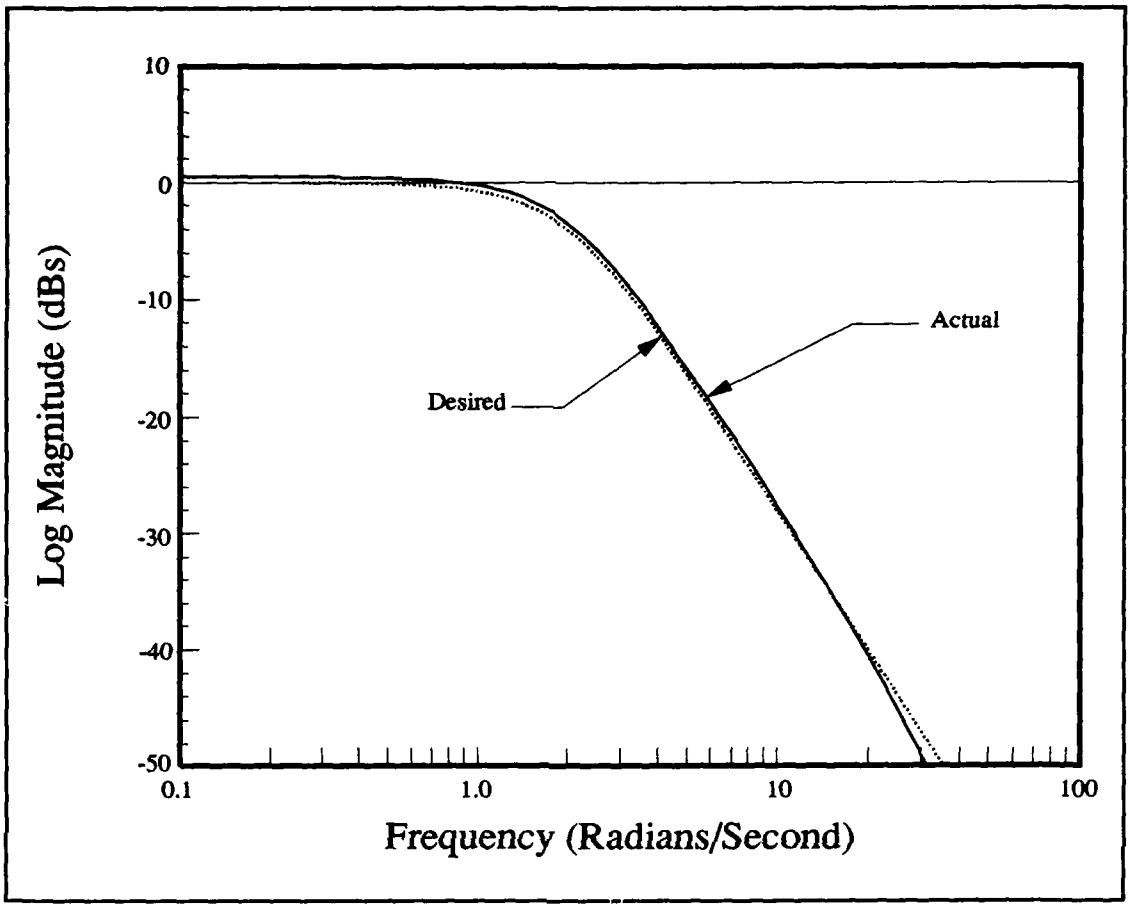

Figure G.5. Closed Loop Frequency Response with Prefilter for Case 6

Appendix H: Nichols Plot Loop Shaping

All loop shaping done in this thesis was accomplished using the software package MathCad (12). MathCad is a personal computer based software package which allows the input and display of mathematical expressions in the format one would use by hand with pencil and paper. Its major strength for loop shaping is that, with the aid of the worksheet developed in the course of this thesis, transfer functions for the plant and a compensator can be entered directly as poles and zeros. A nichols plot of the frequency response of the open loop transfer function is shown on the screen along with a selected M_m contour. The compensator can be changed and the effects immediately show up in the plot. In this way, a minimal order compensator can quickly be designed which produces the desired open loop characteristics. Figures (H.1) through (H.8) show the screen views of the entire worksheet. The worksheet is too large to be viewed all at once. However, only the upper left corner and the lower left corner are needed to use the worksheet.

In the upper left corner enter the basic plant in terms of gain, poles, and zeros. Do not enter any poles or zeros at the origin. Also enter the desired value of the M_m contour. In the lower left corner enter the desired compensator, the desired value of steady state gain and the desired final system type for the open loop transfer function.

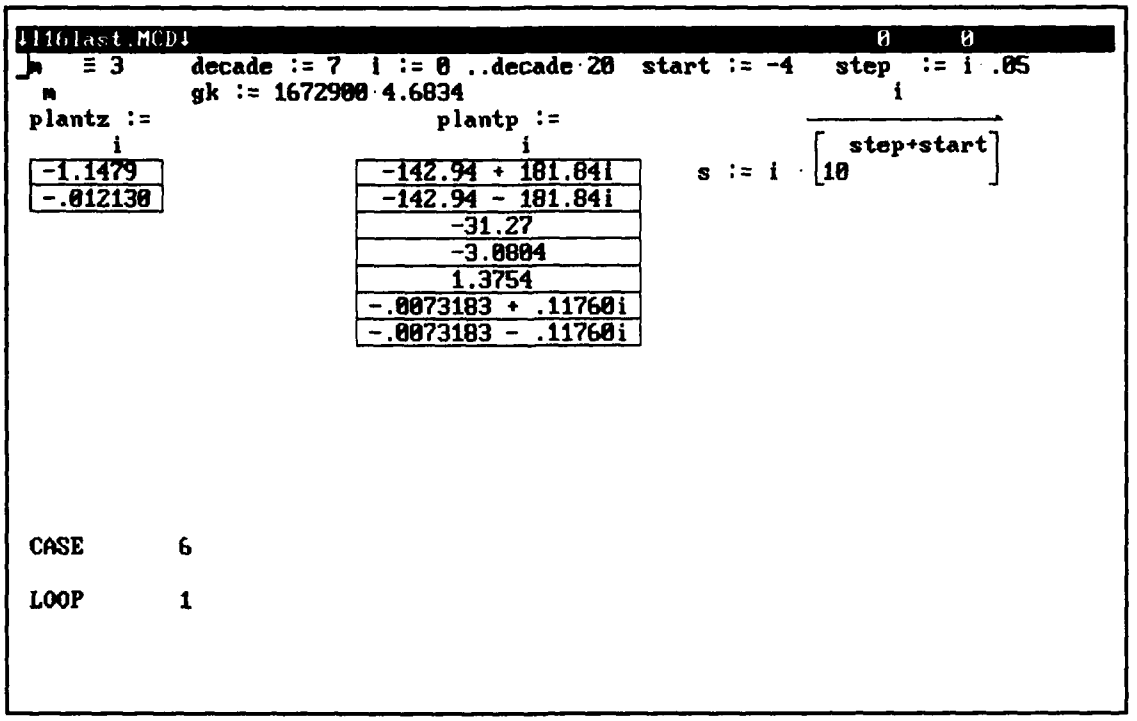

Figure H.1. MathCad Loop Shaping Worksheet 0,0 to 24,79

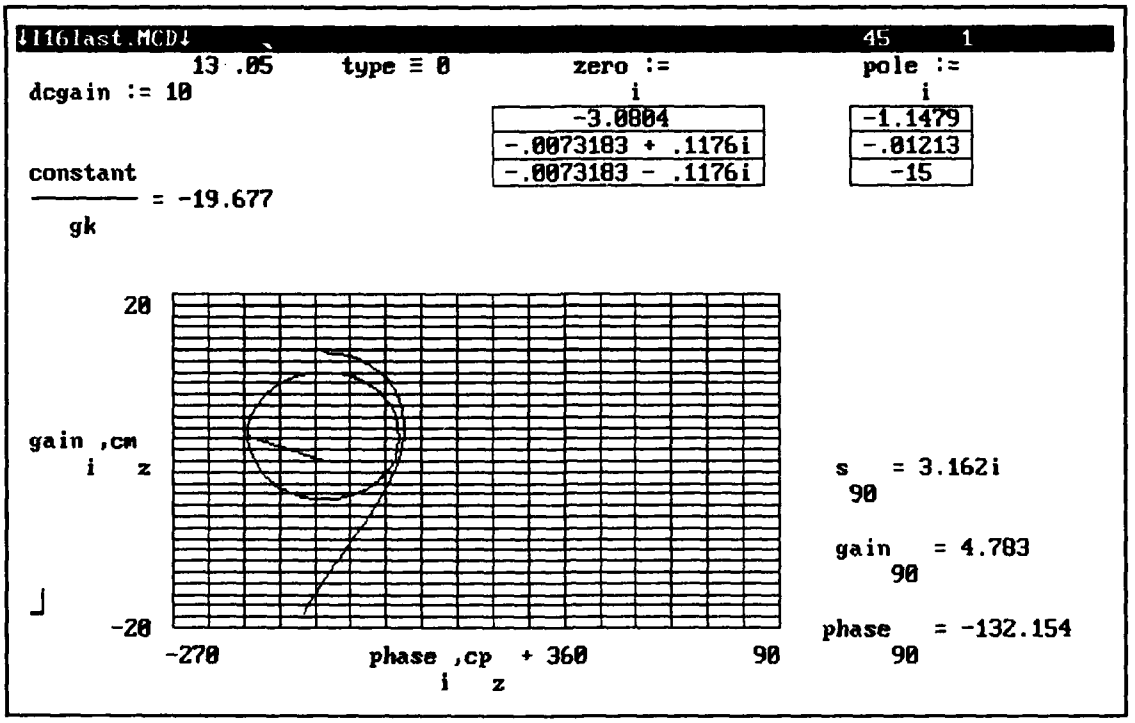

Figure H.2. MathCad Loop Shaping Worksheet 25,0 to 48,79

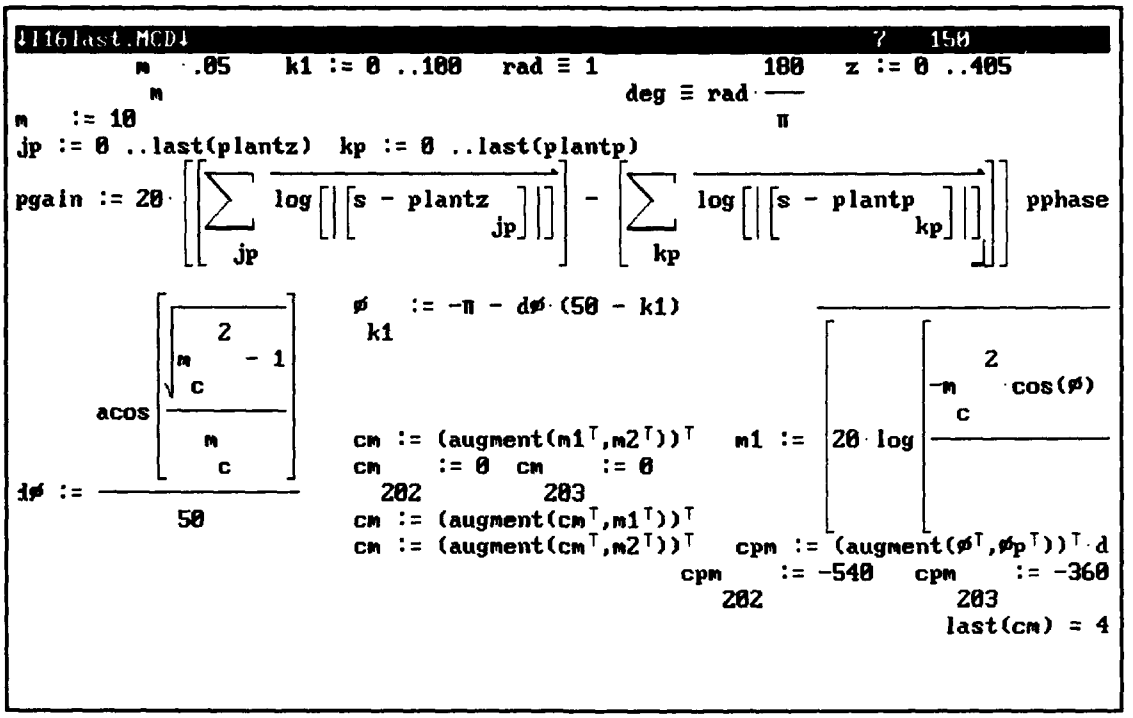

Figure H.3. MathCad Loop Shaping Worksheet 0,80 to 24,159

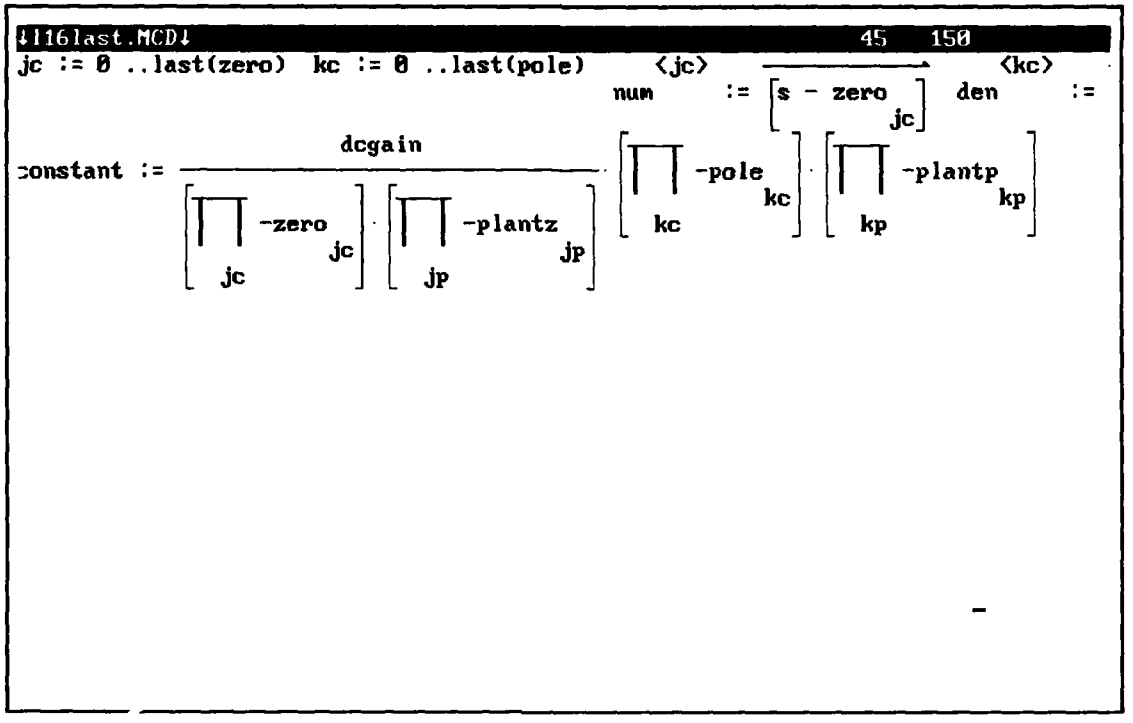

Figure H.4. MathCad Loop Shaping Worksheet 25,80 to 48,159

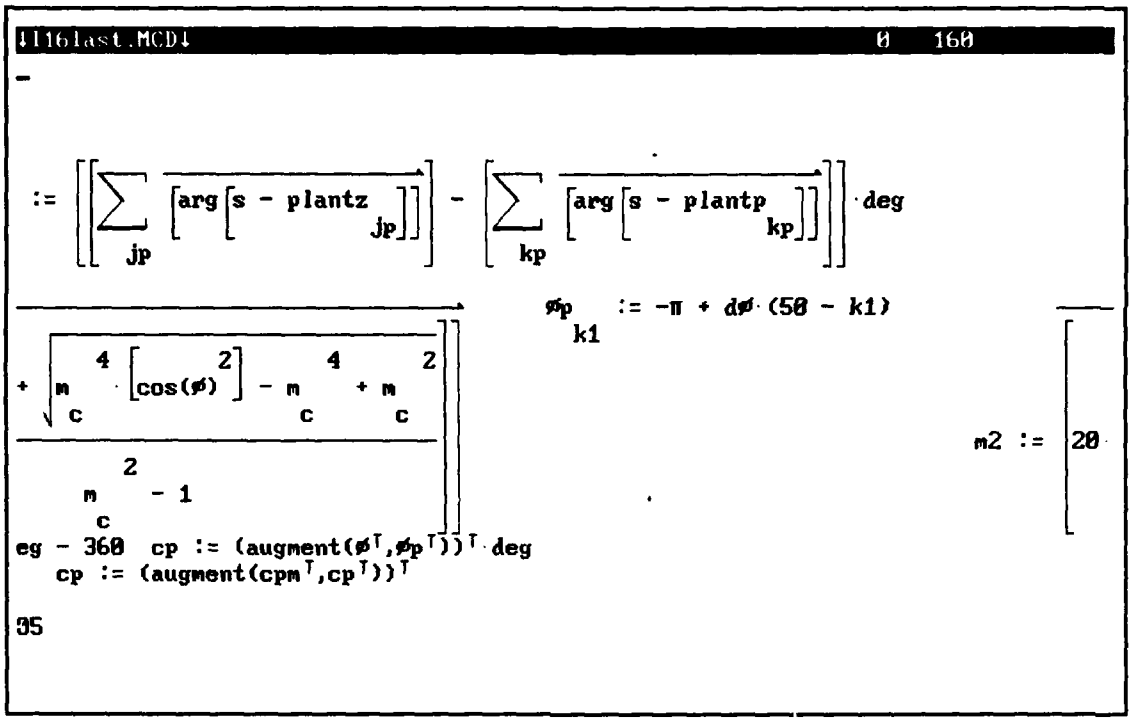

Figure H.5. MathCad Loop Shaping Worksheet 0,160 to 24,239

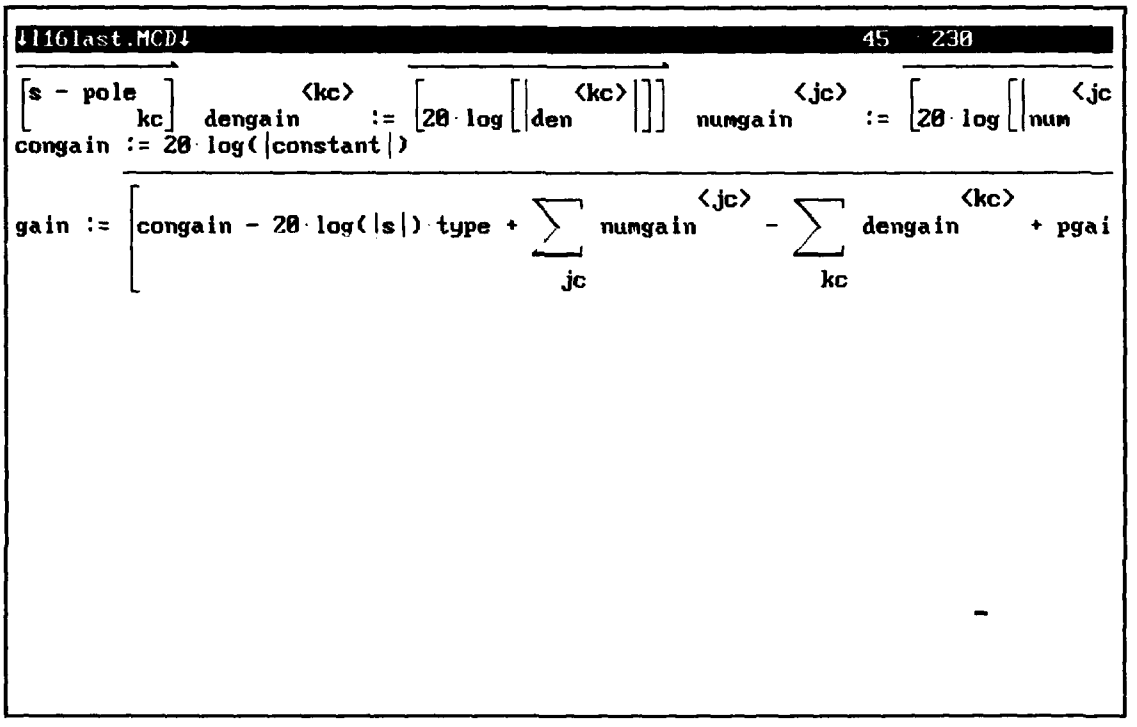

Figure H.6. MathCad Loop Shaping Worksheet 25,160 to 48,239

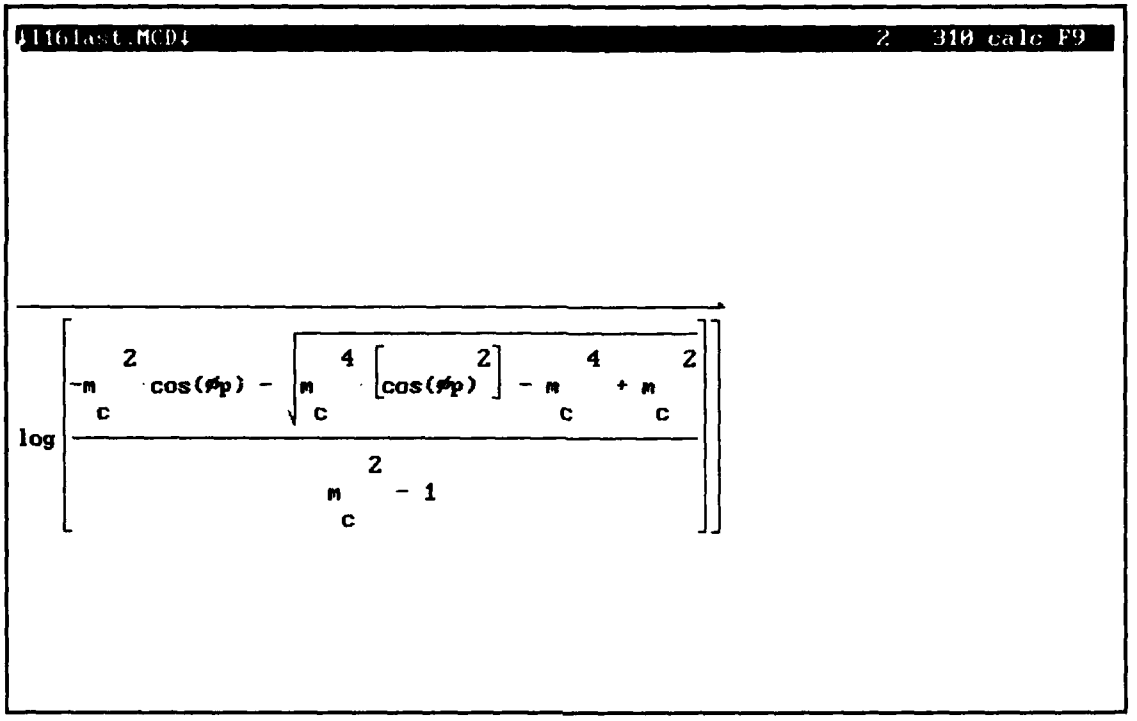

Figure H.8. MathCad Loop Shaping Worksheet 0,240 to 24,319

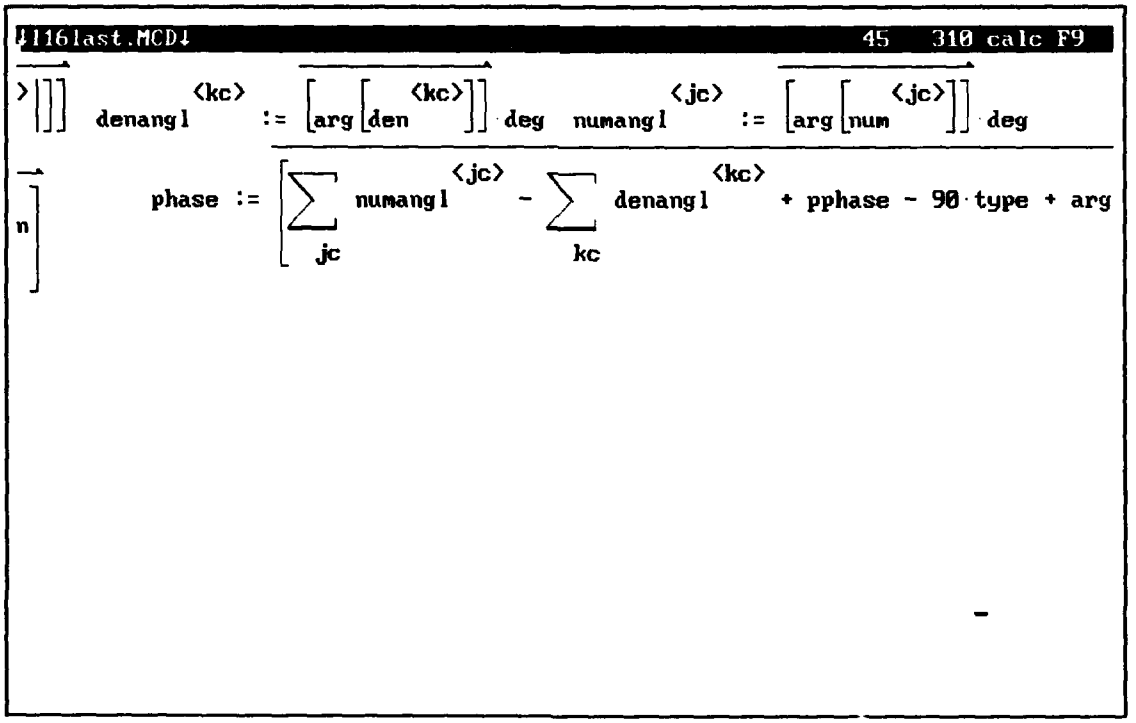

Figure H.8. MathCad Loop Shaping Worksheet 25,240 to 48,319

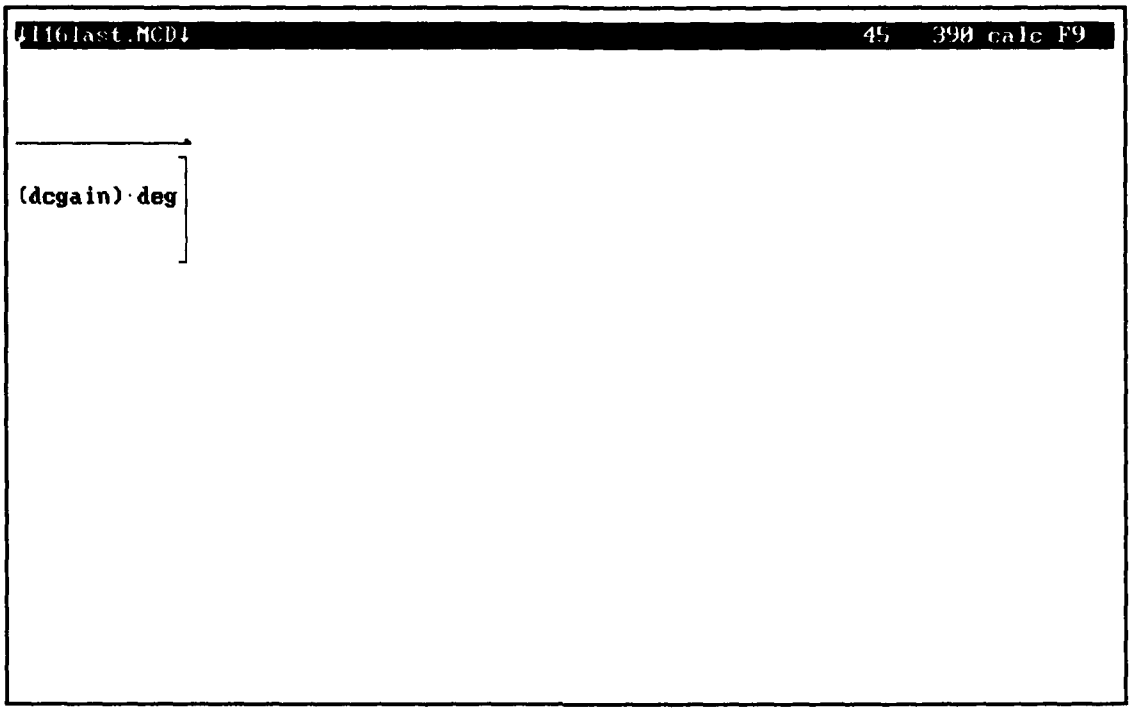

Figure H.8. MathCad Loop Shaping Worksheet 25,320 to 48,399

Bibliography

1. Clough, Capt. Bruce T. Conversation and Discussion. AFWAL/FIGX, Wright-Patterson AFB, OH. April 1988.

2. D'Azzo, John J. and Constantine H. Houpis. Linear Control System Analysis and Design, Conventional and Modern (Second Edition). New York: McGraw-Hill Book Company, 1981.

3. Halliday, David and Robert Resnick Physics, Part I. New York, John Wiley & Sons, Inc., 1962.

4. Horowitz, Isaac M. Conversation and Discussion. AFWAL/FIGL, Wright-Patterson AFT, OH. April 1988 - March 1989.

5. Horowitz, I. M. "A Synthesis Theory for a Class of Saturating Systems", International Journal of Control, 38: 169-187 (July 1983).

6. Horowitz, I. M. and Y. K. Liao. "Quantitative Non-Linear Compensation Design for Saturating Unstable Uncertain Plants," International Journal of Control, 44: 1137-1146 (October 1986).

7. Horowitz, Isaac. "Feedback Systems with Rate and Amplitude Limiting," International Journal of Control, 40: 1215-1229 (December 1984).

8. Horowitz, Isaac M. and Marcel Sidi. "Synthesis of Feedback Systems with Large Plant Ignorance for Prescribed Time Domain Tolerances," International Journal of Control, 16: 677-699 (1981).

9. Houpis, C. H. Quantitative Feedback Theory Technique for Designing Multivariable Control Systems. AFWAL-TR-86-3107. Air Force Wright Aeronautical Laboratory, Wright-Patterson AFB OH, January 1987.

10. Houpis, Constantine H. Class notes in EENG 743, Literature Study in Control Theory. School of Engineering, Air Force Institute of Technology, Wright-Patterson AFB, OH, March-May 1988.

11. Lewantowicz, Zdzislaw. Class notes in EENG 641, Automatic Flight Control II. School of Engineering, Air Force Institute of Technology, Wright-Patterson AFB, OH. March-May 1988.

12. Mathsoft, Inc. MathCad User's Guide. Cambridge, Massachusetts, October 1987.

13. Integrated Systems Inc. $MATRIX_x$ Users Guide, (Version 6.0). Palo Alto, Califomia.

14. Roskam, Jan. Flight Dynamics of Rigid and Elastic Airplanes. Lawrence KS: Roskam Aviation and Engineering Corporation, 1972.

Vita

Captain Oliver J. Merwin [redacted] He graduated from high school in Fairfax, Virginia in 1974 and received a Bachelor of Science Degree in Aerospace Engineering from Northrop University in 1978.

He received his commission in the United States Air Force in July of 1978 through the ROTC program and entered Undergraduate Pilot training at Vance AFB, Ok in May 1979. After completion of pilot training, he remained at Vance as a T-37 instructor pilot. In September of 1983, he was assigned to Scott AFB as a C-140A pilot performing airborne inspection and calibration of ground based navigation, instrument approach, air traffic control, and communication facilities. He was entered into the Graduate Electrical Engineering program at the Air Force Institute of Technology in June of 1987.

[redacted]

REPORT DOCUMENTATION PAGE

Form Approved
OMB No. 0704-0188

1a. REPORT SECURITY CLASSIFICATION UNCLASSIFIED	1b. RESTRICTIVE MARKINGS
2a. SECURITY CLASSIFICATION AUTHORITY	3. DISTRIBUTION/AVAILABILITY OF REPORT Approved for public release; distribution unlimited
2b. DECLASSIFICATION/DOWNGRADING SCHEDULE	
4. PERFORMING ORGANIZATION REPORT NUMBER(S) AFIT/GE/ENG/89M-5	5. MONITORING ORGANIZATION REPORT NUMBER(S)
6a. NAME OF PERFORMING ORGANIZATION School of Engineering 6b. OFFICE SYMBOL (If applicable) AFIT/ENG	7a. NAME OF MONITORING ORGANIZATION
6c. ADDRESS (City, State, and ZIP Code) Air Force Institute of Technology Wright-Patterson AFB OH 45433-6583	7b. ADDRESS (City, State, and ZIP Code)
8a. NAME OF FUNDING/SPONSORING ORGANIZATION AFWAL/FIGX 8b. OFFICE SYMBOL (If applicable) AFWAL/FIGX	9. PROCUREMENT INSTRUMENT IDENTIFICATION NUMBER
8c. ADDRESS (City, State, and ZIP Code) Wright-Patterson AFB OH 45433	10. SOURCE OF FUNDING NUMBERS PROGRAM ELEMENT NO. / PROJECT NO. / TASK NO. / WORK UNIT ACCESSION NO.

11. TITLE (Include Security Classification)
CONTROL DESIGN FOR AN UNSTABLE NON-MINIMUM PHASE AIRCRAFT SUBJECT TO CONTROL SURFACE SATURATION

12. PERSONAL AUTHOR(S)
Oliver J. Merwin, Capt., USAF

13a. TYPE OF REPORT	13b. TIME COVERED	14. DATE OF REPORT (Year, Month, Day)	15. PAGE COUNT
MS Thesis	FROM _____ TO _____	March 1989	152

16. SUPPLEMENTARY NOTATION

17. COSATI CODES			18. SUBJECT TERMS (Continue on reverse if necessary and identify by block number)
FIELD	GROUP	SUB-GROUP	Control Systems Control Surfaces Control Surface Saturation
01	04		

19. ABSTRACT (Continue on reverse if necessary and identify by block number)

Thesis Advisor: Constantine H. Houpis
Professor
Deptartment of Electrical Engineering

20. DISTRIBUTION/AVAILABILITY OF ABSTRACT	21. ABSTRACT SECURITY CLASSIFICATION
☒ UNCLASSIFIED/UNLIMITED ☐ SAME AS RPT. ☐ DTIC USERS	UNCLASSIFIED
22a. NAME OF RESPONSIBLE INDIVIDUAL Constantine H. Houpis, Professor	22b. TELEPHONE (Include Area Code) (513) 255-3576 22c. OFFICE SYMBOL AFIT/ENG

DD Form 1473, JUN 86 *Previous editions are obsolete.* SECURITY CLASSIFICATION OF THIS PAGE

19. Abstract

The purpose of this study is to validate a design technique for the control of unstable aircraft which are subject to limited control authority. This thesis applies the technique to a realistic aircraft model, instead of the simplified models used in the theoretical development, to produce a pitch rate controller for widely spaced regions of the flight envelope.

First the aircraft is stabilized by feeding back pitch rate. Then an adjustable command limiter is placed in the input path for the stable effective plant. The saturation level of the limiter is adjusted by a second feedback loop feeding back the stabilator deflection angle. An outer feedback loop provides the proper command tracking response when the command limiter is not saturated. The final element is a minor feedback loop around the command limiter to provide a second degree of freedom to ensure the limiter comes out of saturation as quickly as possible.

Simulations for step commands ranging from 1 to 50 degrees/second pitch rate show the design is quite successful. The stabilator does not saturate in a manner which causes instability even when responding to extreme commands. Simulations of a pulse command show that the command limiter unstaurates rapidly and the aircraft responds appropriately to a reduced pitch command even when the stabilator is near the limit.

The technique applies relatively simple linear design tools to the non linear problem of control surface saturation.